

Transcription factor Pax6 controls structure and function of the centrosome in cortical progenitors

Dissertation
for the award of the degree

“Doctor rerum naturalium”
of the Georg-August-Universität Göttingen

within the doctoral program
‘Molecular physiology of the brain’
of the Göttingen Graduate School for Neurosciences, Biophysics, and Molecular
Biosciences (GGNB)
of the Georg-August University School of Science (GAUSS)

submitted by
Marco Andreas Tylkowski

from Wedel
Göttingen, 2013

Thesis committee

Prof. Dr. Anastassia Stoykova 1 st Referee	Molecular Developmental Neurobiology Max-Planck Institute for Biophysical Chemistry Göttingen
Prof. Dr. Sigrid Hoyer-Fender 2 nd Referee	Department for Developmental Biology University of Göttingen Göttingen
Prof. Dr. Andreas Wodarz	Stem Cell Biology, Department of Anatomy and cell biology University of Göttingen Göttingen

Extended thesis committee

Prof. Dr. Ahmed Mansouri	Molecular Cell Differentiation Max-Planck Institute for Biophysical Chemistry Göttingen
Prof. Dr. Ernst Wimmer	Department for Developmental Biology University of Göttingen Göttingen
Prof. Dr. Michael Hörner	Department for Cellular Neurobiology University of Göttingen Göttingen

Date of oral exam:

Affidavit

I hereby declare that my doctoral thesis entitled “Transcription factor Pax6 controls structure and function of the centrosomes in cortical progenitors” has been written independently with no other sources and aids than quoted.

Marco Andreas Tylkowski, May 2013

This work has been generated at the Max-Planck Institute for Biophysical Chemistry – Karl-Friedrich-Bonhoefer-Institute – in Göttingen in the research group Molecular Developmental Neurobiology of Prof. Dr. Anastassia Stoykova

INDEX

Abstract	1
I. Introduction	3
I.1. Brain Development.....	3
I.1.1. Neural induction.....	3
I.2. Development of Telencephalon	5
I.2.1. Molecular patterning of Telencephalon	5
I.2.2. Arealisation of cerebral cortex.....	6
I.2.3. Origin of cell diversity in neocortex.....	8
I.2.4. Neurogenesis and layer formation of neocortex.....	9
I.2.4.1. Radial glia progenitor cells	9
I.2.4.1.1. Symmetric proliferative divisions of neuroepithelial cells and transformation into radial glia progenitor cells.....	9
I.2.4.1.2. Asymmetric neurogenic divisions of RGPs and neuronal layer formation	9
I.2.4.1.3. Interkinetic nuclear migration of RGP nuclei.....	12
I.2.4.2. TF Pax6 and interkinetic nuclear migration	13
I.3. The Centrosome.....	15
I.3.1. Structure of the Centrosome	15
I.3.2. Centrosome function	16
I.3.2.1. Centrosome duplication, segregation and maturation	17
I.3.3. Important centrosome proteins	18
I.3.3.1. Common centrosome markers.....	18
I.3.3.2. The appendage protein Ninein.....	19
I.3.3.3. The outer dense fibre 2 (Odf2) protein	19
I.4. The primary cilium.....	22
I.5. Scope of the thesis.....	24
II. Results.....	25
II.1. TF Pax6 influences the centrosome structure and localisation in cortical RGPs.....	25
II.1.1. Interkinetic nuclear migration is disturbed during late neurogenesis in the mouse <i>Pax6/small eye</i> mutant.....	25
II.1.2. Centrosome localisation is disturbed in RGPs of Pax6-deficient cortex...26	
II.1.3. Structural defect of appendages of the mother centriole in RGPs in <i>Pax6/Small eye</i> mice	27
II.1.3.1. Analysis of centriole structure by STED microscopy.....	28
II.1.3.2. Analysis of centriole structure by electron microscopy	29
II.1.4. Diminished number of RGPs extending primary cilia at the ventricular surface of <i>Sey/Sey</i> cortex	32
II.2. RGPs containing the mother centrosome detach the VZ surface in Pax6-deficient cortex	35
II.3. Mechanism of Pax6-dependent control of centrosome structure and function.....	42
II.3.1. Pax6 as a protein-binding partner of centrosome proteins.....	42
II.3.2. Pax6 as a transcriptional regulator of centrosome-specific proteins.....	45
II.4. Functional and mechanistic analysis of <i>Odf2</i> as a Pax6 downstream target	47
II.4.1. Whole mount <i>in situ</i> hybridisation and reporter gene assay indicate <i>Odf2</i> as a downstream target of Pax6.....	47
II.4.2. TF Pax6 binds to the <i>Odf2</i> promoter	48
II.4.1. <i>Odf2</i> expression in WT and <i>Sey/Sey</i> mice	49

II.4.1.1. <i>Odf2</i> expression on mRNA level	49
II.4.1.2. <i>Odf2</i> expression on protein level.....	51
II.4.2. Ninein protein level is reduced at the centrioles of <i>Sey/Sey</i> mice.....	52
II.5. Analysis of <i>Odf2</i> loss of function cortex	53
II.5.1. Generation of <i>Odf2</i> conditional knock out (<i>Odf2cKO</i>) mice.....	53
II.5.2. Analysis of <i>Odf2</i> knock down <i>in vivo</i>	54
II.5.2.1. <i>In vivo</i> transfection of <i>Odf2</i> short-hairpin constructs in developing brain <i>via</i> <i>in utero</i> electroporation	55
II.5.2.2. Analysis of cell cycle exit index	57
III. DISCUSSION.....	59
III.1. Pax6 controls centrosome structure in RGP of developing cortex.....	59
III.2. Pax6 dependent molecular mechanism controls the centrosome function.....	62
III.3. Put the things together.....	66
IV. Material and Methods.....	70
IV.1. Material.....	70
IV.1.1. Biological material.....	70
IV.1.1.1. Bacterial strains	70
IV.1.1.2. Cell lines	70
IV.1.1.3. Vectors	70
IV.1.1.4. Oligonucleotides	71
IV.1.1.5. Enzymes	72
IV.1.1.5.1. Restriction enzymes	72
IV.1.1.5.2. DNA-Polymerase.....	72
IV.1.1.5.3. DNA Ligases	73
IV.1.1.5.4. DNA Phosphatase	73
IV.1.1.6. Antibodies	73
IV.1.1.6.1. Primary Antibodies.....	73
IV.1.1.6.2. Secondary antibodies.....	74
IV.1.1.6.2.1. Secondary antibodies for Westernblot.....	74
IV.1.1.6.2.1. Secondary antibodies for immunohistochemistry / immunocytochemistry	74
IV.1.2. Culture media.....	74
IV.1.2.1. Culture media for <i>E.coli</i> cultures	74
IV.1.2.2. Culture media for eukaryotic cell culture.....	75
IV.1.3. Buffers and solutions.....	75
IV.1.3.1. Gels for SDS-PAGE.....	78
IV.1.4. Chemicals.....	78
IV.2. Methods	79
IV.2.1. Microbiological methods.....	79
IV.2.1.1. Culture of <i>E. coli</i>	79
IV.2.1.2. Storage of <i>E. coli</i> cultures.....	79
IV.2.1.3. Production of competent bacteria	79
IV.2.1.4. Transformation	80
IV.2.1.4. DNA preparation	80
IV.2.1.5. Extraction of genomic DNA from embryonic mouse tissue.....	80
IV.2.1.5. Polymerase chain reaction (PCR)	80
IV.2.1.6. Quantitative real time PCR (q-rtPCR)	82
IV.2.1.7. DNA electrophoresis	82
IV.2.1.8. DNA purification.....	82
IV.2.1.8.1. Isolation of DNA from agarosegels	82
IV.2.1.9. Enzymatic modification of DNA by restriction enzymes	82
IV.2.1.10. De-phosphorylation of DNA 5'-ends	82
IV.2.1.11. Measurement of DNA / RNA concentrations	83
IV.2.1.12. Ligation	83
IV.2.1.13. Electrophoretic mobility shift assay (EMSA)	83
IV.2.2. Cell culture	84

IV.2.2.1. Culture of NIH3T3 cells	84
IV.2.2.2. Plasmid DNA transfection into NIH3T3 cells.....	84
IV.2.2.3. Immunocytochemistry	85
IV.2.2.4. Reportergene assay.....	85
IV.2.2.5. Extraction of proteins after expression in NIH3T3 cells.....	86
IV.2.3. Protein biochemical assays.....	86
IV.2.3.1. SDS-PAGE.....	86
IV.2.3.2. Transfer of proteins to an Immobilon-P Membrane.....	86
IV.2.3.3. Protein detection by antibodies.....	87
IV.2.3.4. Quantitative protein analysis.....	87
IV.2.3.5. Technics for protein-protein interaction analysis.....	87
IV.2.3.5.1. Co-immunoprecipitation analysis of HA-tagged proteins	87
IV.2.4. Animals	88
IV.2.4.1. Animals	88
IV.2.4.2. Animal treatments.....	88
IV.2.4.2.1. BrdU injections.....	88
IV.2.4.2.2. <i>In utero</i> electroporation.....	88
IV.2.5. Histology	89
IV.2.5.1. Cryo conservation and sectioning of mouse brains	89
IV.2.5.2. Organotypic embryonic mice cortical slice culture and photo switch by UV light	90
IV.2.5.3. Immunohistochemistry	90
IV.2.5.4. Generation of DIG-labelled anti-sense RNA probes	91
IV.2.5.5. Electron microscopy of E15.5 embryonic cortex	94
IV.2.6. Software	94
V. Literature	95
VI. Supplemental Material.....	104
VI.1. Abbreviations	104
VI.2. Statistical analysis of electron microscopy micrographs	106
VI.3. Number of appendages.....	107
VI.4. Quantification of primary cilia by IHC of E13.5 WT and <i>Sey/Sey</i> cortex	108
VI.5. Cilia quantification by EM at E15.5 cortex	109
VI.5. Statistical analysis of Kaede-Centrin1 approach.....	110
VI.5.1. Analysis of control brains.....	110
VI.5.2. Analysis of <i>Pax6cKO</i> brains.....	111
VI.5.3. Locations of Yellow centrosomes.....	112
VI.5.4. Location of Centrosomes	112
VI.5.4.1. Location of centrosomes in control brains	112
VI.5.4.2. Location of Centrosomes in <i>Pax6cKO</i> brains.....	112
VI.5.4.3. Comparison of centrosome localisation in control and <i>Pax6cKO</i> brains	112
VI.6. Luciferase assay	113
VI.6.1. Data from Luciferase assay.....	113
VI.6.2. From the data of the Luciferase experiment following result was calculated:.....	113
VI.7. Knock down of <i>Odf2</i> <i>in vivo</i>	114
VI.7.1. Sequences of short-hairpin constructs	114
VI.7.2. Results of quantification of electroporated cells after knock down of <i>Odf2</i>	114
VI.7.3. Statistical analysis of quantification	115
VI.7.4. Statistical analysis of electroporated RGP (Pax6 ⁺ /GFP ⁺) normalized to control.....	115
VI.8. Cell cycle index	116
VI.8.1. Results of cell cycle analysis.....	116
VI.8.2. Statistical analysis of quantification of cell cycle exit after knock down of <i>Odf2</i>	116

VI.9. Figure index	117
VII. Acknowledgements.....	123
VIII. Curriculum vitae	124

ABSTRACT

The mammalian neocortex is a highly complex structure containing more than 100 billions neurons and ten times more glia cells that are generated during development by progenitor cells located at the apical surface of the forebrain ventricular zone (VZ). The cortical progenitors originate from neuroepithelial cells that transform into radial glia progenitor cells (RGPs) at the beginning of neurogenesis. Starting to divide in an asymmetric neurogenic mode each RGP produces a new radial glia progenitor for self-renewal and a neuron. Around mid-neurogenesis, the RGPs switch from this direct mode of neurogenesis to an indirect mode through which each RGP divides to self-renew and generates a new type of progenitor, the intermediate progenitor (IP), located in the subventricular zone (SVZ). Here, the IP undergoes a few symmetric proliferative divisions, thus amplifying the neuronal fate acquired at a particular developmental stage, before entering into a terminal symmetrical neurogenic division to produce two neurons.

The transcription factor (TF) Pax6 is an intrinsic factor of RGPs that regulates multiple functions, e.g. cell morphology, cell cycle length, spindle orientation during mitosis, interkinetic nuclear migration and centrosome localisation. During the last few years some of the mechanistic backgrounds of defects in these processes in *Pax6*-deficiency could be discovered. However, how TF Pax6 controls a proper interkinetic nuclear migration during cell division that is most likely related to centrosome structure / function remains still unclear.

Here, I show results that revealed a novel molecular mechanism, involved in *Pax6*-dependent control of centrosome structure and function. The observed findings could be summarized in the following:

1. Results from the electron microscopy analysis revealed a specific defect of the mother centrioles that were missing subdistal appendages in RGPs located at the cortical apical VZ in the mouse *Pax6/Small eye* mutant. Consequently, the RGPs showed a massive loss of primary cilia at the ventricular surface. Furthermore, analysis of the localisation of mother and daughter centrosomes *in vivo* revealed defect of centriole maturation in the *Pax6*-deficient cortex, evident by a dramatic loss of mother centrioles at VZ surface and a premature exit of RGPs from mitotic cycle.

2. Mechanistically, the presented findings revealed that Pax6 transcriptionally regulates the expression of the appendage specific protein Odf2, thus controlling the maturation of the mother centriole (i.e. the assembly of the subdistal/distal appendages) in RGPs, more strongly during late neurogenesis. This process is of crucial importance for proper centrosome function that includes a correct assembly of primary cilia and the microtubules aster, which is most likely involved in correct interkinetic nuclear migration functioning.

3. In addition, results from *Odf2* knock down assays *in vivo* indicated that a lack of Odf2, RGPs prematurely exit from mitotic cycle, suggesting an intrinsic relevance of *Odf2* expression and centriole maturation for the RGP proliferative capacity and maintenance of cortical progenitor pool for late neurogenesis

To sum up, the shown here direct dependence of appendage protein Odf2 expression by TF Pax6 represents a part of a complex molecular mechanism underlying the correct centrosome maturation and functioning during late cortical neurogenesis.

I. INTRODUCTION

The mammalian brain is a highly complex organ, responsible for cognitive functions like learning and memory. During evolution mammals developed a highly organized forebrain (telencephalon), which is able to fulfil such complex functions. The neocortex (NCX) develops in the dorsolateral part of the telencephalon as a thin sheet of billions of neuronal and glial cells organized radially in six different layers, each built up by neurons with specific morphology, connectivity and function. Tangentially, neurons are organized in numerous distinct areas that are involved in integration and analysis of information brought from the periphery, as well as in performance of distinct functions such as motor, visual, somatosensory or auditory. The proper development of NCX is crucial for the correct function of the brain.

I.1. Brain Development

I.1.1. Neural induction

Generation of the central (CNS) and peripheral (PNS) nervous system starts shortly before the beginning of gastrulation with a process named neural induction. A specific mesodermal structure called Spemann organizer in amphibians (or Node in mice) invaginates inside the gastrulating blastocyst and forms the mesodermal layer below the dorsal ectoderm of the embryo. In amphibians, the earliest involuting part of the organizer induces generation of neuronal fate with anterior (forebrain) characteristic in the overlaying ectoderm. This process is critically dependent on secretion from the organizer/node of Chordin, Noggin and Follistatin, three powerful inhibitors of BMP (bone morphogenic protein)-dependent signalling that is normally existing between the ectodermal cells ('default model of neural induction') (Fietz & Huttner 2011, Meinhardt 2001, Weinstein & Hemmati-Brivanlou 1999). Actually, even shortly before the beginning of neural induction, the anterior endoderm secretes FGF signalling factors that act as inducers of neural fate, which together with the BMP antagonists (secreted from the organizer) ensures the progression of neural

induction. The early involuting mesoderm (the pre-chordal mesendoderm) secretes Wnt blockers and contributes to building up of the head/forebrain, while the latest involuting mesoderm forms subsequently the notochord that induces neuronal fate along the entire AP anlage of CNS / PNS. Initially, the neural plate has molecular characteristic of anterior brain (forebrain). At latest developmental stages however, graded expression of Wnt, FGF and Retinoic acid (RA) secreted from the posterior mesoderm causes region specific transformation of the anterior into caudal neural fate, thus forming the caudal part (spinal cord) of CNS. Wnt inhibitory factors from the anterior visceral endoderm protect the anterior neuronal tissue from posteriolizing activities of these factors (Wilson & Rubenstein 2000). The generated neural plate folds, and after closure forms the neural tube. During this process, the morphogen sonic hedgehog (SHH) secreted from the notochord (Ruiz i Altaba et al 1995) and BMP factors secreted from the dorsal ectoderm defines the dorso-ventral (DV) axis of the neural tube (Gunhaga et al 2003) in which distinct neuronal types are located at distinct positions.

The early brain forms in the most anterior part of the neural tube and is subdivided into three primary brain vesicles: Forebrain (prosencephalon), midbrain (mesencephalon) and hindbrain (rhombencephalon). The forebrain is later subdivided into the diencephalon, which subdivides into epithalamus, thalamus, hypothalamus and telencephalon in which dorsal part develop the two cortical hemispheres (Puelles 2001).

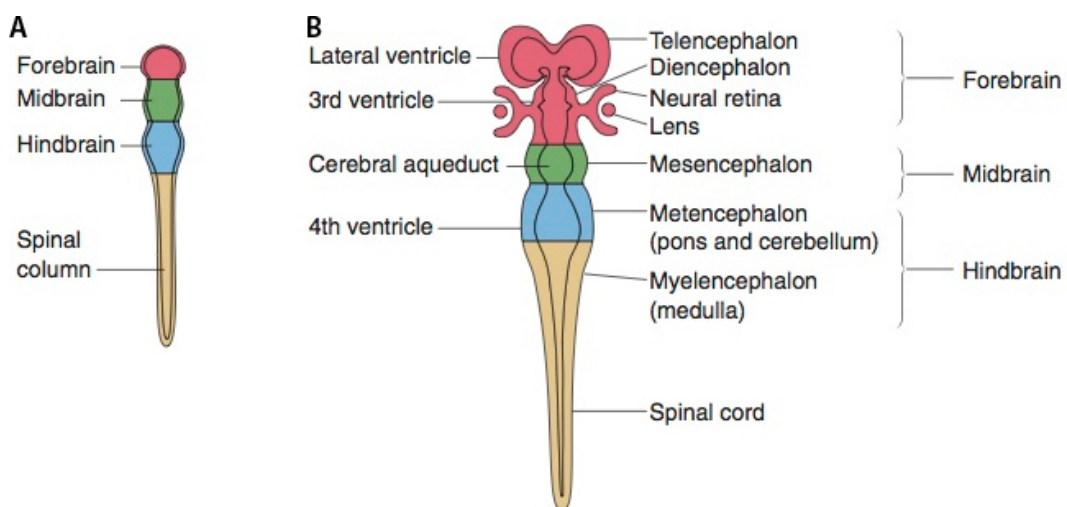


Fig. I.1. Schema showing the primary brain vesicles of forebrain (prosencephalon), midbrain (mesencephalon) and hindbrain (rhombencephalon)(A). The primary vesicles get further subdivided in later stages of development, as indicated in (B) (Sanes et al 2006)

I.2. Development of Telencephalon

I.2.1. Molecular patterning of Telencephalon

During formation of neural plate and tube, anterior-posterior (AP) patterning from the involuting mesoderm generates transverse domains with different competence to a single signalling molecule. Thus, the powerful morphogen SHH, secreted from the notochord / floor plate and the prechordal mesendoderm is able to induce different fates along AP axis, generating thereby Isl⁺ interneurons (INs) in basal forebrain, dopaminergic neurons in tegmentum of midbrain, serotonergic neurons in hindbrain, and motor neurons in ventral spinal cord.

In the forebrain, four inductive centres exist: (a) anterior neural ridge (ANR), formed in the most anterior part of the telencephalon; (b) the roof plate (RP) formed in the most dorsal part of the vesicle, that later invaginates inside the medial wall of the telencephalon, giving rise to (c) the hem; and finally, (d) antihem, formed at the border between the most lateral part of dorsal telencephalon (pallium) with the ventral telencephalon (subpallium). The complex interplay between AP, DV patterning and patterning from these four signalling centres controls the graded expression of transcription factors (TFs) and regulatory molecules in proliferative germinative zone of the pallium generating a grid like map that presages molecular properties of the functional areas (Borello & Pierani 2010, Rakic 1988).

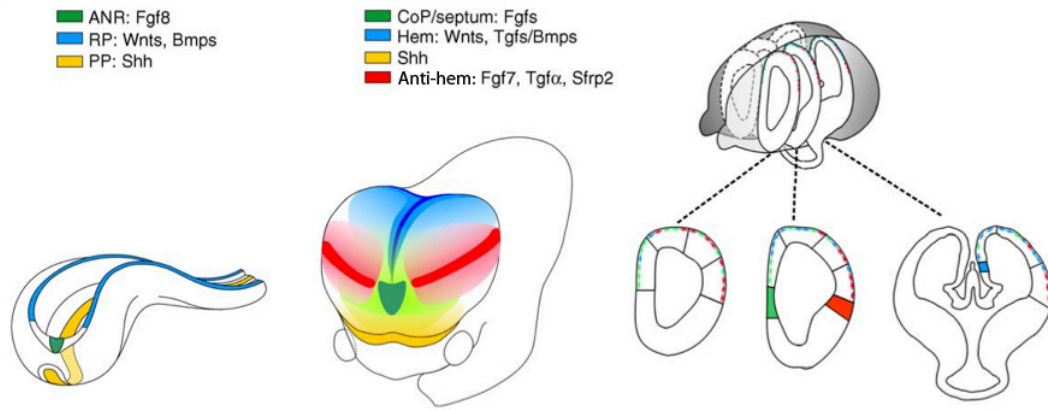


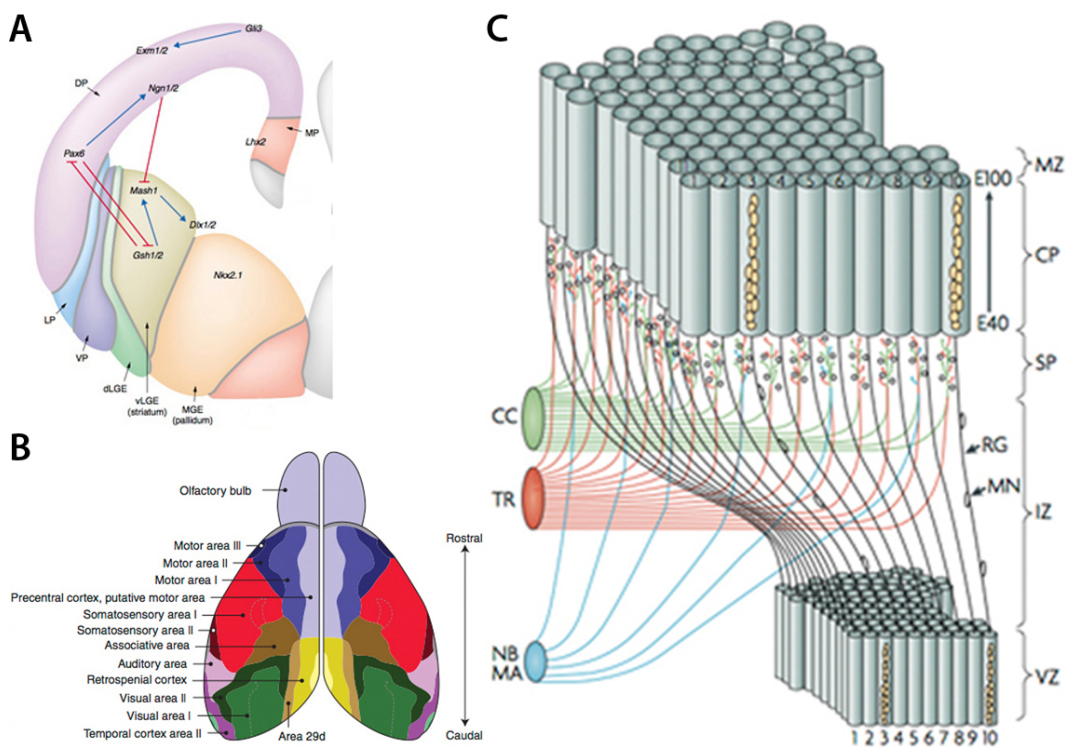
Fig. I.2. Schema showing the different signalling centres and migrating signalling molecules in developing forebrain: FGF8 secreted by the anterior neural ridge (ANR), sonic hedgehog (Shh) by prechordal plate and Wnts and BMPs by the roof plate (RP). After expansion of the telencephalic vesicles Fgfs are expressed anteriorly at the commissural plate (CoP) and septum. The roof plate and the cortical hem secrete morphogenetic factors from Wnts, Tgfs and BMPs families, while the ventral mesendoderm secretes Shh. The anti-hem secretes Fgf7, Tgfa and Sfrp2 (Borello & Pierani 2010)

I.2.2. Arealisation of cerebral cortex

The generation of neocortical progenitor cells depends on two important processes. The first one is DV patterning of telencephalon during which initially the expression of three transcription factors (TFs) defines molecularly different progenitor domains. As early as embryonic (E) stage E9.0, the expression of TF Pax6 is restricted to progenitors of dorsal telencephalon, outlining the anlage of cerebral cortex (pallium). In ventral telencephalon (subpallium) the restricted expression of TFs Gsh2 and Nkx2.1 delineates the regions of the lateral (LGE) and medial ganglion eminences (MGE), respectively (Rallu et al 2002). As a result of cross-repressive interactions between these TFs, a sharp border between pallial and subpallial domains is formed (the pallial-subpallial border, PSB). Similar cross-repressive interactions are established between TF Ngn2 (expressed in pallium) and TFs Mash1 and Dlx1/2- in subpallium. Since *Ngn2* is a direct downstream target of Pax6, the evolutionary conserved and powerful developmental regulator Pax6 exerts a pivotal role for the early patterning of developing forebrain and cortical development (Fode et al 2000, Schuurmans & Guillemot 2002, Stoykova et al 1996, Walther & Gruss 1991) (Fig. I.3.). At early stages of cortical neurogenesis, differential expression of molecular determinants in germinative epithelium subdivides the pallial VZ into different regions

encompassing: dorsal pallium (DP), anlage of the 6-layered neocortex (NCX); medial pallium (MP), anlage of the archipallium (hippocampus); lateral pallium (LP), anlage of paleocortex (pyriform cortex)(Fig I.3A)

Two models were proposed to explain possible mechanisms of cortical arealisation. According to the “protocortex model” neuronal identity of distinct areas is established by signalling brought by thalamo-cortical axons (TCA) coming from distinct sensory nuclei of thalamus (O’Leary 1989). In contrast, the “protomap” hypothesis suggests that the correct molecular identity of neurons of different areas is already encoded in the progenitors in germinative zone (Rakic 1988). The current view assumes that a complex interplay between already existing information in the progenitors and information from outside including the TCA establishes and maintains the neuronal fate in the different areas of the developing cortex (Mallamaci & Stoykova 2006, O’Leary et al 2007, Rakic 1988, Sansom & Livesey 2009).

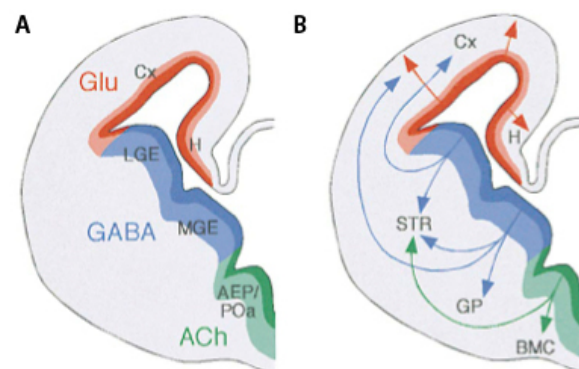


↑Fig. I.3. Patterning of cerebral cortex. **(A)** Based on specific expression of regulatory molecules, the embryonic cortex is subdivided into dorsal (DP), lateral (LP), ventral (VP) and medial (MP) pallium. A complex interplay between TFs Pax6 and Gsh1/2 as well as Ngn1/2 and Mash/Dlx1/2 establishes a sharp boundary between pallium and subpallium (specifically, with the ventral lateral ganglion eminences (vLGE) (Schuurmans & Guillemot 2002). **(B)** Schema of the different functional areas of the mouse telencephalon (Sansom & Livesey 2009). **(C)** Schema of the current view of cortical arealisation. The correct molecular identity is already encoded in radial units in the germinative zone and maintained by information from outside. VZ: ventricular zone; IZ: intermediate zone; SP: subplate; CP: cortical plate; MZ: marginal zone; MN: migrating neuron; RG: radial glia cell; NB: nucleus basalis; MA: monoamine subcortical centres; TR: thalamic radiation; CC: cortico-cortical connections. The timing of neurogenesis (E40-E100) refers to the embryonic age in macaque monkey (Rakic 2009).

I.2.3. Origin of cell diversity in neocortex

Most of the neuronal and glial cells in NCX arise from progenitors (mostly radial glia cells, RGCs, named also progenitors, RGP) in the two germinative zones of dorsal telencephalon. The first one, the VZ, is located directly at the ventricular surface of both hemispheres, while the second one, named subventricular zone (SVZ), is located at some distance of VZ. The neurons in NCX are organized in six layers each containing neurons with distinct shape, molecular properties, used transmitters, connectivity and functions. The majority of neocortical neurons originate from VZ and SVZ. They are excitatory glutamatergic projection neurons, which extend their axons to distant intracortical, subcortical and subcerebral regions (Molyneaux et al 2007). These neurons migrate relatively short distances radially along the basal processes of the RGCs. In addition, the NCX contains GABAergic (γ -aminobutyric acid) interneurons (INs) building up local inhibitory connections. These INs migrate long distances tangentially from their origin, the subpallial progenitors of MGE and LGE to their final locations within distinct cortical layers (Gotz & Sommer 2005, Marin & Rubenstein 2003, Wilson & Rubenstein 2000) (Fig. I.4.)

Fig. I.4. Schema of birthplaces of different neuronal subtypes. GABAergic interneurons are born in the VZ of the lateral and medial ganglion eminences (LGE/MGE) while glutamatergic projection neurons are born in the VZ of the neocortex **(A)** Glutamatergic neurons migrate relatively short distances within the cortex while GABAergic interneurons migrate long distances from LGE and MGE into the cortex **(B)** (Wilson & Rubenstein 2000).



I.2.4. Neurogenesis and layer formation of neocortex

I.2.4.1. Radial glia progenitor cells

I.2.4.1.1. Symmetric proliferative divisions of neuroepithelial cells and transformation into radial glia progenitor cells

Before neurogenesis starts, neuroepithelial cells (NE) in the germinative VZ divide in a symmetric proliferating manner to build up an adequate pool of stem cells (Caviness & Takahashi 1995). At the onset of NCX neurogenesis (around embryonic day (E) 11.5 in mice) the NE cells transform into radial glia progenitor cells (RGCs / RGPs). This change goes along with morphological changes like radial expansion of process and loss of tight junction complexes, but not adherence junctions, together with changes in the expression pattern of specific molecular determinants (Gotz & Barde 2005). The RGPs show a glia like cell shape therefrom they exhibit basal and apical processes, which span the whole wall of the developing NCX (Fietz & Huttner 2011, Heins et al 2002, Rakic 2009). Their cell body including the nucleus is located at the apical surface in VZ. RGPs are the progenitors for all glutamatergic projection neurons of the NCX. After accomplishment of neurogenesis around E18.5 in mouse) and postnatally, the RGPs transform into astrocytes (Campbell & Gotz 2002, Gotz et al 2002, Gotz & Huttner 2005, Malatesta et al 2000, Miyata et al 2010, Noctor et al 2001).

I.2.4.1.2. Asymmetric neurogenic divisions of RGPs and neuronal layer formation

The cortical layers are formed in an “inside first, outside last” manner by asymmetric RGP divisions. At the onset of neurogenesis at E11.5, RGPs start to divide in an asymmetric self-renewing manner. The two generated daughter cells show different cell fates: while one of the daughters becomes a RGP, stays in the VZ and is used for a renewal of the progenitor pool, the second cell adopts neuronal fate and migrates radially along the basal process of the RGP to the cortical plate (CP). During this early neurogenesis (E11.5-E13.5), RGPs participate through such asymmetric divisions (*via* the mode of a “direct neurogenesis”) to the generation of neurons of the lower cortical layers, layer VI

then layer V. From E13.5 the direct neurogenic divisions decline. Instead, after division the RGP produces a RGP (for a renewal) and another type of progenitor, an intermediate progenitor (IP) (named also basal progenitor, BP). This IP migrates to the SVZ where it undergoes a few (2-3) symmetric proliferative divisions before they terminally divide in a symmetric differentiative manner (Fietz & Huttner 2011). In this “indirect mode” of cortical neurogenesis, RGPs predominately produce neurons, firstly of layer IV and then neurons of layer III and layer II (Campbell 2005, Farkas & Huttner 2008, Nieto et al 2004, Tarabykin et al 2001). While each division of a RGP in direct neurogenic mode produces only one neuron, each division of a RGP in the indirect neurogenic mode produces at least 2 neurons. The number of daughter cells increases when the IP does several rounds of proliferating divisions (Haubensak et al 2004). In such a way, the generated neuronal fate through the asymmetric division of RGPs at a particular developmental stage is amplified.

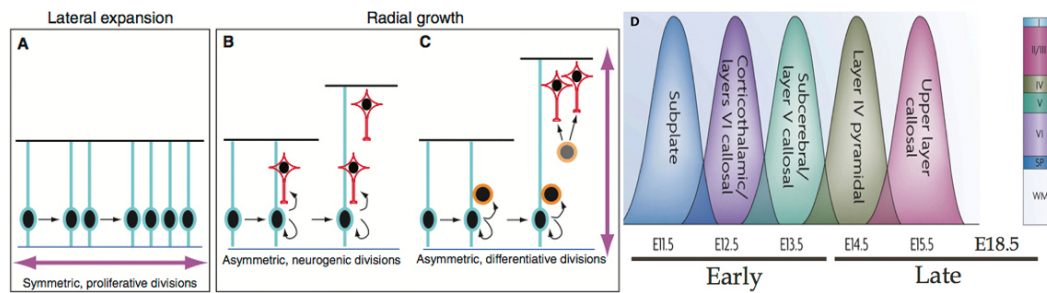


Fig. 1.5. Schema of the different cell division modes of RGPs: **(A)** Symmetric proliferative divisions to expand the progenitor pool, leading thereby to lateral expansion of the cortex; **(B)** asymmetric neurogenic divisions produce RGPs and neurons during early neurogenesis *via* a direct mode of neurogenesis; **(C)** asymmetric differentiative divisions during mid- and late neurogenesis to produce a RGPs and an IPs, the last of which move into SVZ and after limited amplifications, symmetrically divides to generate neurons *via* indirect mode of neurogenesis (Fish et al 2008). **(D)** The time scale shows when the neurons of the different layers are produced. Lower layers (VI, V) are produced first, followed by a subsequent generation of upper layers (IV-II) according to an “inside first outside last” intrinsic program (Molyneaux et al 2007).

Recently published data showed that at least some RGPs are fate restricted neural progenitors. Interestingly, *Cux2*, a marker for upper cortical layers II to IV, is also expressed in a set of RGPs that proliferate during early neurogenesis. However, while *Cux2* negative cells predominantly produce lower layer neurons during early neurogenesis, the *Cux2*⁺ RGPs starts their neurogenic divisions during late neurogenesis, predominantly producing neurons for the upper cortical layers IV to II (Franco et al 2012).

Recently, a new class of progenitor cells located in the outer subventricular zone progenitors (OSVZP) of developing neocortex of mammals has been described (Wang et al 2011). Although they miss the apical process to the ventricular surface they show the same characteristics like RGPs including a basal process and the expression of the RGP marker Pax6. Being relatively rare in mice, these progenitors appear in an increasing number in higher mammals, like monkeys and humans, and seem to be responsible for the higher number of upper layer neurons in those mammals (Fish et al 2008, LaMonica et al 2012, Lui et al 2011, Wang et al 2011).

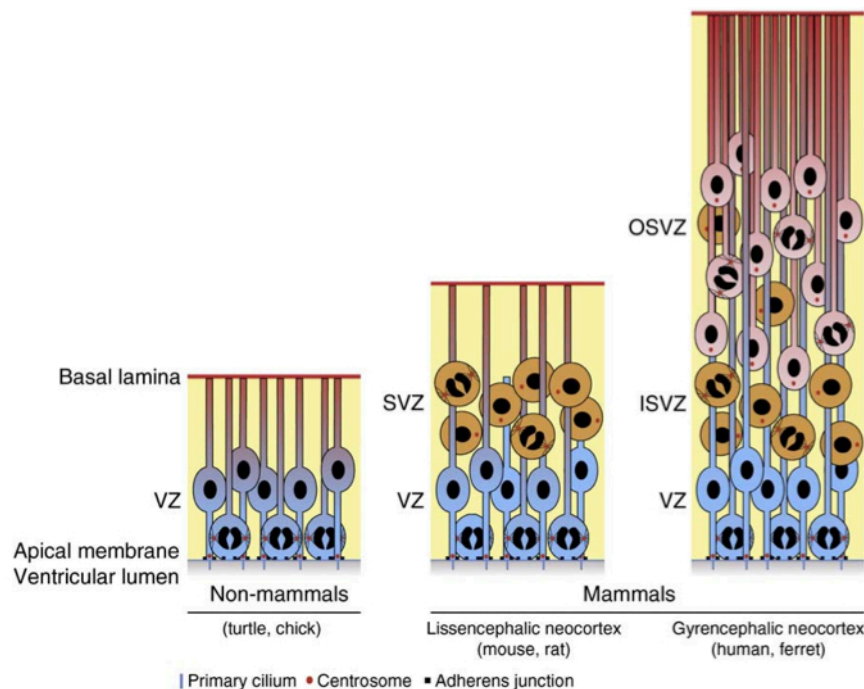


Fig. I.6. Schema showing the different progenitor cell types in vertebrates. During evolution additional germinative layers with additional progenitor subtypes developed to fulfil the higher requirements of a mammalian neocortex (Fietz & Huttner 2011).

I.2.4.1.3. Interkinetic nuclear migration of RGP nuclei

The nuclei of RGPs are located only within the VZ although the cells processes span the whole depth of the embryonic pallium. The distribution of the nuclei within the VZ is not random but strongly connected to the cell cycle. After mitosis of the RGP at the ventricular apical surface, the new-formed nucleus shows an apical to basal movement during G1-phase. The nucleus reaches the most basal part of the VZ shortly before the cell enters the S-phase. After S-phase is completed, the nucleus undergoes a basal to apical transition followed by the M-phase directly at the ventricular surface. This nuclear movement is called interkinetic nuclear migration (INM) (Fujita 1962, Reiner et al 2012, Sauer 1935, Spear & Erickson 2012, Taverna & Huttner 2010).

RGPs have a bipolar cell polarity, showing at the ventricular surface presence of several cell compartments like Par-complex and the centrosome, which are essential for a correct cell division (Bultje et al 2009, Chenn et al 1998, Costa et al 2008). Due to the fact that this mechanism is strongly connected to the cell cycle, the cell actively accomplishes this movement. Therefore, the cell uses the microtubules depending motor protein system to transport the nucleus. During G1-phase, Kif1a, a member of the Kinesin-3-family, which moves along microtubules from the minus to the plus end, performs the apical to basal nuclear migration. For basal to apical transition the Dynein motor protein is used, moving the nucleus along the microtubules from microtubules plus end to microtubules minus end (Tsai et al 2010).

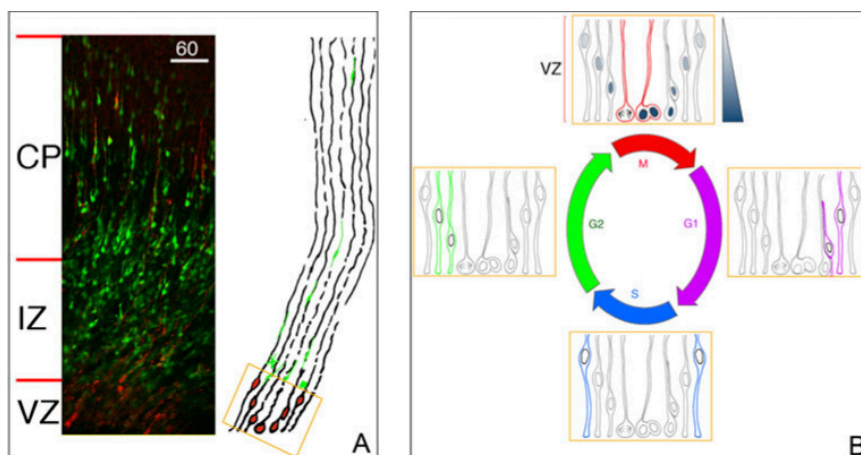


Fig. I.7. Although RGPs span through the whole thickness of the neocortex, the cell bodies including the nucleus are exclusively located in VZ (A). The interkinetic nuclear migration guarantees mitosis at the ventricular surface therefore it is strongly connected to the cell cycle (B) (Reiner et al 2012)

I.2.4.2. TF Pax6 and interkinetic nuclear migration

The TF Pax6 belongs to the evolutionary conserved family of paired-domain developmental regulators of the eye, pancreas and brain (Ashery-Padan et al 2000, Chalepakis et al 1993, Chalepakis et al 1992, Collombat et al 2003, Collombat et al 2009, Georgala et al 2011a, Simpson & Price 2002, St-Onge et al 1997). Expressed specifically in the pallial RGP, Pax6 is an important intrinsic factor determining the correct morphology and cell cycle characteristics of RGP (Gotz et al 1998, Mi et al 2013). Pax6 deficient *Small eye* (*allele Sey/Sey*) mice show severe defects in early dorsoventral patterning of telencephalon (Muzio et al 2002, Stoykova et al 1996, Stoykova et al 2000, Toresson et al 2000). Loss of Pax6 in RGP results in accelerated generation of early-born neurons due to a shortened cell cycle of the RGP (Estivill-Torrus et al 2002, Mi et al 2013, Quinn et al 2007, Tuoc et al 2009). Consequently, RGP of *Sey/Sey* mice show a reduced neurogenic potential and the number of neurons in Pax6 deficient cortex is reduced by half (Heins et al 2002, Stoykova et al 1996). In Pax6 loss-of-function (LOF), the functional arealisation along AP axis of the cortex is affected, showing region specific disproportional size defects (Mi et al 2013, Pinon et al 2008).

The correct functioning of the Pax6 dependent transcriptional network is highly dosage dependent. Overexpression of Pax6 in RGP pushes the system toward neurogenesis, while down-regulation of Pax6 reduces RGP self-renewal and causes a premature cell cycle exit (Heins et al 2002, Sansom et al 2009). However, extreme elevation of the endogenous Pax6 level *in vivo* affects the RG proliferation and leads to progenitor apoptosis during early neurogenesis (Berger et al 2007). Applying a conditional ablation of Pax6 function in developing cortex, recent work confirmed an almost complete loss of upper layer neurons of the layers IV to II due to a premature cell cycle exit of the RGP (Georgala et al 2011b, Tuoc et al 2009).

Interestingly, in Pax6 deficient rats, the loss of Pax6 leads to a disturbed INM: the basal to apical transition is slowed or incomplete, resulting in a slower cell cycle or mis-position of mitotic RGP (Tamai et al 2007). Furthermore, the position of the centrosome, a subcellular organelle involved in the microtubules network, shows a disturbed localisation. Normally, the centrosomes are located at the RGP-cell membrane, lining the ventricular surface of the RGP, while only few of them are localized more basally. Time lapse imaging of the centrosomes

during the cell cycle in the embryonic cortex of the rat *Small eye* mutant reveals a defective anchorage of centrosomes to the cell membrane at the ventricular surface indicated by an up and down movement of the centrosome as well as in apical to basal movement to the nucleus of the RGP (Tamai et al 2007).

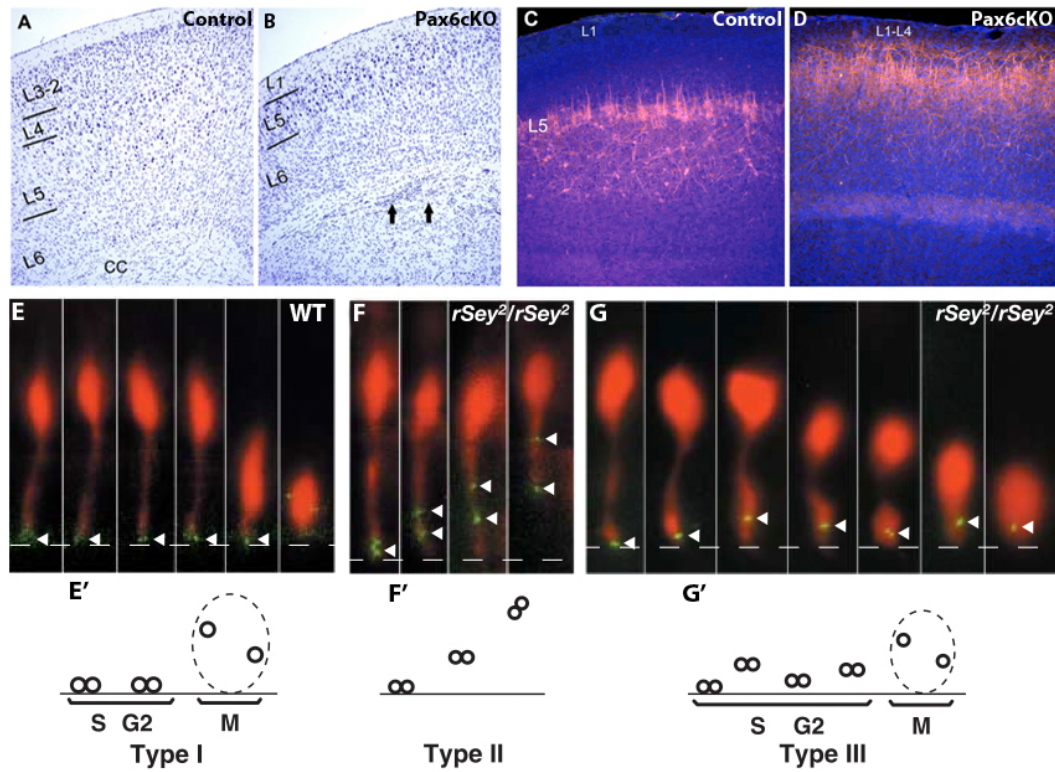
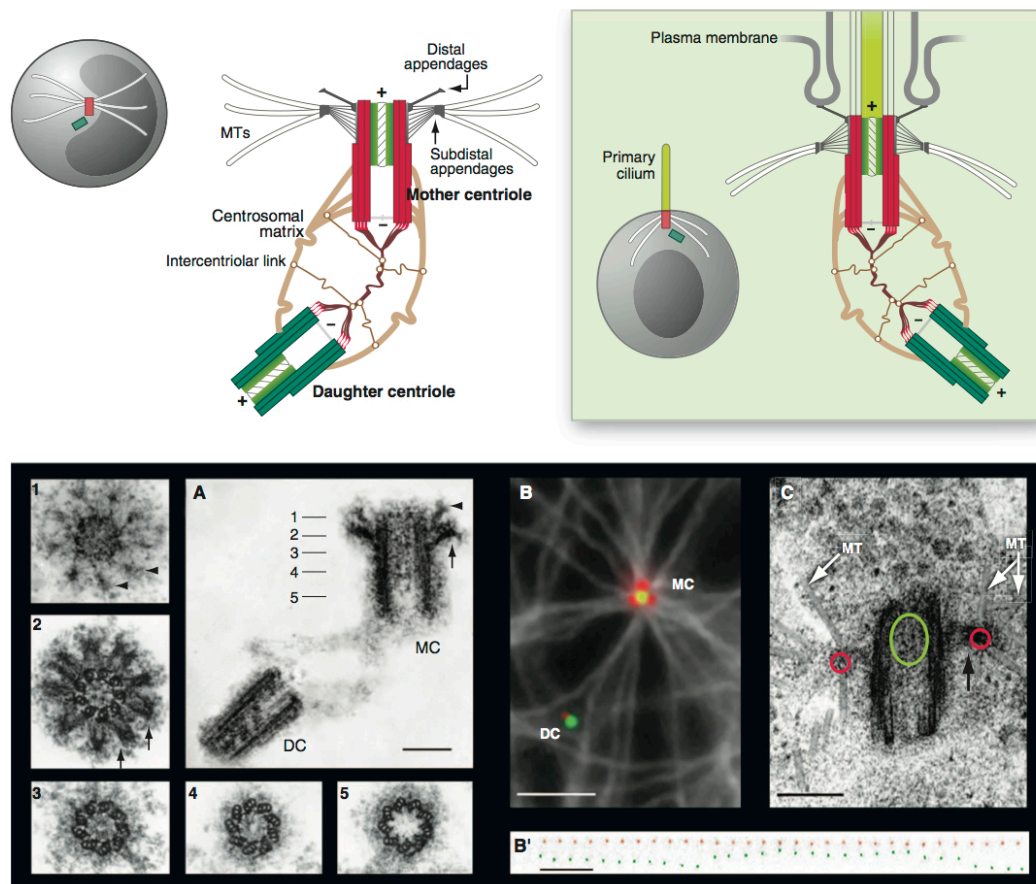


Fig. I.8. Pax6-deficient cortex shows almost a complete loss of neurons of layer 3-2 and 4 (**B and D**) compared to control (**A and C**) (Tuoc et al 2009). Interkinetic nuclear migration (INM) and centrosome localisation are disturbed in Pax6 loss-of-function. The nucleus migrates fast from the basal part of the VZ to the apical surface in WT animals. The centrosome (arrowhead) stays at the ventricular surface during nucleus migration (**E+E'**). In Pax6 LOF cortex, the nuclear migration is incomplete or absent; instead the centrosome (arrowhead) is moving towards the nucleus (**F and F'**) or nucleus migration is retarded and the centrosome (arrowhead) 'jumps' up and down (**G and G'**) (Tamai et al 2007).

I.3. The Centrosome

I.3.1. Structure of the Centrosome

The centrosome consists of two microtubule (MT)-based centrioles embedded in the pericentriolar material (PCM). Each centriole contains nine MT triplets arranged in a ring (around $0.5\mu\text{m}$ in length and $0.2\mu\text{m}$ in diameter). Centrioles are polarized along their proximal-distal axis. The two centrioles differ in shape and age. The older centriole or mature centriole, named also mother centriole (MC) at the earliest assembled two cell cycles ago, contains distal and subdistal appendages. The younger immature centriole, called daughter centriole (DC), assembled during the last cell cycle, misses these structures. The so-called “linker matrix” links both centrioles within the PCM (Azimzadeh & Bornens 2007, Bornens 2002).



↑Fig. I.9. Schematic illustration of the centrosome structure. The mother centriole (red) shows distal and subdistal appendages. At the subdistal appendages are microtubules of the microtubules aster anchored. The daughter centriole (green) misses these structures (A). The mother centriole in the function of basal body of the primary cilium binds to the membrane *via* its distal appendages (B). Electron microscopy pictures of the centrosome, showing the distal (1 and arrowhead) and subdistal (2 and arrow) appendages of the mother centriole (C). ICC of the centrosome as MTOC. Centrin (green) marking the centrioles, Ninein (red) marking the mother centriole, microtubules (white) staining shows that only the mother centriole functions as MTOC (D). Electron microscopy picture of the mother centriole shows that the microtubules are anchored at the subdistal appendages (E). Analysis of the centriole mobility shows that the mother centriole has a stable position due to its connection to the microtubules aster while the daughter centriole is able to move around (F) (Bornens 2012)

I.3.2. Centrosome function

The centrosome is the microtubules organizing centre (MTOC) of the cell, regulating microtubules nucleation and organization. γ -tubulin-ring-complexes (γ -TuRC) in the PCM are essential for MT assembly (Moritz & Agard 2001). The subdistal appendages of the mother centriole are able to bind microtubules minus ends and are therefore essential for the assembly of the microtubules aster (Bettencourt-Dias & Glover 2007, Bornens 2002). Cell components can move along these microtubules in a Kinesin / Dynein dependent manner (Tsai et al 2010). A second function of the centrosome is the formation of the spindle-pole-bodies and assembly of the spindle. Therefore, the centrosome plays an important role in cell division, cell migration and cell polarization. During interphase of the cell, the mother centriole is able to anchor to the cell membrane *via* its distal appendages where it serves as the basal body of the primary cilium (Azimzadeh & Bornens 2007). Each centriole is able to recruit PCM, which is essential for their function as MT nucleation centre. The daughter centriole is able to nucleate microtubules but neither able to dock microtubules minus ends nor able to anchor to the cell membrane (Bettencourt-Dias & Glover 2007).

The centrosome asymmetry after cell division plays an important role during asymmetric cell divisions. *Drosophila* male germ line stem cells (GSCs) divide asymmetrically under influence of signalling from hub cells. The centrosome containing the mother centriole, therefore called mother centrosome, is always inherited by the stem cell while the centrosome containing the daughter centriole (daughter centrosome) enters the differentiating cell (Yamashita 2009). After RGP division in the developing NCX, the cell containing the mother

centrosome re-enters the cell cycle and becomes a new RGP, while the cell containing the daughter centrosome exit the cell cycle, migrates out of the VZ and becomes an IP or a neuron (Wang et al 2009). Interestingly, a knock down of the appendage-specific protein Ninein in RGP causes an exit of mitotic cycle of the RGP, indicating that the maturation of the mother centriole is an intrinsic factor for RGP maintenance (Wang et al 2009). The reasons for this mechanism are still not completely known. Most probably, the strong connection of the mother centriole to the microtubules system is an intrinsic factor for stem cell inheritance.

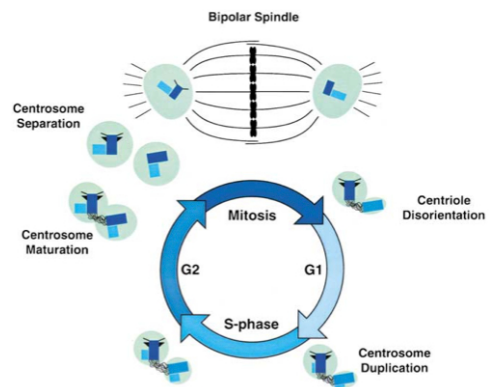
As recently shown, in *Drosophila* the neuroblast cells (the stem cells that generate neuronal cell lines) inherit the daughter centrosome upon division (Januschke et al 2011). This controversial fact becomes clear, having in mind that microtubules anchorage to centrioles in *Drosophila* is independent of subdistal appendages because *Drosophila* mother centrioles miss these structures. Interestingly, the daughter centrosome exhibits the MTOC activity due to an appendage independent mechanism for microtubules anchorage (Januschke et al 2013). This indicates that the MTOC activity of the mother centrosome is indeed the essential factor for stem cell maintenance.

1.3.2.1. Centrosome duplication, segregation and maturation

The strict control of centrosome duplication and segregation is crucial for correct chromosome segregation during mitosis. Each centrosome comprises two centrioles and these have to be duplicated exactly once in each cell cycle. Therefore, the centrosome duplicates in a semi-conservative manner and the duplication is regulated by cyclin-dependent kinase 2 (CDK2), and therefore strongly connected to the cell cycle (Hinchcliffe & Sluder 2001). With the start point of S-phase, each centriole starts to assemble a new centriole at its proximal end. As a result of this duplication mode, each centrosome contains an old or mature centriole and a new assembled one (Azimzadeh & Bornens 2007). Before the cell enters the M-phase centrosome separation starts. Each centrosome recruits PCM as an intrinsic factor for mitotic spindle assembly. At the same time, the immature parental centriole acquires maturation markers like Ninein and Odf2/Cenexin. After mitosis centrosome disorientation starts meaning the new

assembled daughter centriole releases from the mother centriole (Meraldi & Nigg 2002).

Fig. I.10. Schematic illustration of the centrosome cycle. After mitosis centriole disorientation occurs, meaning the new-formed daughter centriole is detached from the mother centriole. At G1 S-phase transition centrosome duplication starts which is accomplished at the end of the S-phase. During G2 phase, the new centrosome matures - that means it recruits PCM. Before the cell enters mitosis, centrosome separation starts to build up the spindle pole bodies during cell division (Meraldi & Nigg 2002)



I.3.3. Important centrosome proteins

I.3.3.1. Common centrosome markers

γ -Tubulin is the most common centrosome/centriole marker, although only 10 % to 20 % of the entire protein amount is located at the centrosome while 80 % to 90 % of the protein is evenly distributed in the cytoplasm. In the centrosome, it accumulates at the outside of the centriole cylinders and is part of the γ -Tubulin-ring-complex. The γ -Tubulin-ring-complex is involved in microtubules assembly and anchorage (Mogensen et al 2000). Centrin is the second important centriole marker and has almost the same distribution then γ -Tubulin. Only a relatively small amount of the protein is located in the centrosome but it accumulates in the inner part of the centriole cylinder and serves a good marker for the Centrosome/Centrioles. Percentrin is a third important marker for the centrosome. This protein is almost exclusively located in the centrosome. It accumulates at the outside of the centriole cylinders but is also present in the PCM. Therefore this protein works more as a centrosome marker and less as a centriole marker (Bornens 2002).

I.3.3.2. The appendage protein Ninein

Ninein is a protein concentrating at the subdistal appendages of the mother centriole but it is also located at the proximal ends of both centrioles. It was shown that Ninein plays an important role in capping the microtubules minus ends and in the positioning and anchorage of microtubules minus ends (Mogensen et al 2000). Therefore, it plays a crucial role for the function of a microtubules organizing centre and for the formation of the microtubules aster (Ou et al 2002). It was shown that microtubules nucleation by microtubules minus end capping and microtubules anchorage at the mother centriole are two independent processes (Delgehyr et al 2005). This indicates that Ninein plays an important role in microtubules stabilisation not only at the centrosome but also in the cytoplasm (Moss et al 2007). Interestingly, Ninein plays an important role of re-entering the cell cycle after RGP division in the developing neocortex. Down regulation of Ninein causes the RGP to exit the mitotic cycle after division (Wang et al 2009).

I.3.3.3. The outer dense fibre 2 (Odf2) protein

Odf2, also named Cenexin, was first found as a stabilizing protein in the sperm tail. Here it is localized in the outer dense fibres, which are associated with the axon. The nine outer dense fibres are characteristic cytoskeleton structures surrounding the axon from the neck along the middle piece until the principal piece of the sperm tail. In the middle piece are the outer dense fibres surrounded by the mitochondrial sheath. Two of the nine outer dense fibres entre the fibrous sheath in the principal piece (Fawcett 1975). The outer dense fibres play an important role for the proper function of the sperm tail because they support the beating of the tail and they protect the tail against shear forces during ejaculation (Baltz et al 1990, Burfeind & Hoyer-Fender 1991).

The outer dense fibres consist of many different protein most of them are not characterized yet (Oko & Clermont 1988, Olson & Sammons 1980, Vera et al 1984). One of the main polypeptides is an 84 kDa Protein named Odf2. It contains two Leucine-zippers, which are important for the interaction with a second outer dense fibre protein named Odf1 (Burfeind & Hoyer-Fender 1991, Shao et al 1998).

Odf2 is a coiled coil protein and able to interact with other Odf2 proteins and it is associated with microtubules (Donkor et al 2004).

The *Odf2* mRNA is been spliced alternatively and the different splice variants differ in at the N as well as at the C-terminal end (Hoyer-Fender et al 2003, Hoyer-Fender et al 1998, Huber et al 2008, Huber & Hoyer-Fender 2007, Rivkin et al 2008, Soung et al 2006).

In 2001 it was found that *Odf2* is expressed at the centrosome of chick liver cells. Further investigations showed that Odf2 is localized at the appendages of the mother centriole (Nakagawa et al 2001). This applies to mammal cells too. It was shown that Odf2 builds up a structure that is associated with microtubules. An interaction of Odf2 and microtubules could not be shown (Hoyer-Fender et al 2003).

The appendage protein Odf2 is mandatory for the development. A gene trap knock out results in pre-implantation lethality (Salmon et al 2006). To investigate the function of *Odf2*, Odf2 deficient cells (*Odf2*^{-/-}) were produced. These cells showed a loss of the appendages of the mother centriole. As a consequence of that Ninein was not detectable at the subdistal appendages (Ishikawa et al 2005).

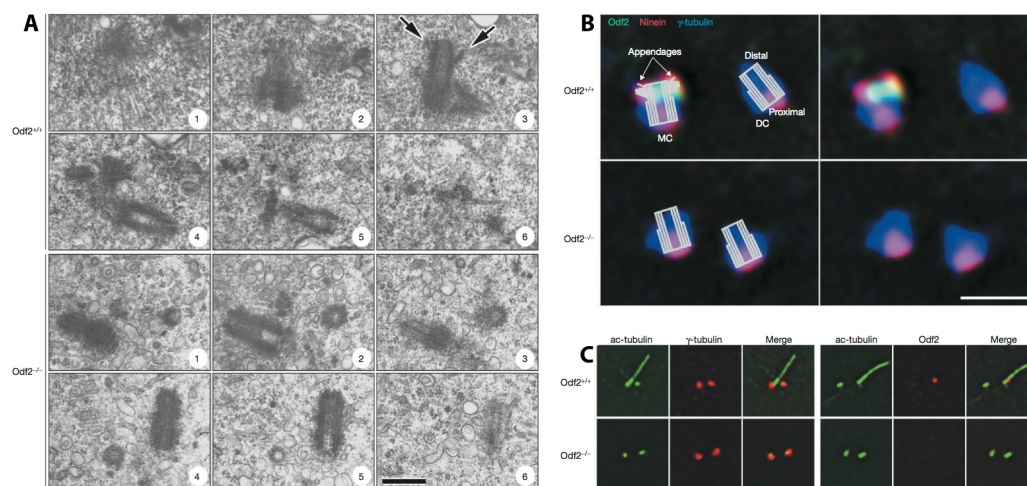


Fig. I.11. Odf2 deficient cells miss the characteristic appendages at the mother centriole (arrows) (A). As a consequence of that *Odf2* knock out cells show a loss of Ninein at the subdistal appendages (B). A second important defect in *Odf2*^{-/-} cells is the loss of primary cilia (C) (Ishikawa et al 2005).

Further investigations showed that Odf2 is necessary for the recruitment of Trichoplein a protein that binds Ninein to the subdistal appendages of the mother centriole (Ibi et al 2011). As a second consequence of *Odf2* loss of function, *Odf2*^{-/-} cells were not able to assemble primary cilia (Ishikawa et al 2005). Recent investigation showed that *Odf2* plays an important role in polarization of cilia in

multi-ciliated trachea cells. Here, the basal body does not form up to nine subdistal appendages, instead there is only one structure called basal foot. By binding to the microtubules system the basal foot defines the orientation of the basal body and therefore also for the motile cilium. Defective *Odf2* leads to an uncoordinated and undirected beating of cilia in the trachea and therefore to a disturbed transport of mucus (Kunimoto et al 2012).

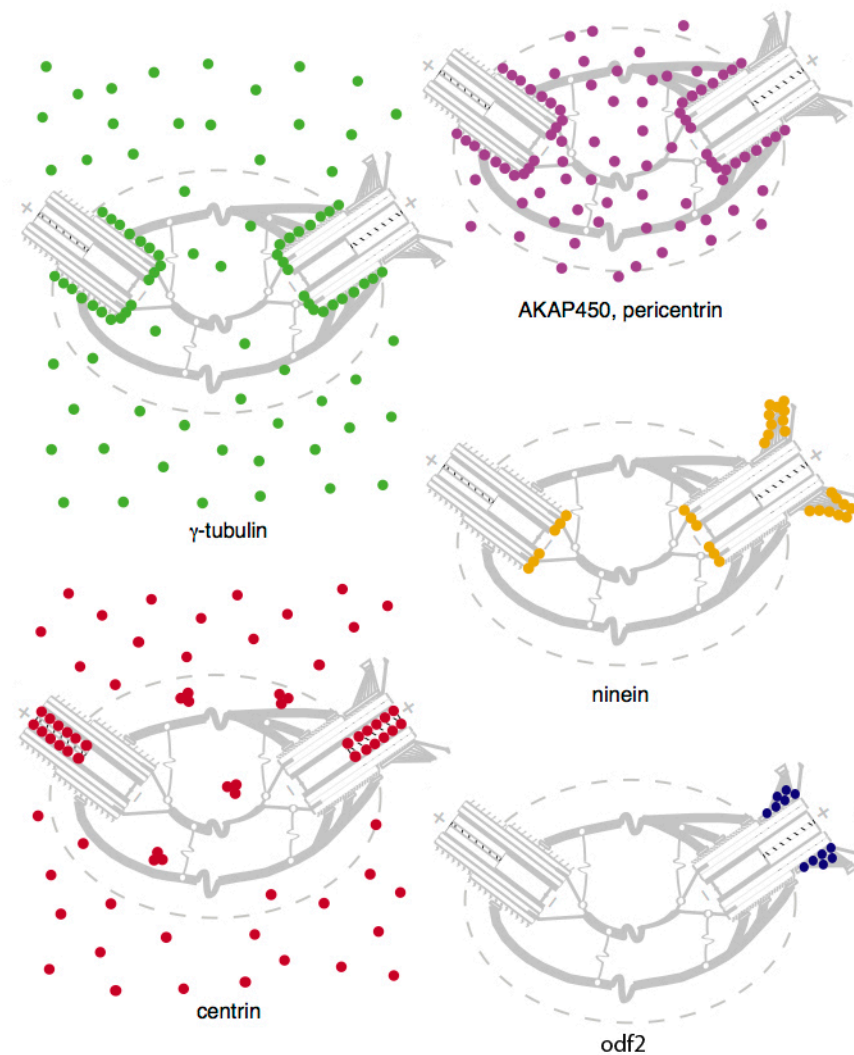


Fig. I.12. Countless proteins accumulate in the centrosome, and especially in the PCM. Here are shown some of the most important proteins like γ -Tubulin and Centrin, which localize outside respectively inside of the centrioles and are the most common marker protein for the centrioles. Pericentrin localized predominantly around the centrioles and in the PCM is a marker for the whole centrosome. Ninein is predominantly localized at the subdistal appendages although it is also expressed at the proximal ends of the centrioles adopted from Bornens, 2002 (Bornens 2002).

I.4. The primary cilium

Cilia are microtubules based structures at the cell surface. It is distinguished two types of cilia motile and immotile. In general, motile cilia have a 9+2 axonem, meaning two centrally located microtubules surrounded by 9 microtubules duplets. Immotile cilia have a 9+0 axonem meaning they miss the two centrally located microtubules. The immotile 9+0 cilia are called primary cilia. The central two microtubules of the axonem are necessary for the movement of the cilia. Exceptions are the cilia of the embryonic node. Although they miss the central microtubules pair they are motile. They exhibit a Dynein-based machinery and are essential for the correct left-right determination (Nonaka et al 2002, Supp et al 1997).

The structural base of the primary cilium is the basal body, which is the mother centriole of the centrosome. The basal body attaches to the cell membrane by the distal appendages (Hoyer-Fender 2010, Kobayashi & Dynlacht 2011). The axonem of the primary cilium grows out of the distal end of the basal body and forms the backbone of the cilium. Important for the primary cilia assembly is the intraflagellar transport (IFT). The IFT is a microtubules motor-based transport machinery transporting cilia components to the tip (anterograde transport) or towards the basal body (retrograde transport) (Rosenbaum & Witman 2002). A defect of cilia function is often caused by a defect of the IFT (Pazour et al 2000). For correct function of the sonic hedgehog the IFT is mandatory (May et al 2005).

Primary cilia are single cilia at the cell surface and located at almost all mammalian cell types like fibroblasts, kidney cells and neurons (Barnes 1961, Sorokin 1962). Primary cilia are the mechanic and chemosensory antenna of the cell. They are able to detect changes like fluid flow of extracellular liquids in the environment of the cell and are able to transfer the signal into the cell. Also chemical and molecular changes in the environment can be detected. Therefore the cilia membrane is the location for several receptors of signalling pathways. The most common signalling pathway, which is associated with the primary cilium, is the hedgehog pathway. The receptor patched is only localized within the membrane of the cilia (Rohatgi et al 2007). Also the receptor-tyrosin kinase PDGFR α is associated with the primary cilium (Schneider et al 2005). Additionally several other signalling pathways are associated with the primary

cilium or the basal body like the wnt pathway (Eggenchwiler & Anderson 2007, Gerdes et al 2007, Ross et al 2005, Simons et al 2005, Watanabe et al 2003).

A multitude of diseases are caused by non-functional primary cilia like polycystic kidney disease, diseases of pancreas and liver, *situs inversus*, Bardet-Biedl-syndrome and cancer. A defect of primary cilia can also effect the development of the brain and can cause hydrocephalus, microcephalus and mental retardation (Badano et al 2006, Murcia et al 2000, Nigg & Raff 2009).

I.5. Scope of the thesis

Although multiple functions of TF Pax6 have been so far reported, the molecular mechanisms involved are only partially elucidated. The recently discovered abnormalities of interkinetic nuclear migration and centrosome localization in absence of Pax6 in developing rat cortex (Tamai et al 2007) and the importance of the mother centriole maturation for RGP re-entering in mitotic cycle (Wang et al 2009) suggest a novel aspect in RGP function controlled by Pax6.

The main goal of this study was to investigate the relationship between the TF Pax6 and the centrosome of RGPs during cortical neurogenesis on structural and functional level. Consequently, the aims of this work were:

1. To analyse the structure of centrosomes in RGPs during cortical neurogenesis in Pax6-deficient *Small eye* mouse mutant.
2. Identification and analysis of Pax6-dependent molecular mechanism involved in centrosome structural malformation in Pax6 loss-of-function and its significance for centrosome function.

II. RESULTS

II.1. TF Pax6 influences the centrosome structure and localisation in cortical RGPs

II.1.1. Interkinetic nuclear migration is disturbed during late neurogenesis in the mouse *Pax6/small eye* mutant

As reported by Tamai et al., (2007), centrosomes show an incorrect movement during interphase of RGPs in Pax6-deficient rats (*rSey²/rSey²*). To investigate whether the interkinetic nuclear migration (INM) is disturbed also in *Pax6/Small eye* mutant mice (allele *Sey/Sey*), immunohistochemistry (IHC) was performed using antibody for the mitotic marker phosphorylated Histone H3 (pH3). To study whether the probable defect of INM is dependent on different types of RGP divisions during corticogenesis, the IHC was done on sections from mutant (*Sey/Sey*) and control (wild type WT) brains and stages E13.5 (early neurogenesis) and E15.5 (late neurogenesis). In WT cortex, the dividing RGPs at both stages were predominantly located at the surface of VZ (Fig. II.1 A, B arrowheads), while much less cells were located at some distance from VZ surface, outlining the position of the second germinative zone, the SVZ (arrows in Fig. II.1 A, B). In between those two positions for cell divisions, there were almost no dividing cells. In contrast, in *Sey/Sey* mutant cortex at E13.5 and even much more dramatically at E15.5, less dividing RGPs were detected at the ventricular apical surface, that seems to be displaced and chaotically distributed within the germinative VZ and SVZ, without delineating a real SVZ at some distance from the apical surface. These results suggest a defect of INM in the mouse *Sey/Sey* mutant cortex, especially during late corticogenesis when are generated predominantly neurons with a fate of upper layer neurons.

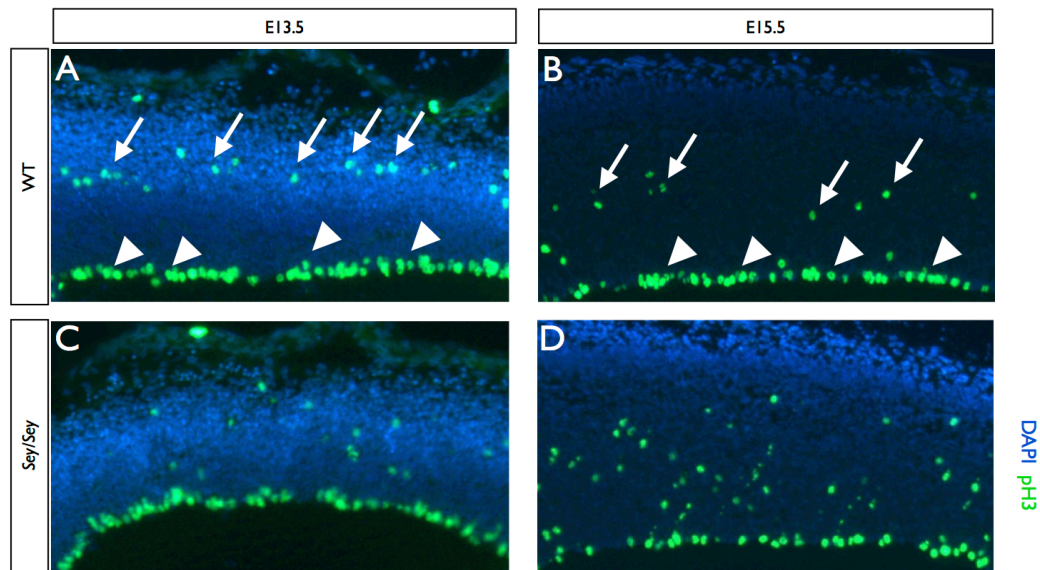


Fig. II.1. IHC with phosphorylated histone H3 (pH3) antibody on brain sections from E13.5 and E15.5 *Sey/Sey* and wild type embryos as indicated. **(A and B)** In WT animals note that two germinative zones (VZ, arrowheads; SVZ arrows) are visible. RGP's divide directly at ventricular surface while IP's divide mostly in SVZ located basally from VZ surface. **(C and D)** In *Sey/Sey* animals less cells divide at the ventricular surface. Instead cells divide in the basal part of the VZ indicating a defect of INM. At E15.5 this phenotype is more drastic than at E13.5.

II.1.2. Centrosome localisation is disturbed in RGP's of

Pax6-deficient cortex

To analyse whether the centrosome localisation is disturbed in *Pax6^{LOF}* mouse cortex, IHC with an antibody for γ -Tubulin was performed. In WT embryo brain, the centrosomes were located directly at the ventricular surface anchored at the cell membrane at the apical process of the RGP's and the centrosomes were stringed like a pearl necklace at the ventricular surface. Only very few centrosomes were visible more basally to build up the spindle pole bodies during mitosis. In *Sey/Sey* mice the centrosomes were neither located directly at the ventricular surface, nor strictly ordered; instead they were displaced chaotically above VZ.

Together, these data indicate that in *Pax6^{LOF}* both centrosomes and dividing RGP's are mis-located in germinative zones of developing cortex, suggesting that Pax6 could control the centrosome structure and/or function.

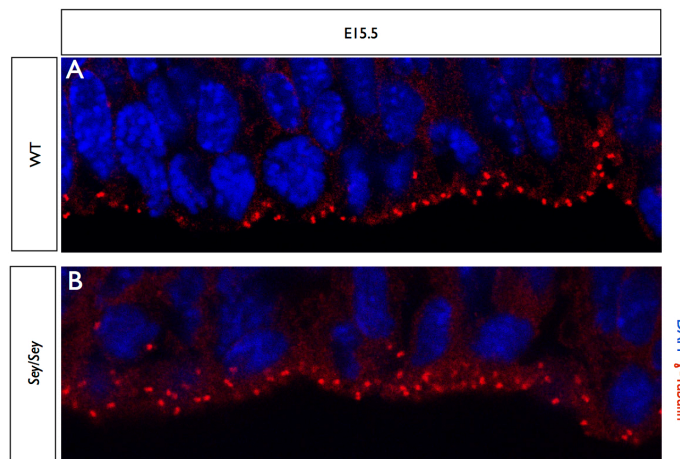


Fig. II.2. IHC for γ -Tubulin shows a disturbed localisation of centrosomes in *Pax6*^{LOF} cortex. **(A)** In WT, centrosomes form a line at the ventricular surface. **(B)** In *Sey/Sey* cortex centrosomes are scattered in the basal part of RGPs

II.1.3. Structural defect of appendages of the mother

centriole in RGPs in *Pax6/Small eye* mice

Due to the fact that the centrosomes were not anymore located at the ventricular surface of the developing *Sey/Sey* cortex, a question arose whether a structural defect at the appendages of the mother centriole causes this effect. The appendages are necessary to anchor the mother centriole of the centrosome to the cell membrane, and this way to become the basal body of the primary cilium. A structural defect of the appendages of the mother centriole would explain the miss-localisation of the centrosome due to an incomplete anchorage at the cell membrane. A defect especially at the subdistal appendages would also influence the composition of the microtubules aster.

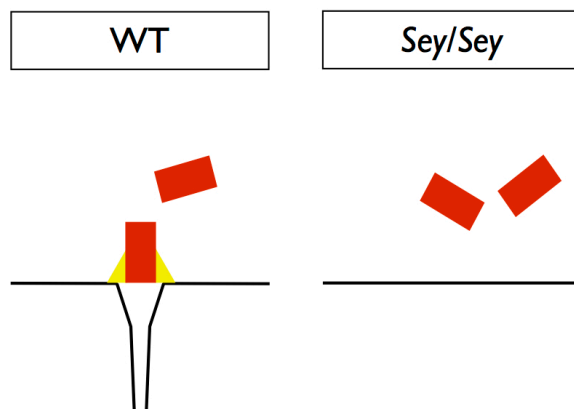


Fig. II.3. Schematic overview of the hypothesized effect of Pax6 loss of function on centrosome structure and behaviour. A loss of distal/subdistal appendages due to a lack of Pax6 would explain miss-orientation and ectopic position of the centrosome due to a missing anchorage to the cell membrane. As a consequence assembly of the primary cilium at the ventricular surface would be disturbed.

II.1.3.1. Analysis of centriole structure by STED microscopy

Because normal confocal microscopy has no adequate resolution allowing to study the centrosome structure, we turned to the STED microscopy. The stimulated emission depletion (STED) microscopy is a relatively new approach and an enhancement of classical confocal microscopy. Due to a second laser, which selectively deactivates fluorophores to enhance the imaging in the area, a super resolution of up to 2.4 nm instead of 200 nm with a confocal microscope is possible (Wildanger et al 2012). Unfortunately, STED microscopy turned out not to be helpful in visualizing the structure of the mother centrioles appendages. Therefore, electron microscopy (EM) was chosen as an alternative method.

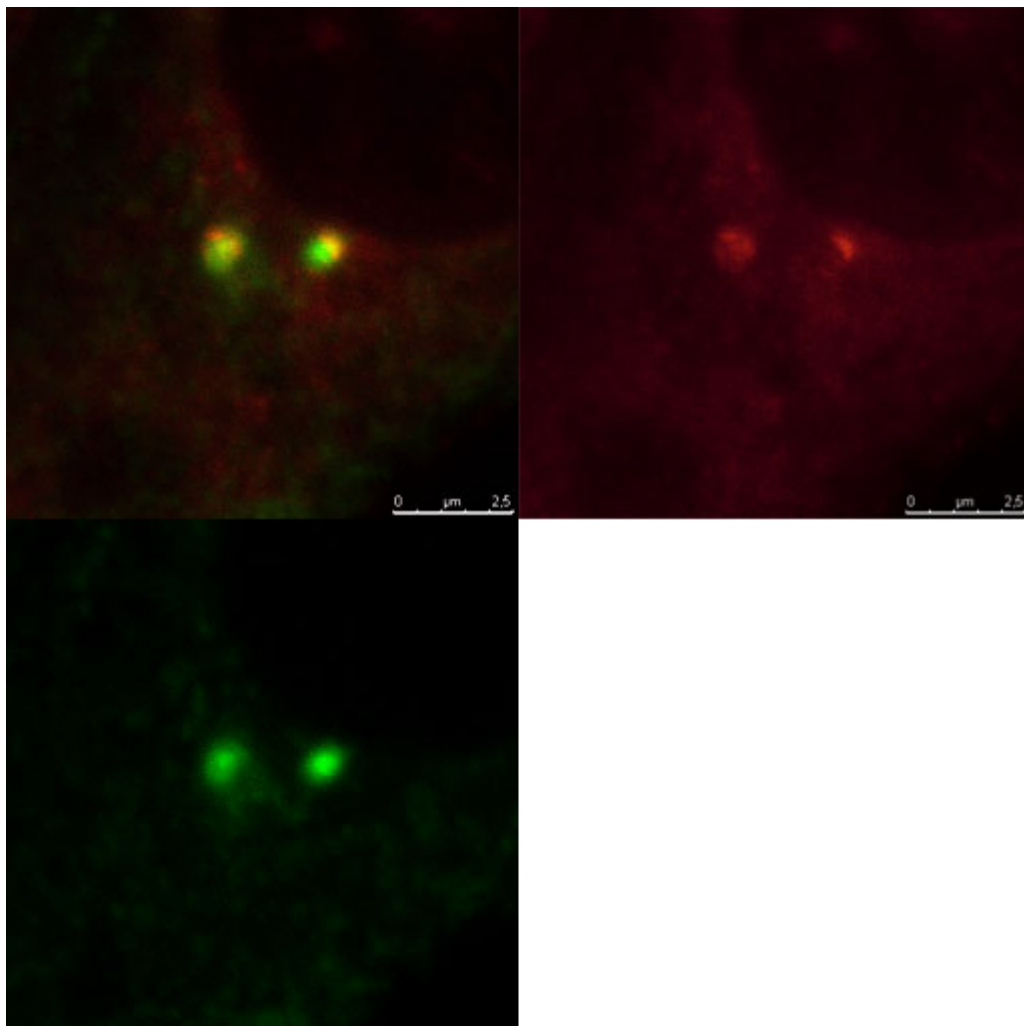


Fig. II.4. STED microscopy picture of Ninein (red) at the centrosome of a NIH3T3 cell combined with a confocal picture of γ -Tubulin (green). Although the resolution of STED microscopy is much higher than confocal microscopy, STED microscopy is not able to visualize details of the appendages at the centrioles.

II.1.3.2. Analysis of centriole structure by electron microscopy

The mother centriole structure in VZ of the neocortex of three E15.5 embryo couples (*Sey/Sey* vs. WT) was investigated. The identified centrioles were counted and analysed whether they show subdistal appendages or not. All together 276 centrioles from 3 WT and 3 *Sey/Sey* animals were analysed.

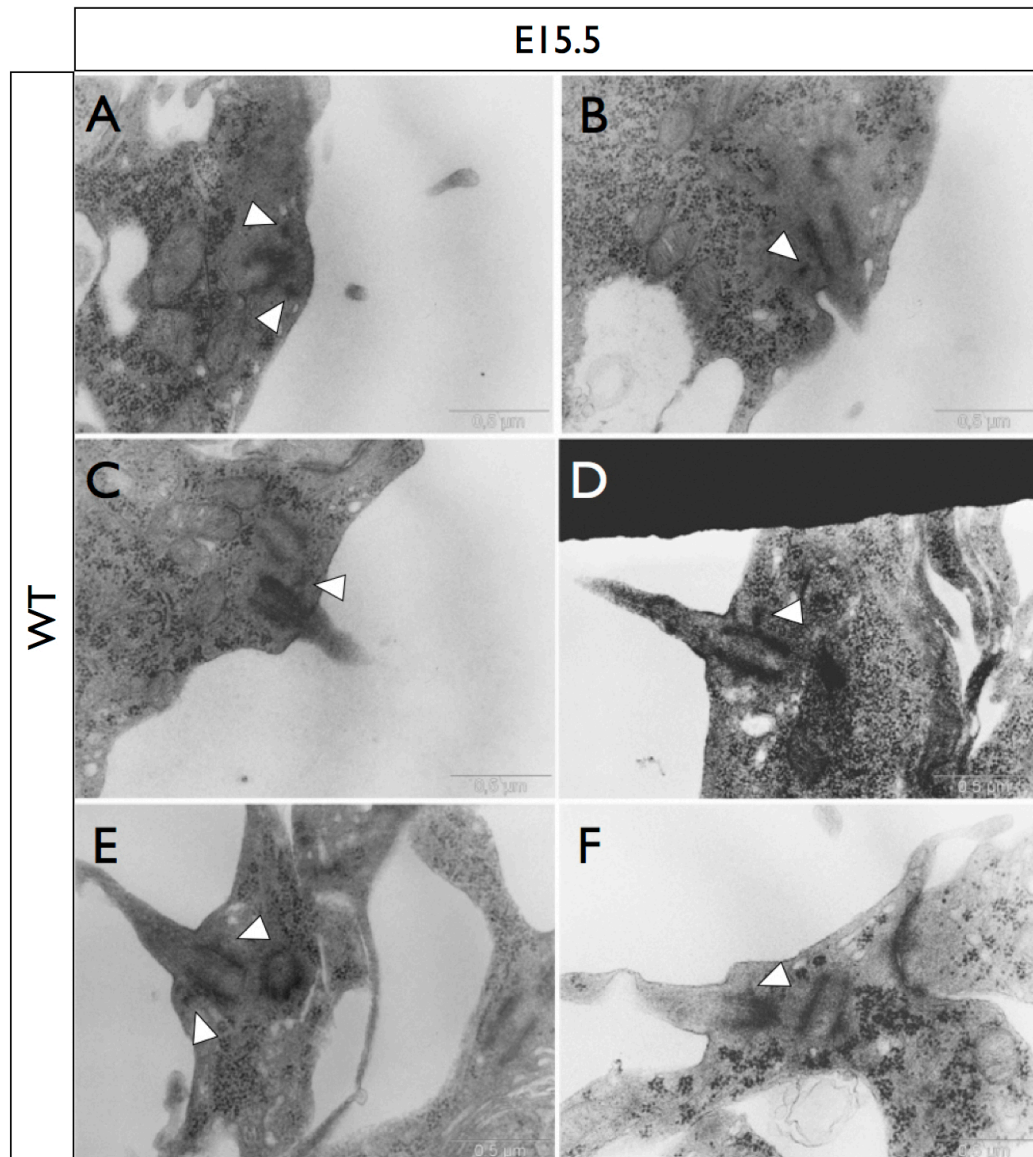


Fig. II.5. Electron microscopy pictures of centrioles at the ventricular surface of WT E15.5 embryos. Counting reveals that 50 % of the centrioles possesses subdistal appendages (arrowheads). Most centrioles possessing subdistal appendages are the basal body of a primary cilium (B-F).

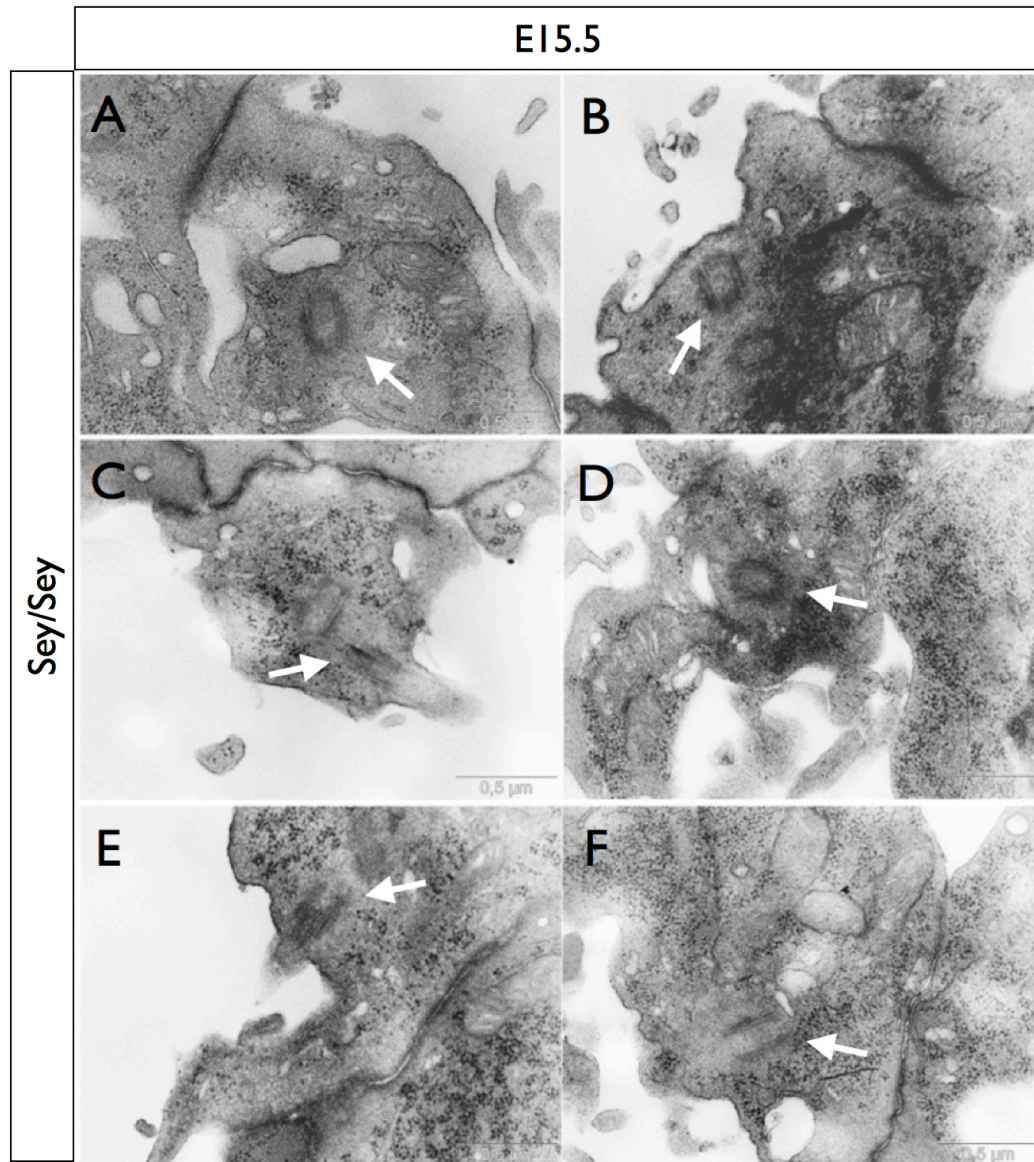


Fig. II.6. Electron microscopy pictures of centrioles at cortical ventricular surface of *Sey/Sey* E15.5 embryos. Around 78 % of the centrioles miss appendages (arrows) while only around 22 % of the centriole show subdistal appendages even when they are connected to a primary cilium (**C+E**). Most centrioles are not located directly at the ventricular surface even when they are mother centrioles identified by the vesicle at their distal end (**A+D**).

The quantitative analysis (with a student's T-test statistic relevance) indicated that 51.26 % (± 6.21) of the centrioles in WT embryos showed the characteristic for the mother appendages centriole, while 48.74 % (± 6.21) did not. In contrast only 21.8 % (± 7.13) of the centrioles in the *Sey/Sey* cortex showed the appendages, and 78.2 % (± 7.13) did not.

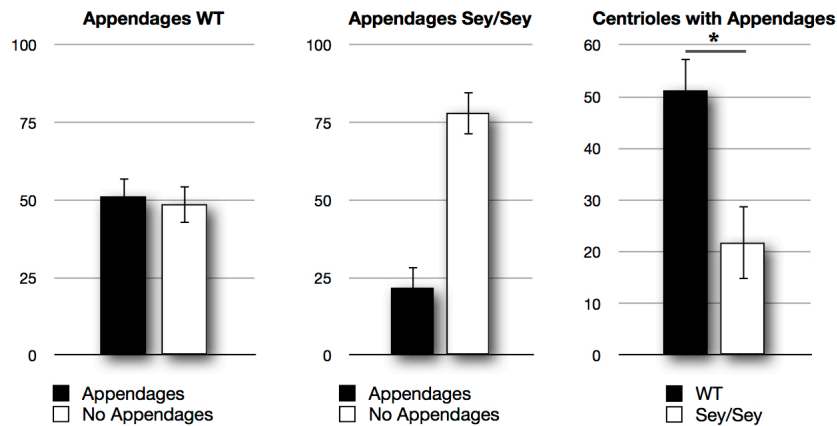


Fig. II.7. Statistic evaluation of EM analysis of centrosomes at the ventricular surface of WT and *Sey/Sey* E15.5 embryos. WT embryos show ~50 % centrioles with and without subdistal appendages. In *Sey/Sey* embryos only ~22 % of the centrioles contain subdistal appendages. Taken together the results indicate a reduction of more than 50 % of matured centrioles in *Sey/Sey* cortex. The student's T-test shows a statistical relevance (Appendages: $p=0.012$; no appendages: $p=0.01$)

Additionally, the number of appendages was counted. WT embryos showed an average number of $1.51 (\pm 0.08)$ appendages while *Sey/Sey* embryos showed an average number of $1.23 (\pm 0.16)$. Student's T-test reveals no statistical relevance ($p=0.114$).

Taken together these results indicate a defect of mother centriole maturation, especially affecting the subdistal appendages that are either not formed or at least incompletely formed.

A direct consequence of missing or reduced subdistal appendages is the loss of primary cilia (Ishikawa et al 2005) therefore it is mandatory to analyse whether primary cilia assembly is normal in *Sey/Sey* cortex.

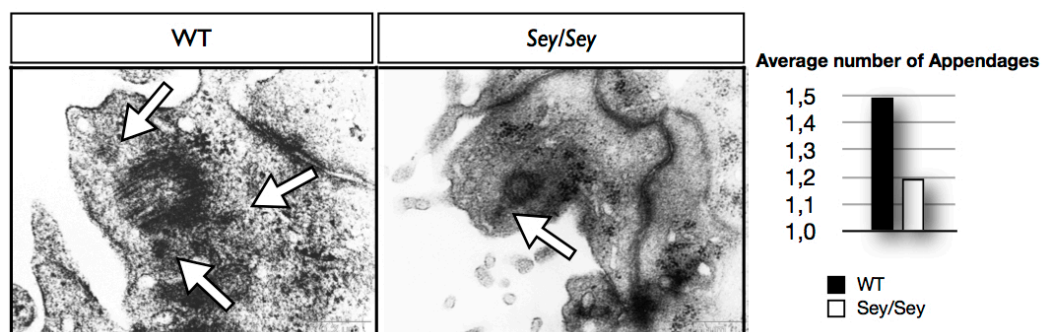


Fig. II.8. Analysis of the number of subdistal appendages (arrows) of each centriole in WT and *Sey/Sey* E15.5 embryos. The average number of appendages of WT centrioles are 1.5 but only 1.2 in *Sey/Sey* embryos indicating an incomplete maturation of the mother centriole. Student's T-test reveals no statistical relevance ($p=0.114$).

II.1.4 Diminished number of RGP's extending primary cilia at the ventricular surface of *Sey/Sey* cortex

Because the centrosomes in the *Pax6/Small* eye cortex loose the connection to the cell membrane, next the formation of cilia at the ventricular surface was examined. A double IHC was performed with an antibody against acetylated tubulin as a marker for primary cilia together with γ -tubulin antibody on brain sections from E13.5 wild type and *Sey/Sey* embryo brains. The results indicated a reduction by 43.53 % (± 10.2) of primary cilia number in the mutant, as compared to control brains (statistical relevance $p=0,015$) (Fig. II.9).

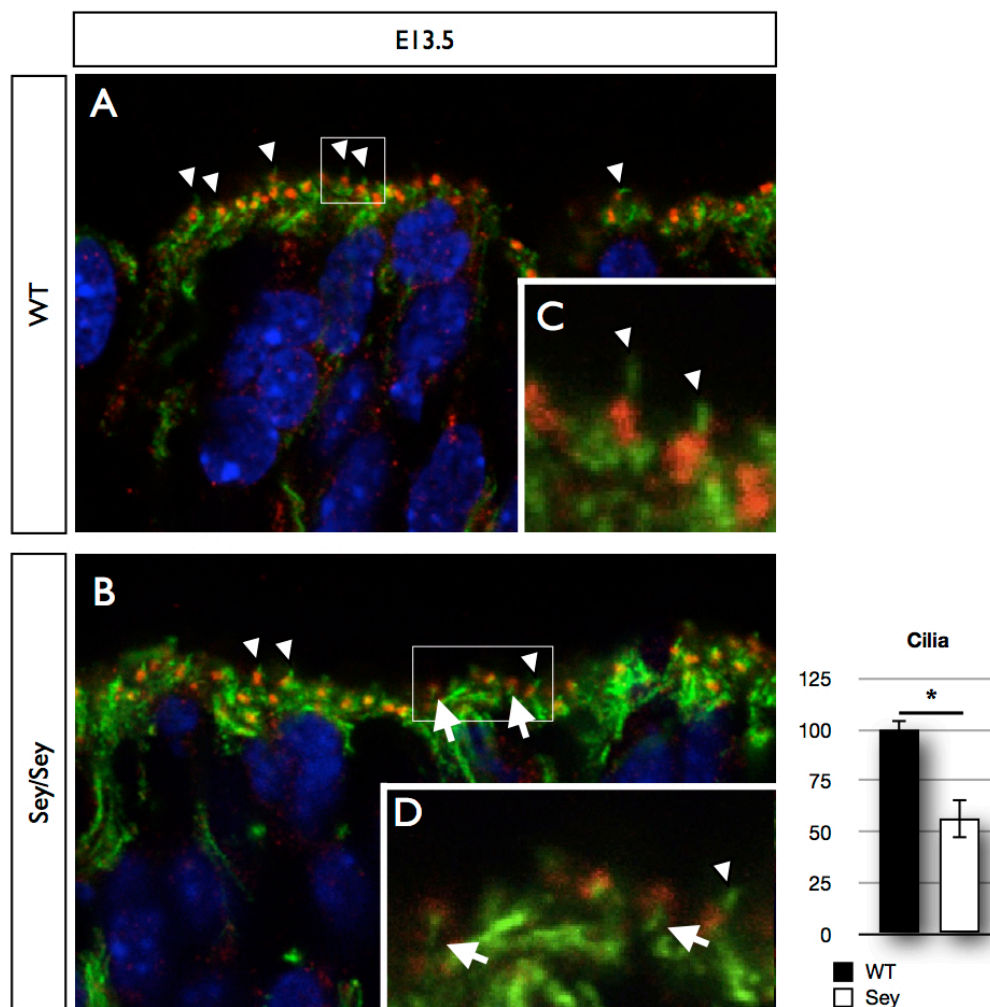


Fig. II.9. IHC for γ -Tubulin (red), acetylated Tubulin (green) and DAPI. On cross brain sections at E13.5, the *Sey/Sey* cortex shows reduced primary cilia (arrowheads) at the ventricular surface (A) as compared to WT (B). Higher magnification pictures ((in the frames) indicates a mis-orientation of some cilia (arrows) in *Sey/Sey* (D) but not in WT cortex (C). Statistical analysis reveals a reduction in primary cilia number in *Sey/Sey* cortex by more than 40 % (43.53 %; $\pm 10,02$; $p = 0,015$) compared to the WT.

The performed double IHC analysis on E15.5 embryos brains however failed due to the fact that the concentration of acetylated tubulin at the apical surface of the RGP is too high to allow identification of single / individual primary cilia.

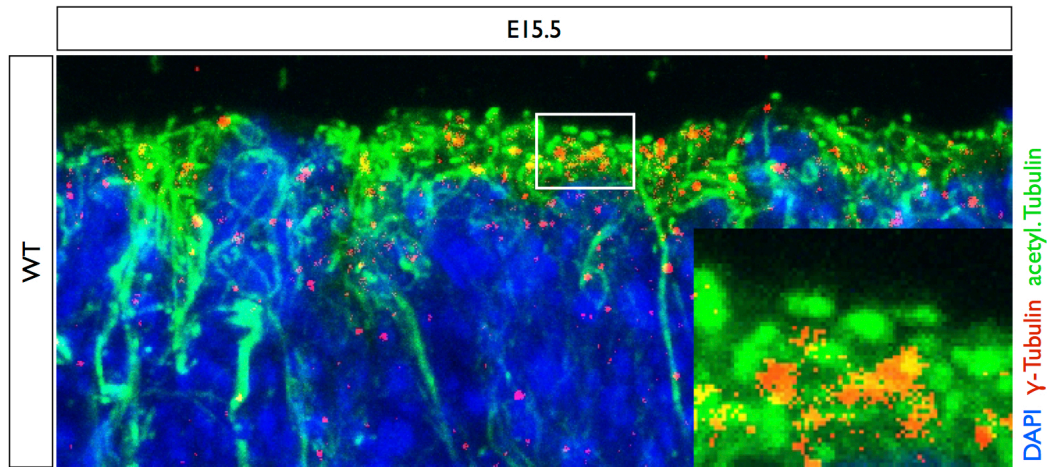


Fig. II.10. IHC for γ -Tubulin (red) and acetylated tubulin (green). Due to the strong expression of acetylated tubulin in the apical process of RGP an identification of primary cilia is not possible.

As an alternative approach to analyse the presence of primary cilia in RGP during late neurogenesis, electron microscopy was used. Electron micrographs of cortical ventricular zone on sections from E15.5 brains were made and the number of centrioles of RGP connected to primary cilia was counted in both WT and *Sey/Sey* embryos. Remarkably, strongly diminished number of RGP with cilia in *Sey/Sey* cortex was found, much more drastic at E15.5 than at E13.5. While in E15.5 WT cortex 34.89 % (± 9.24) of the centrioles were connected to primary cilia, only 6.01 % (± 4.42) of the centrioles in *Sey/Sey* embryos were with a cilium (Fig. II.10). The student's T-test reveals a statistical relevance ($p=0.031$).

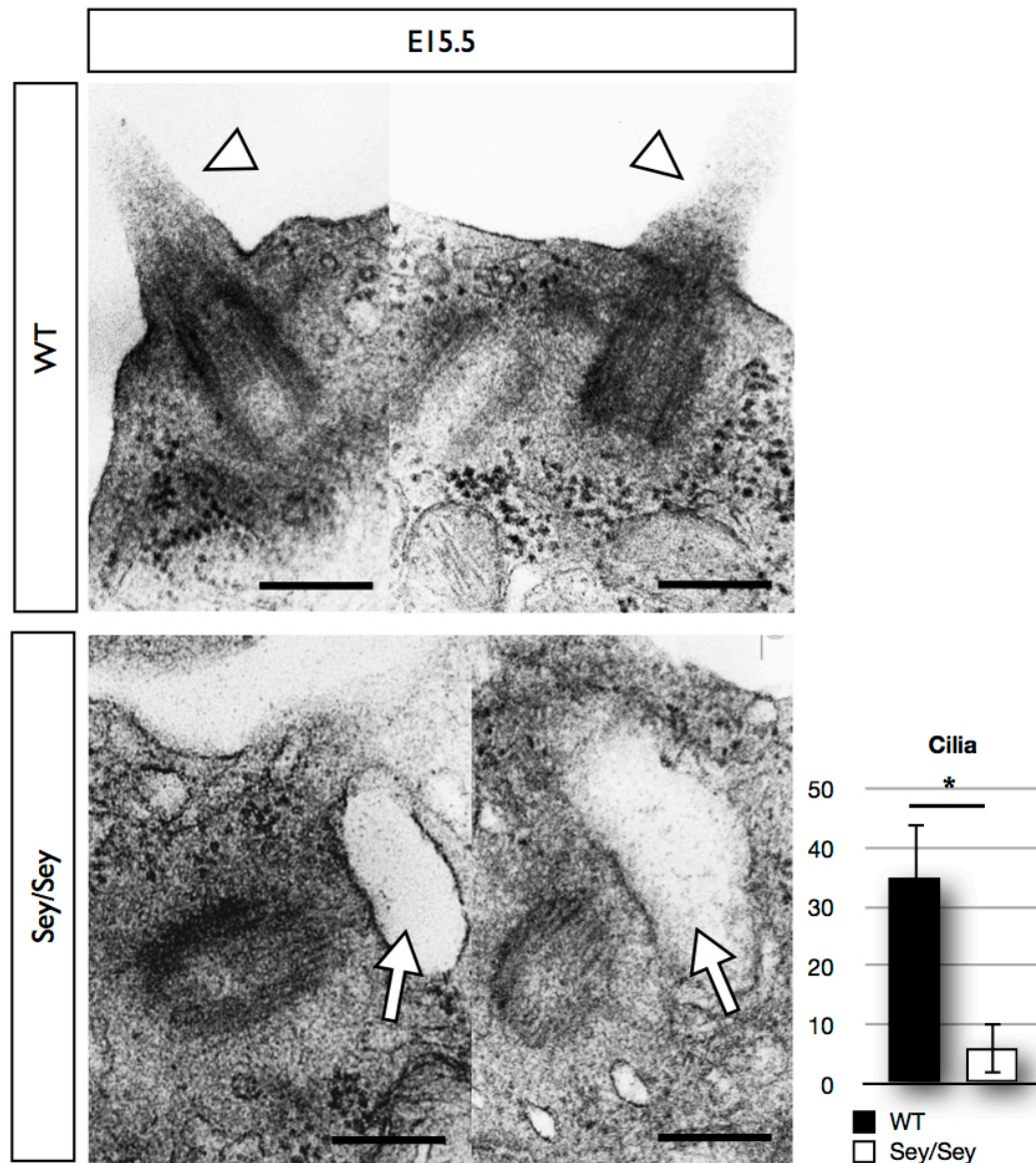


Fig. II.11. Quantitative analysis of centrioles connected to primary cilia using electron microscopy. Considerably less centrioles were connected to primary cilia (arrowheads) in *Sey/Sey* than in WT cortex. Centrioles in *Sey/Sey* cortex showed very often a vesicle at their distal end (arrows). However they failed to connect to the cell membrane and to assemble a primary cilium. Statistical analysis (C) indicates a strong reduction of the number of primary cilia at the ventricular surface compared with the wild type (WT: 34.89 % \pm 9.24; *Sey/Sey*: 6.01 \pm 4.42; $p = 0.031$).

These results indicate that in Pax6-deficient cortex, RGP show a malformation at the subdistal appendages of the mother centriole, leading to a loss of primary cilia at the ventricular surface.

II.2. RGPs containing the mother centrosome detach the VZ surface in Pax6-deficient cortex

Recent data indicates that loss of Ninein, an important protein of the subdistal appendages with a role for the connection of microtubules to the mother centriole, causes a premature exit of RGPs from mitotic cycle (Wang et al 2009). We hypothesized therefore that the discovered loss of subdistal appendages in *Sey/Sey* might cause a similar defect in Pax6-deficient cortex. To investigate directly this question, I decided to master and introduce in the Lab a recently published approach (named thereafter “Kaede-Centrin1 approach”) (Imai et al 2010, Wang et al 2009).

Kaede is a fluorescent protein, which is able to change its fluorescence from green after expression to red after exposure to UV light (350 – 400 nm). The fusion protein Kaede-Centrin1 is specifically expressed at the centrioles of the centrosome. After expression of Kaede-Centrin1 and photo switch to red fluorescence, all centrosomes appear in red. After the next mitosis all centrosomes appear in yellow due to the red fluorescence of the older centriole and a green fluorescence of the new assembled green centriole. However, after the second mitosis (following the photo switch) it is possible to distinguish between cells containing a mother centrosome (yellow, respectively red and green) and a cell containing a daughter centrosome (green) (Fig. II.12). This is important for analysing the centrosome distribution after asymmetric division of RGPs. By localisation of the centrosome it is possible to identify the cell type to which the centrosome belongs. Centrosomes of RGPs are exclusively located in VZ mostly at the apical ventricular surface, while centrosomes of differentiating cells leave the VZ and migrate basally with the nucleus of these cells.

As described previously, the mother centrosome is essential to maintain RGPs in the VZ (Wang et al 2009). To analyse the centrosome distribution in RGPs *in utero* electroporation approach was used. Therefore, a plasmid coding for Kaede-Centrin1 was injected into the lateral ventricle of an E13.5 embryo. By electroporation of the plasmid in the embryo head, the negatively charged plasmid DNA is able to enter the RGPs in VZ of the lateral ventricle. This method is an excellent approach to manipulate the expression of a single gene. By

electroporation of the Kaede-Centrin1 fusion protein it is possible to visualize the location of the protein within the cortex or even within a single cell.

24 hours after electroporation of the plasmid coding for photo switchable Kaede-Centrin1 fusion protein the mouse was sacrificed and the electroporated brains were dissected and cut into 300 μm slices. Then the photo switch was executed *ex vivo* by a short (5 s) exposure to UV light (350 - 400 nm). After 48 hours incubation (humidified incubator; 37 °C; 5 % CO_2) the brain slides were fixated and analysed with a confocal microscope.

The disadvantage of *ex vivo* photo switch is the harmful cutting of the brains. This might lead to changes in the location of single cells and therefore also to wrong localisation of single centrosomes. Due to the fact that the slices were 300 μm thick this can be neglected because cells within the slice were not affected. A second negative point might be that the cell migration during incubation time is affected. The brain slices are embedded in 2 % low melting agarose, which inhibit a basal expansion of the cortex. This might lead to defects in the migration of newborn neurons or IPs. Additionally, the optimal conditions of *in utero* incubation can only roughly simulated *in vitro*, which might also have a negative effect. The pro for an *ex vivo* photo switch is that a second operation of the mother is not necessary. Due to the fact that the experiments were performed in transgenic mice and embryos, it is more complicated then in WT animals (Imai et al 2010, Wang et al 2009). Transgenic mice and especially Pax6-deficient embryos die very often after the electroporation procedure. The mother as well as the embryos would hardly survive a second operation for photo switch.

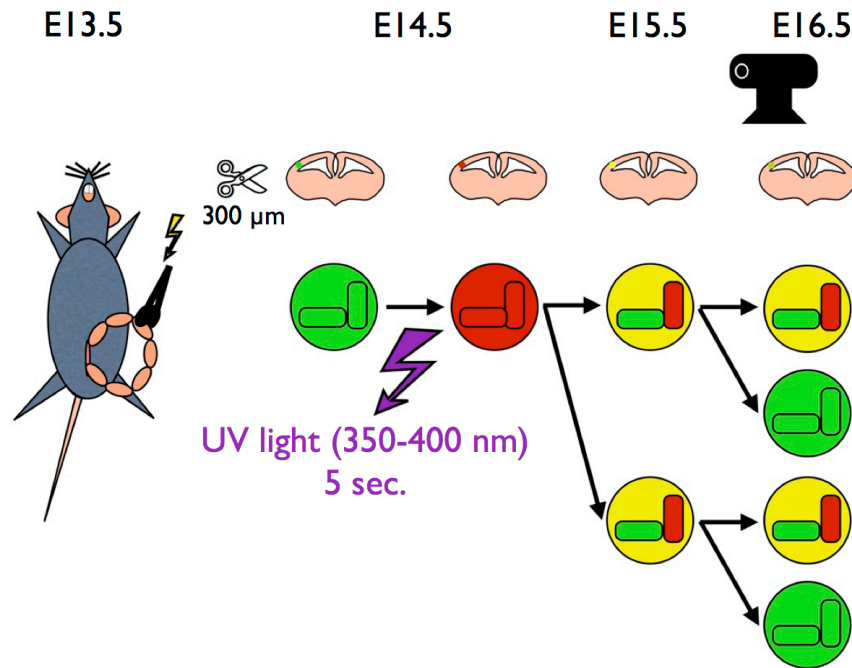


Fig. II.12. Schematic overview of the Kaede-Centrin1 approach to evaluate the centrosome maturation. The embryos were electroporated at E13.5. At E14.5 the mouse was sacrificed and the electroporated brains were cutted into 300 μm slices followed by photo conversion by exposure to UV light (350 – 400 nm) for 5 seconds. After two cell cycles (48 hours) it is possible to distinguish between mother centrosome (yellow/green and red) and daughter centrosome (green).

For establishment of the new technic in our laboratory, initially experiments were proceed with CD1 WT mice to test whether the photo switch and the incubation were working. Analysis with a confocal microscope revealed a successful photo switch evident by detection of yellow marked centrosomes. The fact that the centrosomes appear in yellow and that there were green marked centrosomes located basally of the VZ indicated that the cells survive and migrate during the incubation time (Fig. II.13).

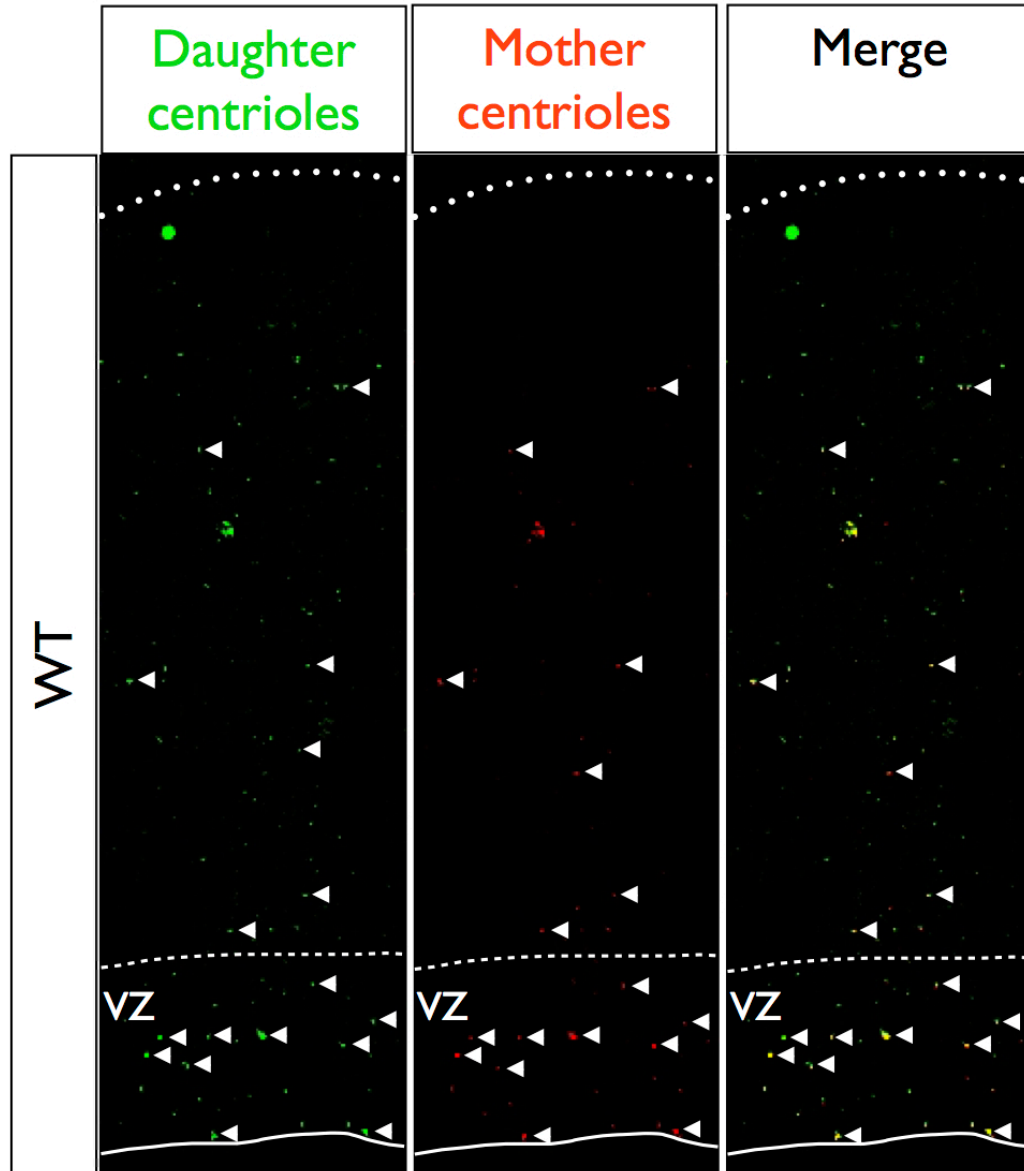


Fig. II.13. Confocal microscopy of WT cortex after *in utero* electroporation of Kaede-Centrin fusion protein at E13.5, photo switch *ex vivo* at E14.5 and 48 hours of incubation (37 °C; 5 % CO₂; humidified). Analysis showed yellow and green marked centrosomes indicating that photo switch was successful. Green marked centrosomes located basally from VZ indicate a proper cell division of RGP and proper migration of differentiating cells. Distribution of the centrosomes indicates a higher percentage of mother centrosomes (yellow) in the VZ. Statistical analysis was not performed.

Sey/Sey mice turned out to be not practicable for electroporation; due to massive malformations of the mutant head and brain, the embryos do not easily survive the procedure of electroporation. Therefore, Kaede-Centrin1 electroporation was performed in cortex-specific *Pax6cKO* embryos. Therefore *Pax6^{fl/fl}* mice (Ashery-Padan et al 2000) were crossed with *Pax6^{fl/fl};Emx1Cre^{+/-}* mice driving recombinase activity in cortical progenitors (Gorski et al 2002). Due to statistical distribution 50 % of the embryos were Cre⁺ while 50 % were Cre⁻. Embryos were

electroporated randomly; genotyping identifying *Cre*⁺ embryos was performed from embryonic tissue after brain dissection. *In utero* electroporation was performed at E13.5 after 24 hours the mouse was sacrificed, the embryonic brains were dissected and cut into 300 µm slices and transferred to Minicell cell culture inserts (0,4µm; 30mm Diameter; Millipore) in 6 wells containing 1.5 ml Brain slice culture medium. By exposing the brain sections to UV light (350 – 400 nm) for 5 seconds the photo switch was performed. After two days of *in vitro* incubation, the brains were fixated with PFA and prepared for cryo-sectioning. The brains were cut into 20 µm slices and prepared for IHC. To identify the VZ an IHC with an antibody for Sox2 was performed on the brains slices. *Cre*⁻ embryos were used as control.

Analysis of the centrosome location revealed a reduced amount of centrosomes in the VZ of *Pax6LOF* cortex compared to WT, suggesting that more cells (then only the differentiating cells) leave the VZ. Although the student's T-test revealed no statistical relevance, this was an indication that RGPs prematurely leave the VZ, which leads to a reduced total amount of Centrosomes in VZ.

As shown by Wang et al., (2009), cells containing the mother centrosome stay in the VZ to become a new RGP (thus maintaining the progenitor pool), while cells containing the daughter centrosome leave the VZ towards the CP and differentiate into a neuron. Analysis of the location of the mother (yellow/red and green) and daughter (green) centrosomes showed obvious differences between the control and *Pax6* loss-of-function brains. In accordance with Wang et al., (2009) in the control brains 68.69 % (± 0.32) of the mother centrosomes were located within the VZ and 31.31 % (± 0.32) were found outside (Fig. III.14; Fig. III.15). Notably, in *Pax6LOF* brains only 37.65 % (± 8.31) of the mother centrosomes were located in the VZ while 62.35 % (± 8.31) were located outside of the VZ (Fig. III.14; Fig. III.15). These results strongly suggest that in *Pax6 LOF*, RGPs containing the mother centriole, instead of staying in VZ, prematurely leave the VZ.

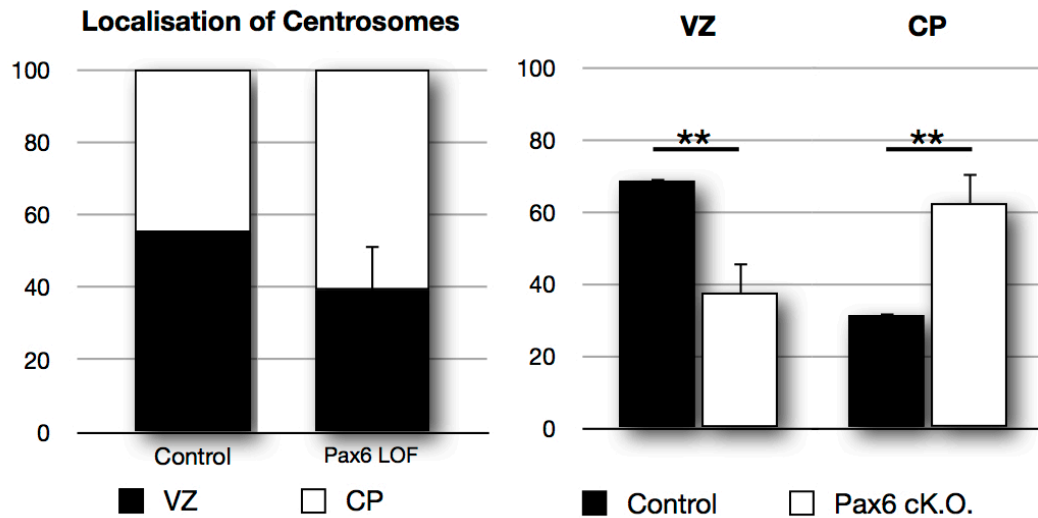
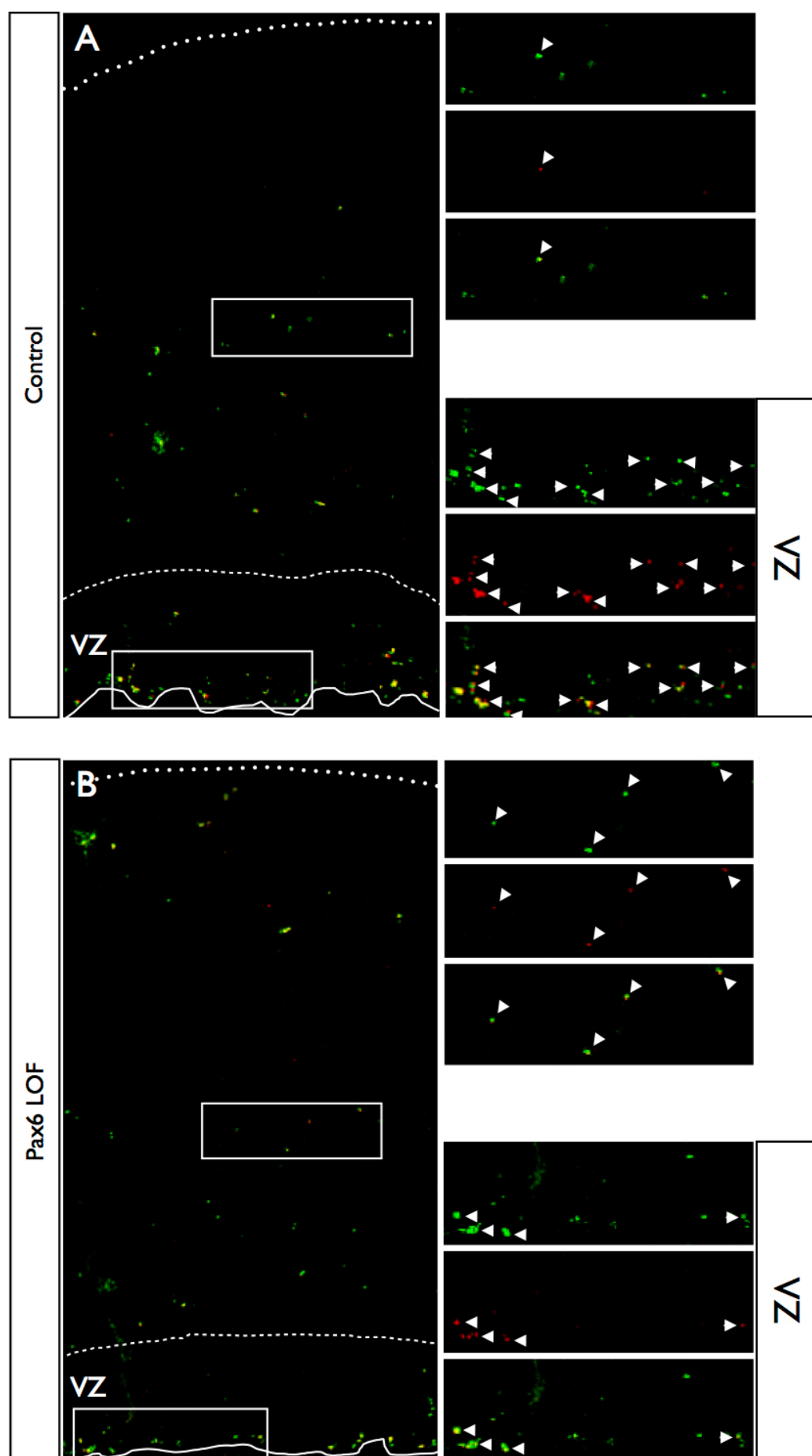


Fig. II.14. Statistical analysis of Kaede-Centrin1 experiment. The analysis indicated a general reduction of centrosome number in the VZ of *Pax6* deficient cortex although there is no statistical relevance (WT: 55.02 % \pm 0.45; *Sey/Sey*: 44.98 % \pm 12.59; $p = 0.3$). Clearer was the result from analysis of the location of the mother centrosomes. While in WT almost 70 % of the mother centrosomes are located in the VZ, only less than 40 % are in *Pax6* deficient cortex indicating a loss of cells containing the mother centrosome (WT: VZ: 68.69 % \pm 0.32, CP: 31.31 % \pm 0.32; *Sey/Sey*: VZ: 37.65 % \pm 8.31, CP: 62.35 % \pm 8.31; ** = $p < 0.01$; $p = 0.0074$).



↑Fig. II.15. Confocal microscope pictures of control (A) and Pax6 deficient cortex (B) after electroporation of Kaede-Centrin1-plasmid, photo switch after 24 h and 48 h incubation *in vitro*. The Pax6-deficient cortex shows remarkably lower number of mother centrosomes (green and red / yellow; arrowheads) in the VZ as compared with the control cortex (A, VZ and B, VZ). In the Pax6-deficient cortex more mother centrosomes are distributed in basal regions (the intermediate zone, IZ and cortical plate, CP).

Taken together, the results from the structural analysis of the centrioles revealed that in absence of Pax6 in RGP of developing cortex, there is a loss of subdistal appendages of the mother centrioles and therefore, incomplete maturation of the mother centriole. As a direct consequence of missing subdistal appendages, the mother centrioles in Pax6-deficient cortex are not able to transform into basal body of the primary cilium, which fails to extend into the ventricle. As a secondary effect, RGPs containing such defective mother centrioles leave the VZ.

II.3. Mechanism of Pax6-dependent control of centrosome structure and function

II.3.1. Pax6 as a protein-binding partner of centrosome proteins

Results from previously performed in the group yeast-two-hybrid screen identified at least 3 centrosome associated proteins as possible protein-binding partners of TF Pax6. The first one Nedd9, is a scaffolding protein of the Cas family, member of the β 1-intergrin signalling pathway, and involved in the TGF β signalling pathway (O'Neill et al 2000, Vogel et al 2009). The second candidate was Kif2a, a Kinesin motor protein belonging to the kinesin-13 family that plays an important role in microtubules depolymerisation (Wordeman 2005). The third candidate was Hook2; a linker protein to bind cargo complexes to microtubules based motor proteins. This protein localizes to the centrosome and binds to centriolin/CEP110 (Szebenyi et al 2007).

In order to verify possible protein-protein interactions, I performed co-transfections of Pax6 together with Nedd9, respectively Kif2a or Hook2 *in vitro*. Therefore NIH3T3 cells were cultured in a six well plate on coverslips. One day

thereafter the cell were transfected with an expression plasmid encoding for Pax6 under the control of a CMV promoter (*pCMV-Pax6*) together with an expression plasmid for HA-Nedd9 (*pCMV-HA-Nedd9*) respectively HA-Kif2a (*pCMV-HA-Kif2a*) or HA-Hook2 (*pCMV-HA-Hook2*). After one day of incubation, the cells were fixated on coverslips. To visualize locations of Pax6 and the possible protein-binding partners within the cells, double immunocytochemistry (ICC) was performed with antibodies for Pax6 and HA-tag. The HA-tag was used to detect Nedd9, respectively Kif2a or Hook. After ICC cells were covered with Vectashild Mounting-Medium containing DAPI. The cells were analysed by confocal microscopy.

The analysis indicated that Pax6 is exclusively expressed in the nuclei of transfected cells, while all three co-transfected constructs were expressed in the cytoplasm. All three proteins showed a bubble like expression pattern. Kif2a (Fig. II.16A) and Hook2 (Fig. II.16B) seemed to be expressed mostly next to the cell membrane; Nedd9 (Fig. II.16C) seemed to be evenly distributed all over the cytoplasm. Kif2a and Hook2 showed at least some co-localisation within the nuclei. In order to analyse whether this is indeed a co-localisation and therefore an interaction of Kif2a, respectively, Hook2 with Pax6 or an expression in the cytoplasm above or beneath the nucleus, a co-immunoprecipitation (CoIP) was performed.

Therefore, NIH3T3 cells were cultured in 10 mm culture dishes to get an adequate amount of overexpressed protein. One day after transfer, the cells were co- transfected with Pax6 and Kif2a, respectively Hook2 or Nedd9 expression vectors and after 24 hours the cells were harvested with Trypsin. After Trypsin was inactivation through washing with DMEM-medium containing 10 % FCS, cells were counted. After washing twice with PBS cells were lysed with a to the cell number adequate volume of lysis buffer. CoIP was performed with the ProFound™ Mammalian HA Tag IP/Co-IP Kit. A Westernblot was performed with the eluate and with the lysate (Input) as control.

None of the performed CoIPs showed an interaction of the HA-tagged probes with Pax6. Kif2a (Fig. III.16D) and Hook2 (Fig. III.16E) (that showed a possible co-localisation in ICC) showed no interaction in the co-immunoprecipitation. Also Nedd9 (Fig. III.16F), as expected, showed a negative result.

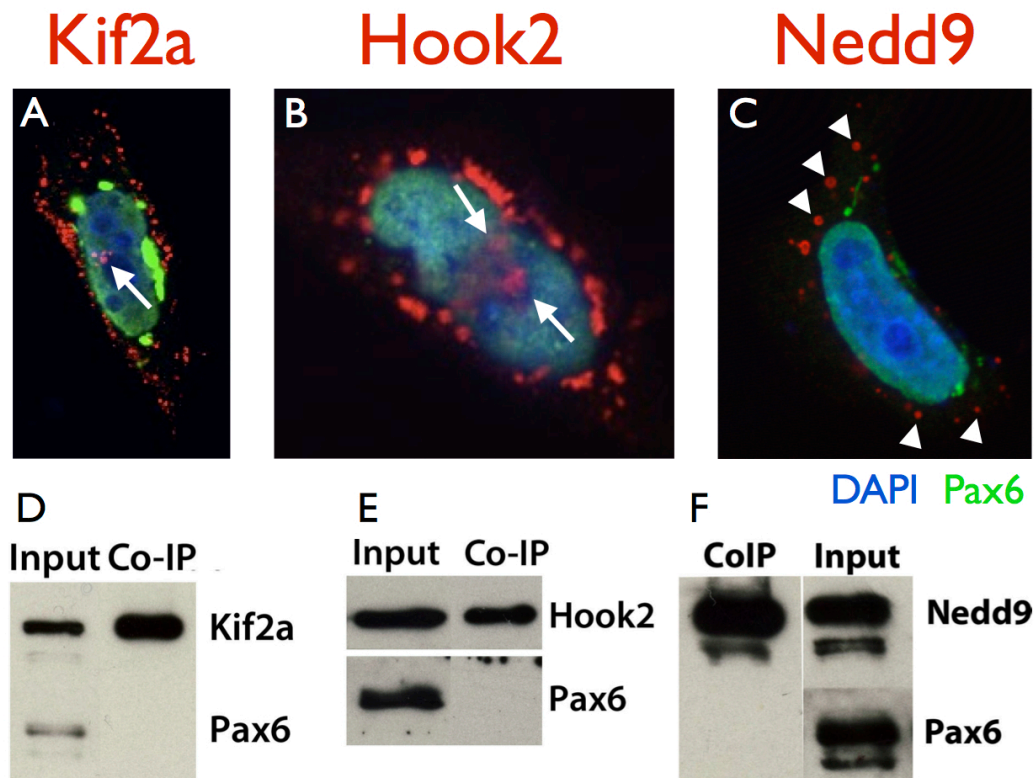


Fig. II.16. Co-transfections and Co-immunoprecipitations (CoIPs) of Pax6 with of potential Pax6 protein binding partners. Nedd9 protein was distributed in the cytoplasm (arrowheads) showing no co-localisation with Pax6, which is exclusively expressed in the nucleus. Kif2a and Hook2 showed at least a partially co-localisation (arrows) (**A and B**). CoIPs were performed with the centrosome-associated proteins Kif2a (**D**), Hook2 (**E**) and Nedd9 (**F**). None of the proteins showed a positive interaction with Pax6 *in vitro*.

Co-immunoprecipitation (CoIPs) showed no interaction of the three candidates Kif2a, Hook2 and Nedd9 with Pax6 *in vitro*. To analyse whether there is a co-localisation of Pax6 and the centrosomes in RGP, a double IHC for Pax6 and γ -Tubulin was performed on WT brain sections. The wild type brain was dissected at E13.5 fixated by 4 % PFA and cryo-sectioned into 16 μ m slices. The immunohistochemistry was performed with antibodies for Pax6 and γ -Tubulin and DAPI and analysed with confocal microscopy.

The analysis showed no co-localisation of Pax6 with the centrosome in interphase of RGP. Pax6 is exclusively expressed in the nucleus during interphase - therefore potential interactions with centrosome proteins would be not possible during interphase. During mitosis however, the nuclear membrane is degraded and Pax6 is evenly distributed over the cytoplasm. At this time point, a co-localisation of Pax6 and the spindle poles is present, although there is no higher concentration of Pax6 at the spindle poles.

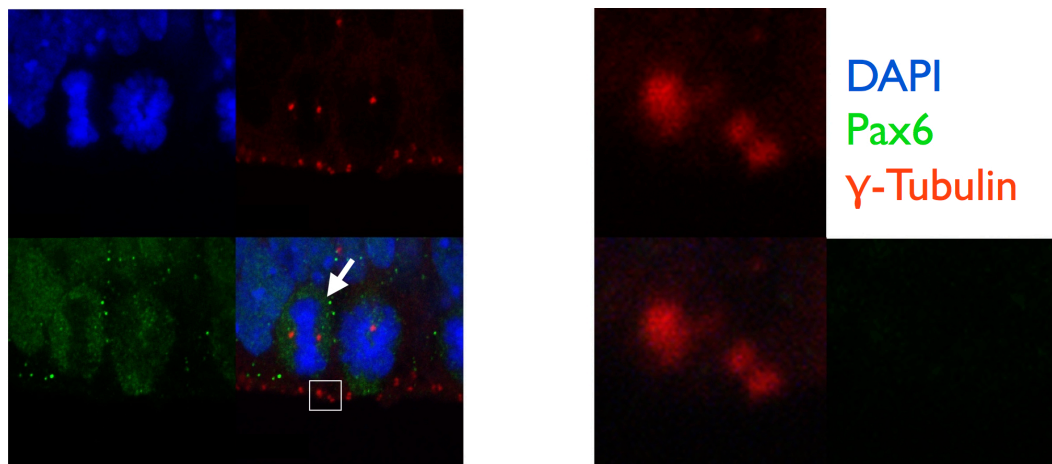


Fig. II.17. Immunohistochemistry (IHC) with antibodies for Pax6 (green) and γ -Tubulin (red). Pax6 and centrioles of interphase cells show no co-localisation. During mitosis the nuclear membrane is degraded and Pax6 is evenly distributed in the cytoplasm (Arrow). Therefore an interaction would be only possible during cell division.

To sum up, because of distinct subcellular localisation, protein-protein interactions between Pax6 and the studied centrosome proteins, Kif2a, Hook2 and Nedd9 could not be established during interphases. However, during mitosis, Pax6 interaction with centrosome/spindle pole proteins might be possible but such interactions would not interfere neither with centrosome function / behaviour nor with interkinetic nuclear migration.

II.3.2. Pax6 as a transcriptional regulator of centrosome-specific proteins

I hypothesized therefore, that being a powerful developmental regulator, TF Pax6 might influence the transcription of some centrosome-specific proteins. As noticed above, our structural analysis showed a defect of centriole maturation in *Pax6*-deficient cortex. We assumed therefore that Pax6 function might be required for expression / function of a protein of the subdistal appendages. The first candidate for such appendage-specific protein is Ninein. Noteworthy, knock down of Ninein causes a premature exit of RGP from the mitotic (Wang et al 2009). Premature exit from the mitotic cycle is also known for RGP in *Pax6*-deficient mice (Quinn et al 2007, Tuoc et al 2009). Although Ninein has been not shown to act as a direct Pax6 downstream target gene, Ninein expression on mRNA level is down regulated in *Pax6*-deficient brains (Asami et al 2011).

A second possible target gene that could be regulated by TF Pax6 could be *Odf2*, encoding the outer dense fibre 2 protein located at the subdistal appendages (Nakagawa et al 2001). Without Odf2, primary cilia assembly and recruitment of

Ninein to subdistal appendages fails (Ishikawa et al 2005). Due to this similarity to the phenotype of *Pax6*-deficient cortex, I hypothesized that the subdistal appendage-specific Odf2 protein could be regulated by Pax6 at transcriptional level.

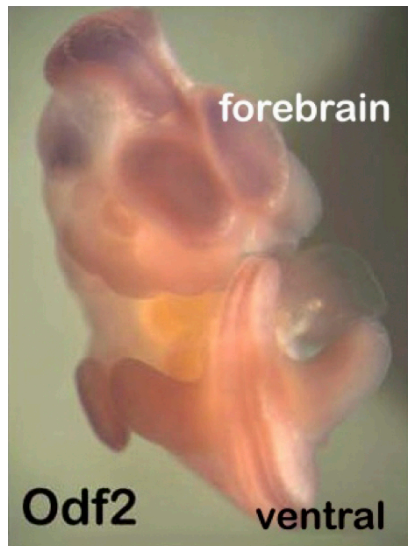
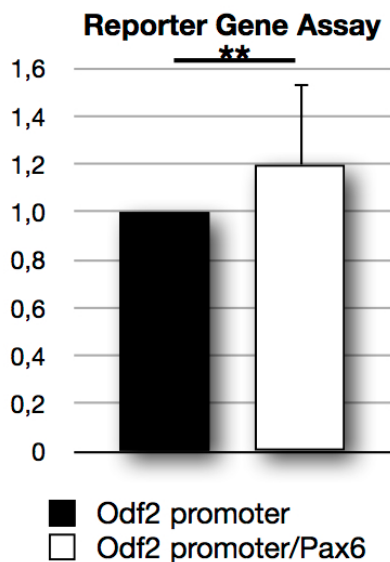


Fig. II.18. View on the ventral part of an E12.5 WT embryo after whole mount *in situ* hybridisation for *Odf2* in a WT E12.5 embryo. Expression pattern of *Odf2* reveals a strong expression of *Odf2* in the developing CNS, including a strong expression in E12.5 forebrain of WT embryos. Collaboration with Prof. Hoyer-Fender.

II.4. Functional and mechanistic analysis of *Odf2* as a Pax6 downstream target

II.4.1. Whole mount *in situ* hybridisation and reporter gene assay indicate *Odf2* as a downstream target of Pax6

The restricted expression of *Odf2* in developing CNS, including a strong expression in E12.5 forebrain (Fig. III.18), was similar to the *Pax6* expression (Walther & Gruss 1991), suggesting possible regulation between these genes. To examine further this possibility, I performed a reporter gene assay in NIH3T3 cells using an expression plasmid, in which firefly luciferase acts as a reporter under the control of *Odf2* promoter (collaboration with Prof. Hoyer-Fender). After co-expression of the *Odf2*-promoter-luciferase construct together with a CMV-*Pax6* expression plasmid, an increased activity of the luciferase reporter was detected. The experiment was performed 30 times for the control (single transfection of *Odf2*-promoter-luciferase construct) and 30 times for the



experiment (co-transfection *Odf2*-promoter-luciferase construct and *CMV-Pax6*). Average calculation indicated an enhancement of 20 % after co expression with Pax6. (Reporter construct (Control) = 1; Pax6 + Reporter construct = 1,2; $\pm 0,34$; $p = 0,0084$).

Fig. II.19. Luciferase reporter with the control of the *Odf2* promoter. Co-expression of Pax6 revealed an increased reporter gene activity of ~20 % compared to single expression of reporter construct. Reporter construct (Control) = 1; Pax6 + Reporter construct = 1,2; $\pm 0,34$; ** = $p < 0.01$; $p = 0,0084$.

II.4.2. TF Pax6 binds to the *Odf2* promoter

To investigate whether Pax6 is able to bind directly to the *Odf2* promoter, the *Odf2* promoter sequence was searched for Pax6 binding sites. Three possible binding sites were identified within the *Odf2* promoter. The capacity of Pax6 to bind each of these sites was analysed using an electrophoretic mobility shift assay (EMSA) (Baumer et al 2003). Oligonucleotides of the possible binding sites were marked with γ -P32-ATP and incubated with Pax6 protein. After electrophoresis the γ -P32-ATP was detected through autoradiography. Oligonucleotides, which are bound to Pax6, move slower through the gel than unbound oligonucleotides, showing an upward shift relatively to the unbound oligonucleotides. The result revealed a strong binding of Pax6 to the third binding site (Fig. II.20, SQ3). To verify further this result a second EMSA was performed. Additionally to the shift of the Pax6-oligonucleotide complex a supershift experiment was performed. Therefore an antibody targeting Pax6 was added to the Pax6-oligonucleotide complex and incubated for 15 minutes. The antibody binds to Pax6 within the complex to generate an antibody-Pax6-oligonucleotide complex to verify the specific binding of Pax6. The antibody-Pax6-oligonucleotide complex migrates even slower than the Pax6-oligonucleotides complex and therefore performs a super shift.

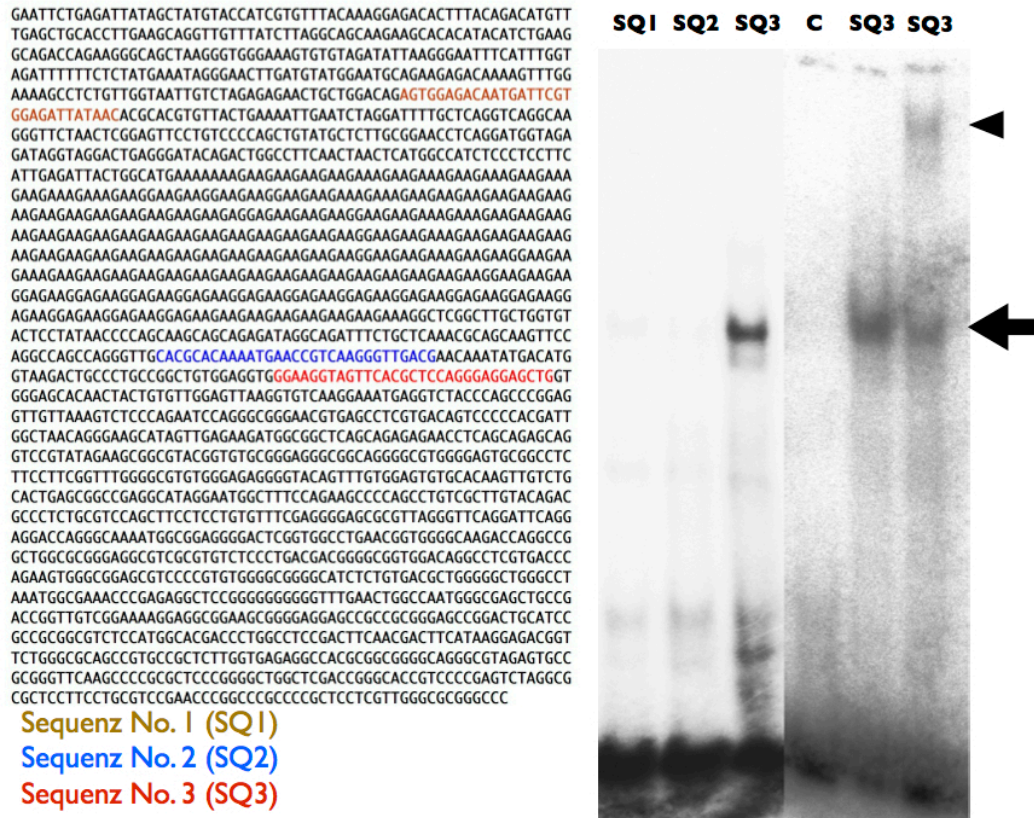


Fig. II.20. Left panel: Sequence of the *Odf2* promoter containing possible Pax6 binding sites (coloured); right panel: EMSA of the three Pax6-binding sequences (SQ1, SQ2, SQ3) in *Odf2* promoter. The third binding sequence (red; SQ3) showed a very strong binding to Pax6 (arrow), which band was supershifted (arrowhead) in the additional presence of Pax6 antibodies.

Taken together, the results indicate that *Odf2* is a direct downstream target gene of TF Pax6 in the performed *in vitro* assays.

II.4.1. *Odf2* expression in WT and *Sey/Sey* mice

II.4.1.1. *Odf2* expression on mRNA level

Next, I investigated whether expression of *Pax6* *in vivo* could also regulate *Odf2* expression. In order to analyse the expression of *Odf2* in the cortex of WT and *Pax6*-deficient *Sey/Sey* embryos an *in situ* hybridisation was performed on cross brain sections at E13.5 and E15.5. At E13.5 only a slight reduction of *Odf2* mRNA expression was visible in *Sey/Sey* cortex, compared with the control. At E15.5, however this difference becomes more apparent, showing a regulation of *Odf2* by Pax6, especially during late cortical neurogenesis (Fig. II.21).

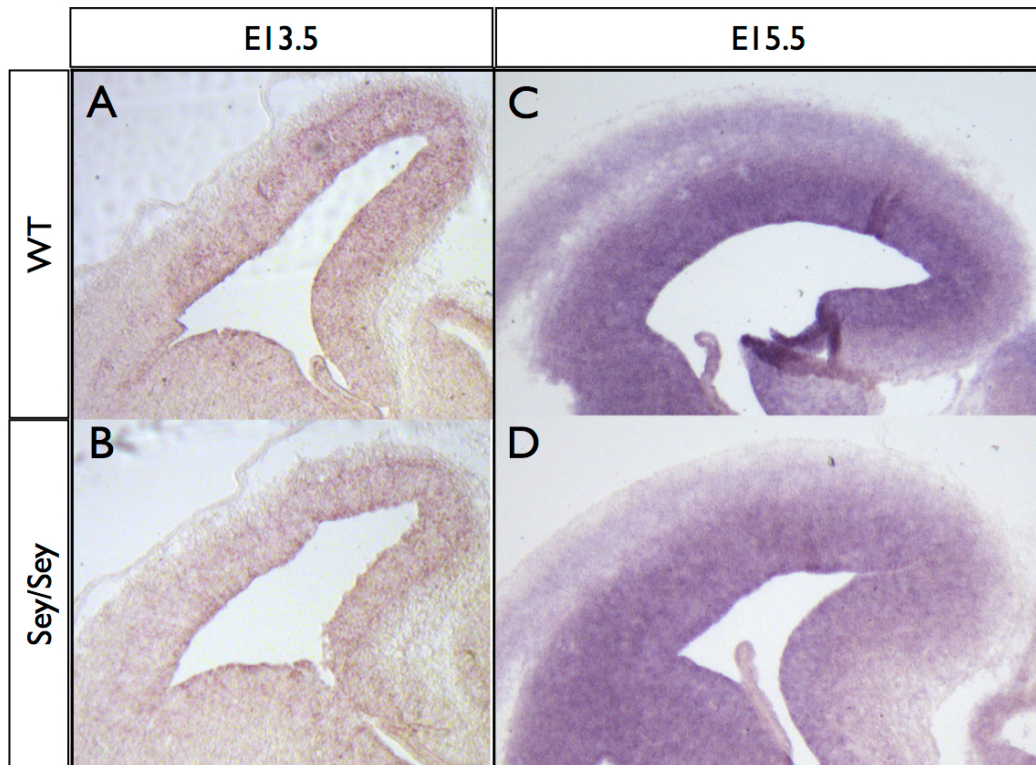


Fig. II.21. *In situ* hybridisation analysis of *Odf2* expression at E13.5 and E15.5 of WT and *Sey/Sey* brains as indicated. ISH at E13.5 reveals a slight reduction of *Odf2* expression in *Sey/Sey* embryos (A, B). At E15.5 ISH shows a much stronger down regulation of *Odf2* in *Sey/Sey* embryos (C, D).

To get a further support of the observed dependence of *Odf2* expression from TF Pax6, I performed quantitative real time PCR assays, RT-PCR (collaboration with Prof. Hoyer-Fender). Cortices from E15.5 WT and *Sey/Sey* embryo brains were prepared from which mRNA was extracted and subjected to RT-PCR in three independent experiments. At E15.5, the expression of *Odf2* at mRNA level was strongly down regulated with a small variation between the three experiments. (q-rtPCR experiment 1: 45.64 %; q-rtPCR experiment 2: 55.51 %; q-rtPCR experiment 3: 60.69 %). Taken together, these results indicated that Pax6-deficient cortex *in vivo*, the expression of *Odf2* is down regulated to 53.95 % (± 6.24). The experiment is statistical relevant ($p=0.009$) (Fig. II.22).

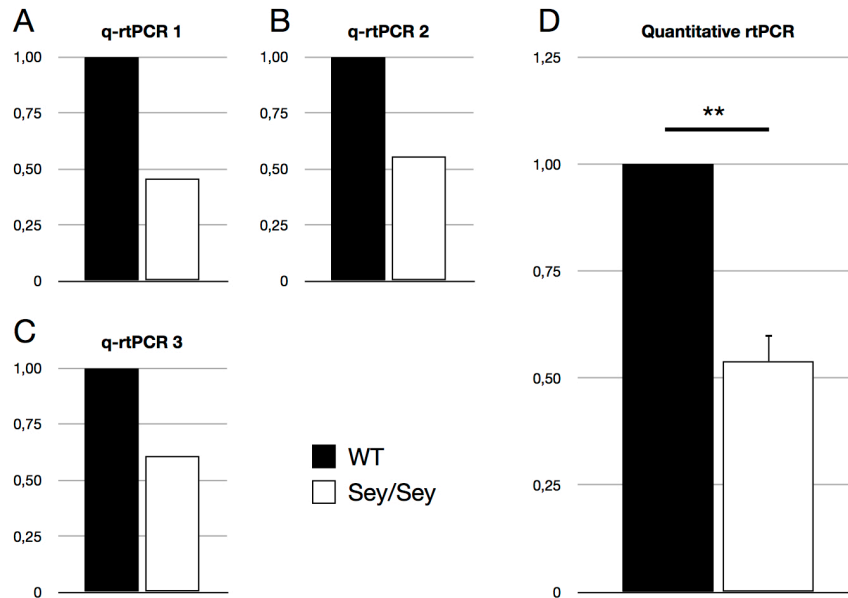


Fig. II.22. Quantitative rtPCR (E15.5). Quantitative rtPCR showed a reduction of more than 50 % in the *Sey/Sey* cortex (D) as compared with control (53.95 % \pm 6.24; ** = $p < 0.01$; $p = 0.009$).

II.4.1.2. Odf2 expression on protein level

To study furthermore the protein level of *Odf2* in WT and Pax6 deficient brains, an IHC with antibodies for γ -Tubulin and Odf2 on brain cross sections was performed. In accordance with the *in situ* data presented above, already at E13.5 a small reduction of Odf2 protein was visible at the centrioles in the Pax6-deficient brains (Fig. II.23C). Remarkably, at E15.5 this effect was much stronger (Fig II.23D) when almost no Odf2 protein was detectable at the centrioles in *Sey/Sey* cortex. Due to the fact that some appendages were still present (as detected in the EM assay at E15.5) it is likely that some Odf2 was still present at such “residual” mother centrioles, however, the sensitivity of the antibody seems to be not high enough to detect such low levels of Odf2 protein.

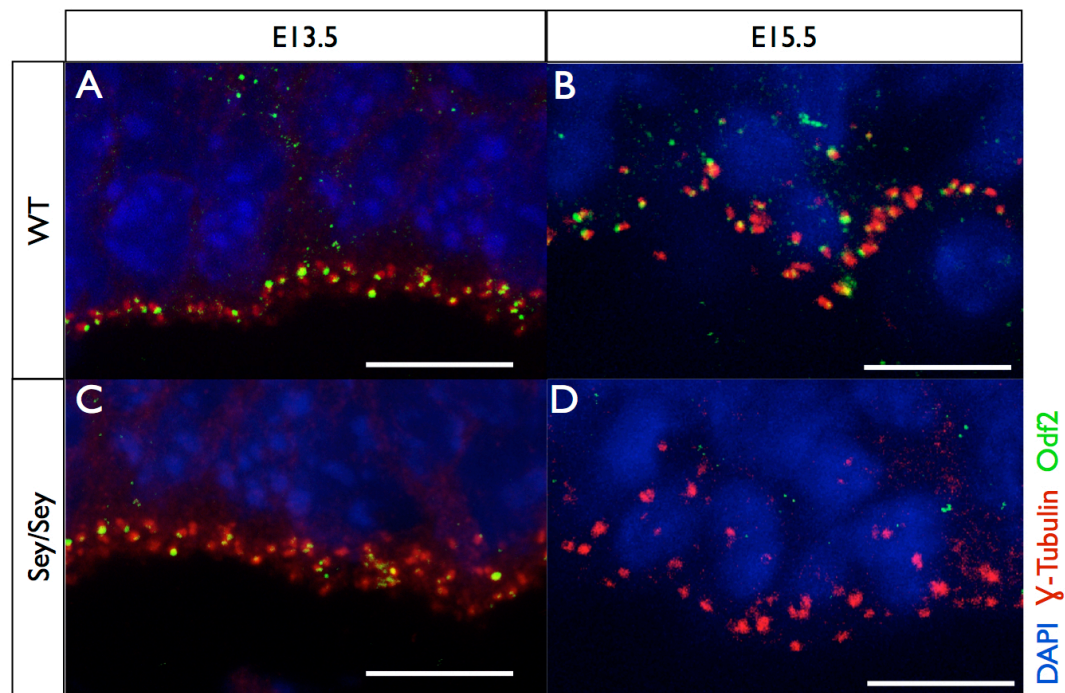


Fig. II.23. IHC with antibodies for γ -Tubulin (red) and Odf2 (green) revealed a reduction of Odf2 at the centrioles of E13.5 *Sey/Sey* embryos compared with WT. At E15.5 no Odf2 was detectable at the centrioles indicating a complete loss respectively massive down regulation of *Odf2*.

II.4.2. Ninein protein level is reduced at the centrioles of

Sey/Sey mice

Because the discovered loss of Odf2 at the centrioles of *Sey/Sey* cortex, an investigation of Ninein expression at the centrioles was mandatory due to previous investigations (Asami et al 2011, Ibi et al 2011, Ishikawa et al 2005). An IHC with an antibody for γ -Tubulin and Ninein was performed on cross sections of wild type and *Sey/Sey* embryo brains to visualize the Ninein expression at the centrioles. As expected, Ninein expression was dramatically reduced at the centrioles of the mutant cortex.

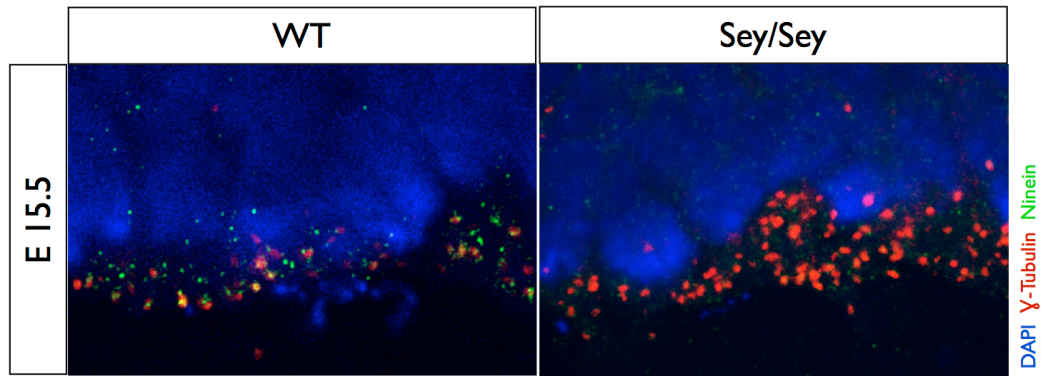


Fig. II.24. IHC with antibodies for γ -Tubulin (red) and Ninein (green) at E15.5 showed a strong reduction of Ninein at the centrosomes indicating a loss of subdistal appendages in *Sey/Sey* cortex.

To sum up, the results from these *in vivo* experiments support the findings from my *in vitro* assays and morphological analyses. More specifically, the results strongly suggest that due to a direct regulation of *Odf2* expression by TF Pax6, the subdistal appendages at centrosomes of RGP are mis-built, reflecting in severe structural defects of the centrosomes, including a loss of Ninein at the centrosomes (as an indirect consequence of the Pax6LOF).

II.5. Analysis of *Odf2* loss of function cortex

II.5.1. Generation of *Odf2* conditional knock out (*Odf2cKO*) mice

In order to analyse the direct effect of loss of *Odf2*, I decided to generate *Odf2KO* mice. Due to the fact that *Odf2KO* mice are lethal at very early stages of embryogenesis (Salmon et al 2006) I planed to generate a transgenic line for conditional inactivation of *Odf2*. Luckily, the research group of Prof. Hoyer-Fender possessed already generated *Odf2cKO* ES cells. The *Odf2cKO* (ES) IDG3.2 cells (F1 hybrid ES cells from 129SV and C57-bl.6 background) (obtained from Prof. Dr. Hoyer-Fender, University of Göttingen) and were aggregated or injected into CD1 WT embryos for generation of chimeric mice. The injection failed to give rise to any chimeras due to unknown reasons, while the aggregation gave rise to 13 chimeras. Unfortunately, crossing of chimeras with CD1 WT animals failed to give a germ line transmission.

II.5.2. Analysis of *Odf2* knock down *in vivo*

As an alternative approach to the generation of *Odf2cKO* mice, electroporation of *Odf2* short-hairpin (SH) constructs were performed. Four *Odf2* SH constructs were purchased from OriGene together with control plasmids. In addition 8 *Odf2* SH constructs were generated with pSilencer 2.0-U6 vector.

RNA interference is able to mediate sequence specific post-transcriptional gene silencing. RNAi is regulating gene silencing *via* double stranded RNA or short-hairpin RNA. These RNA molecules are cleaved by dicer, a RNase III enzyme, to 21-23 nucleotide molecules with a 2 nucleotide overhang at the 3'-end (Bernstein et al 2001, Zamore et al 2000) Dicer is also involved in the formation of RNA-induced silencing complex (RISC) which contains a small single-stranded RNA generated from the double stranded RNS or the short-hairpin construct. The RISC complex is then able to identify the target mRNA via the small single stranded RNA binds to it and cleaves the complementary RNA for degradation (Hammond et al 2000). The advantage of shRNA constructs over double stranded RNA is that short-hair-pin RNA is encoded in plasmid DNA under the control of a polymerase III promoter (in my case a U6 promoter) (Kawasaki & Taira 2003) and therefore much better suitable for *in utero* electroporation then double stranded RNA.

All twelve SH constructs were tested together with the controls in NIH3T3 cells after over expression of *HA-Odf2*. HA-Odf2 was then detected by a westernblot with an antibody for HA. As a loading control an antibody for β -Actin was used.

The SH constructs SH3 and SH5 showed a strong capability to reduce the *Odf2* protein amount to a minimum. Therefore these two constructs were used for the *in vivo* assay *via in utero* electroporation experiments. The control plasmid K07 was used as a non-targeting control plasmid.

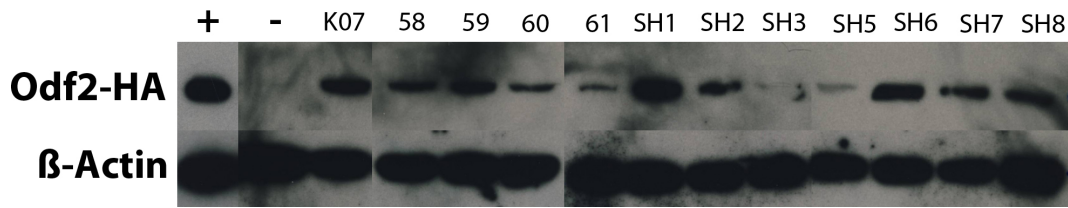


Fig. II.25. Functional test of *Odf2* short-hairpin constructs. The constructs SH3 and SH5 caused a strong knock down of *Odf2*. Construct K07 is a non-targeting construct used as control. Construct 58, 59, 60, 61 were from Origene, constructs SH1-SH8 were generated with pSilencer 2.0-U6 vector. Ligation of SH4 construct with pSilencer2.0-Ug vector failed.

II.5.2.1. *In vivo* transfection of *Odf2* short-hairpin constructs in developing brain *via in utero* electroporation

In utero electroporation was used to manipulate the expression of *Odf2* in RGP cells in the developing *in vivo* cortex. The advantage of this method is that one can quickly manipulate gene expression (either *via* overexpressing constructs or knock down by a specific short-hairpin containing plasmids). Each of the effective *Odf2* SH constructs (SH3, SH5) and the control plasmid K07, were electroporated in E13.5 embryo brains *in utero* together with an expression plasmid coding for GFP. The mouse was sacrificed at E16.5. For each construct 3 embryos were analysed. An IHC was performed with an antibody for GFP and Pax6 as a marker for RGP cells. Statistical analysis showed a dramatic loss of GFP⁺/Pax6⁺ cells after electroporation of either SH3 or SH5, compared with control (Fig. II.26). After electroporation of the control plasmid, 9.31 % (± 0.29) of GFP⁺ cells were also Pax6⁺ and 90.68 % (± 0.29) were only GFP⁺. After electroporation of the *Odf2* SH3 construct, however, only 1.88 % (± 0.58) of the GFP⁺ cells were also Pax6⁺ and 98.12% (± 0.58) were Pax6⁻ cells. Similarly, electroporation of *Odf2* SH5 resulted in 2.45 % (± 0.49) GFP⁺/Pax6⁺ and 97.55 (± 0.49) were GFP⁺/Pax6⁻ progenitors. Normalized to control, the *Odf2* knock down causes a dramatic reduction of GFP⁺/Pax6⁺ cells of 79.81 % (± 6.18) (SH3) respectively of 73.67 % (± 5.27) (SH5). This indicates a dramatic loss of RGP cells (GFP⁺/Pax6⁺) after the knock down of *Odf2*. Both experiments showed a statistical relevance (SH3: $p = 0.00053$; SH5: $p = 0.00027$). These results indicate a loss of RGP cells after reduction of the *Odf2* protein.

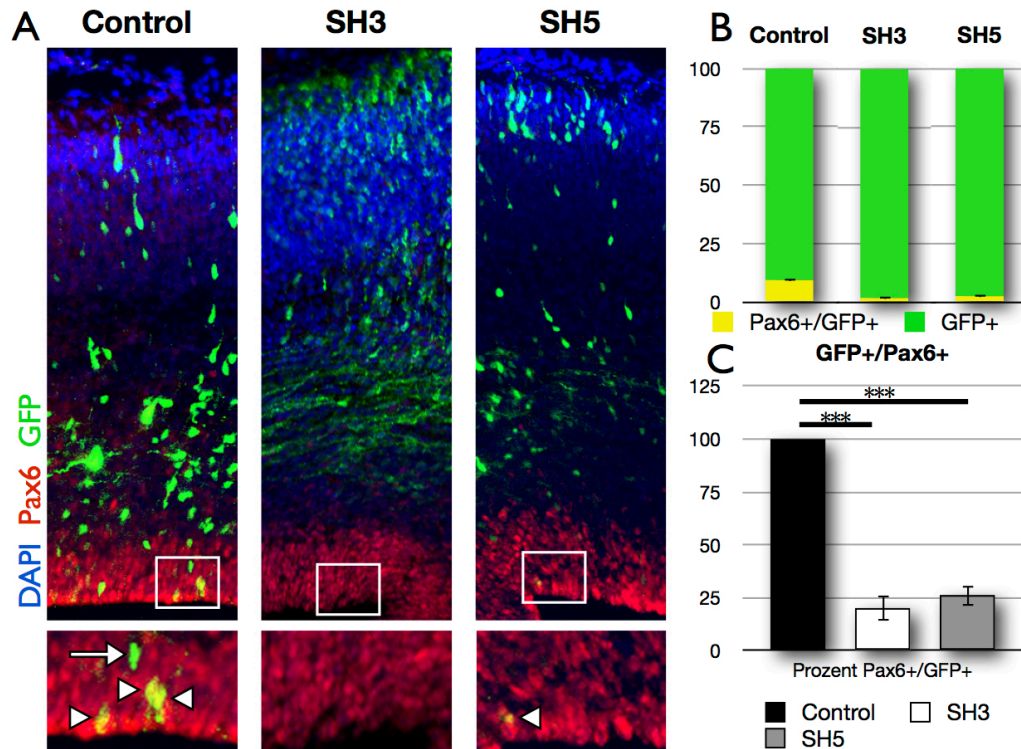


Fig. II.26. Analysis of the neocortex after *Odf2* knock down *in vivo*. Electroporation of embryo brains with *Odf2* SH constructs SH3 and SH5 and the control plasmid K07 together with GFP was done at E13.5 and the analysis was made at E16.5. Each SH construct was electroporated together with GFP-plasmid to mark the electroporated cells. **(A)** After electroporation of a control plasmid 9.3 % (± 0.29) of electroporated cell were GFP⁺/Pax6⁺. After electroporation of SH3 respectively SH5 1.88 % (± 0.58) respectively 2.45 % (± 0.49) were GFP⁺/Pax6⁺ indicating a loss of RGPs. Normalized to control, *Odf2* knock down causes a reduction of RGP amount of ~80 % (20.19 % ± 6.18 GFP⁺/Pax6⁺) respectively ~75 % (26.33 ± 5.28 GFP⁺/Pax6⁺) (***) = $p < 0.001$; SH3: $p = 0.00053$; SH5: $p = 0.00027$). Diagram representing the whole amount of electroporated cells indicated a reduction of GFP⁺/Pax6⁺ cells (represented in yellow) after knock down of *Odf2* compared to control **(B)**. Diagram representing GFP⁺/Pax6⁺ normalized to control indicates a massive reduction of electroporated RGP after the knock down of *Odf2* **(C)**.

II.5.2.2. Analysis of cell cycle exit index

The loss of Pax6⁺ RGPs in *Odf2* knock down could reflect either a loss of apical processes (the RGPs become dislocated in SVZ) or alternatively, could be a consequence of a premature exit of RGPs from the mitotic cycle. To examine the second possibility, the cell cycle exit index was defined after *in vivo Odf2KD* in cortical progenitors. *In utero* electroporation with SH3 plasmids or control plasmid was performed in wild type embryo brains at E13.5 and 24 hours thereafter the pregnant mouse was injected with BrdU. After additional 24 hours, the mouse was sacrificed and the embryos removed, the brain dissected and fixated. IHC analysis with antibodies for GFP, BrdU and Ki67 was performed and analysed by fluorescence microscopy. BrdU labels cells, which pass through S-phase, therefore after a 24 hours BrdU pulse all cells are labelled, which passed through S-phase within the last 24 hours. Cells, which are already out of the mitotic cycle, are not labelled and therefore, BrdU⁻ cells were not considered for analysis. Ki67 is a protein specifically expressed in cell within the mitotic cycle. Therefore the combination of a 24 hour BrdU labelling together with a Ki67 labelling marks cells which re-entered the cell cycle after their division within the last 24 hours (considering that an RGP needs less then 24 hours from S-phase to mitosis). As a consequence BrdU⁺ Ki67⁻ cells exit the mitotic cycle after last mitosis within the last 24 hours.

In control embryos, 58.08 % (± 3.04) of RGPs were mitotically active (GFP⁺, BrdU⁺ and Ki67⁺) while 41.92 % (± 3.04) were GFP⁺, BrdU⁺ and Ki67⁻ and therefore they were out of the mitotic cycle. Remarkably, after knock down of *Odf2* only 26.31 % (± 2.1) of the cells were GFP⁺, BrdU⁺ and Ki67⁺ while 73.69 (± 2.1) were GFP⁺, BrdU⁺ and Ki67⁻ cells, indicating an enhanced premature exit of RGPs from the mitotic cycle after knock down of *Odf2*. These results indicate that RGPs exit the mitotic cycle prematurely after *Odf2* knockdown and therefore leave the VZ. These results are statistical relevant ($p = 0.0005$).

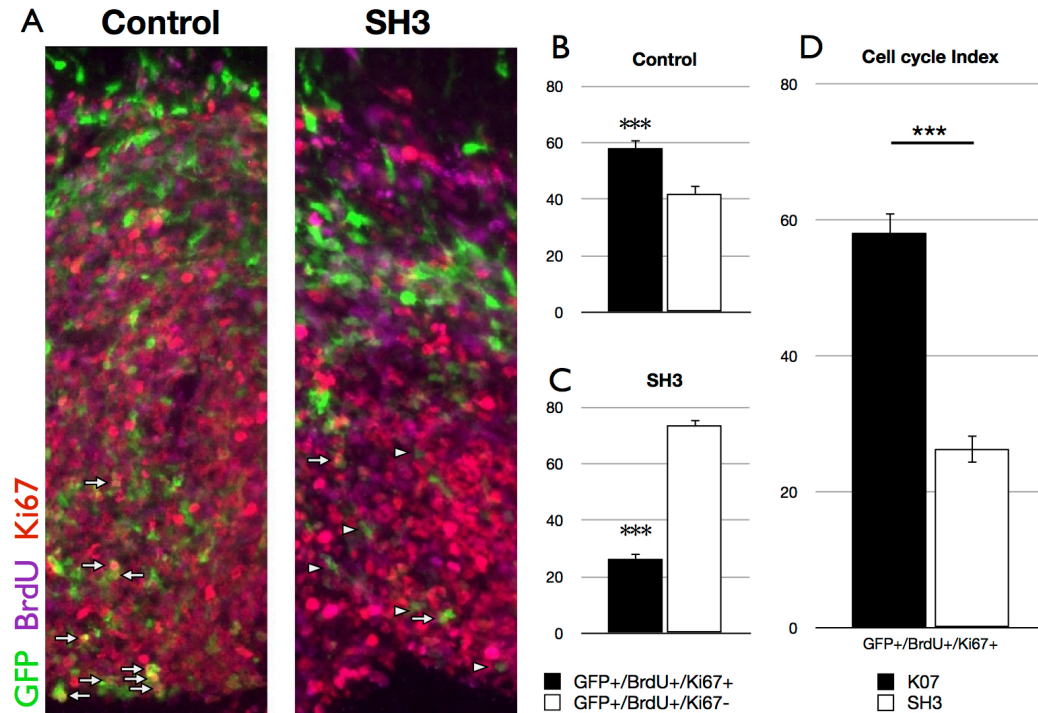


Fig. II.27. Analysis of cell cycle exit index after knock down of *Odf2*. (**A**, **B** and **C**) After electroporation of control plasmid K07 at E13.5, BrdU injection 24 hours later and analysis of E15.5 brains, 58.08 % (± 3.04) of the electroporated cells were in the cell cycle (GFP⁺/BrdU⁺/Ki67⁺) (arrows). (**D**) However, after electroporation of SH3, only 26.31 % (± 2.1) of the RGP were still in the cell cycle, and a higher number (73.69; ± 2.1) exited from the mitotic cycle (GFP⁺/BrdU⁺/Ki67⁻) (arrowheads) (***) = $p < 0.001$; $p = 0.00051$). The diagrams showing the cell cycle index after electroporation of control plasmid and *Odf2* knock down construct SH3 indicating a strong diminishing of cells within the cell cycle (black bars).

Taken together, these findings indicate Pax6 controls mother centriole maturation by regulating the expression of the appendages protein Odf2. In a loss of Pax6, Odf2 expression is strongly suppressed and appendages are not or not properly formed. The missing or incomplete maturation of the mother centriole leads to a premature exit of mitotic cycle of RGP, especially during late neurogenesis.

III. DISCUSSION

III.1. Pax6 controls centrosome structure in RGP of developing cortex

Similarly to the Pax6 deficiency in the rat brain, the presented in this work results revealed a disturbance of INM, more specifically during late neurogenesis. Together with previous data from our lab suggesting a specific loss of upper layer neurons (Tuoc et al 2009), these results further support the view that Pax6 plays an intrinsic role mostly during the late corticogenesis. As shown by Tamai et al., (2009), in the rat *Small eye* cortex not only the INM but also the centrosome localisation was severely affected. INM is a microtubules motor protein-dependent process suggesting that the structure of the centrosome / centrioles, maybe be involved in correct functioning of INM. I show here that during RGP proliferation, TF Pax6 controls the correct structural assembly specifically of the mother centriole. During S-phase of the mitotic cycle, the centrioles duplicate to produce a pair of centrioles for each daughter cell (Kochanski & Borisy 1990). After cell division, one of the daughter cells keeps the mother centrosome (containing the former mother centriole), while the second cell receives the daughter centrosome (containing the former daughter centriole). Depending on their age, the two types of centrioles have structural differences. In a process designated as centrosome maturation, only the mother centriole acquires distal and subdistal appendages, while the daughter centriole lacks such structures (Azimzadeh & Bornens 2007, Azimzadeh & Marshall 2010). Consequently, only the mother centriole is in a position directly to anchor to cytoplasmic MTs at its appendages, e.g. at the VZ surface (Bettencourt-Dias & Glover 2007, Bornens 2002, Bornens & Azimzadeh 2007, Mogensen et al 2000, Nigg & Raff 2009).

Accumulating recent evidence indicate that asymmetric segregation of mother and daughter centrosomes could be a conserved mechanism involved in maintenance of the progenitor pool vs. differentiation capacity in eukaryotes (Wang et al 2009, Yamashita et al 2007). Cortical neurogenesis is a particularly clear example for a tight coordination between the asymmetric centrosome

inheritance and acquisition of specific cell fate. As recently reported, in developing cortex the mother centrosomes are preferentially inherited by the cells that remain in VZ for RGP renewing, while the daughter centrosomes are exclusively inherited by cells that differentiate and migrate towards CP (Wang et al 2009).

Using electron microscopy, I showed here for the first time profound structural abnormalities of the centrioles in RGPs of *Pax6/Small eye* mutant cortex. The performed analysis revealed that the number of centrioles with appendages in RGPs of E15.5 *Pax6*-deficient cortex was 2.5 folds diminished (~22 %) as compared with WT control brains (50 %). Furthermore, in contrast to the control brains where most of the centrioles were directly at (or at least very near to) the VZ surface and were connected to a primary cilium, in the *Sey/Sey* mutant very few centrioles extended a primary cilium, and the majority of them were at some distance from the ventricular surface. Before primary cilia assembly, the mother centrioles normally connect to a vesicle at their distal end. Centrioles with such a “mother-like” appearance were also detected in the *Sey/Sey* cortex. However, in accordance with data reported for the rat *Small eye* mutant (Tamai et al 2007), also in the mouse *Pax6*-mutant cortex such centrioles never connected to the cell membrane, suggesting abnormal maturation of the mother centrioles in *Pax6**LOF* condition.

Previous analysis indicated that centrioles in human lymphoblastoma cells (KE37 cell line) have up to nine distal and subdistal appendages (Paintrand et al 1992). Whether every mother centriole in every cell contains 9 appendages is still not clear. While some centrioles in RGPs from WT cortex contained up to three appendages, only few centrioles in *Sey/Sey* cortex showed up to two, and most of them showed only one appendage. Interestingly, basal bodies of multi-ciliated trachea cells contain only one subdistal appendage, called basal foot (Kunimoto et al 2012) that transmits the polarisation of the cell to the motile cilium and guarantees a coordinated beating and fluid flow. Thus, the structure of subdistal appendages appears to be not a static structure, but rather a structure that is optimized for specific function in the different cell types. Due to the fact that none of the centrioles of WT and *Sey/Sey* brains showed more than three appendages, it

is most likely that the mother centriole in cortical RGPs contains much less than 9 appendages.

The primary cilium is acting as a sensory organelle involved in registration/mediation of intracellular of intracellular signal transduction pathways such as Wnt/ β -catenin and Shh pathways (Goetz & Anderson 2010, Wallingford & Mitchell 2011). My results from the performed quantitative analysis using antibody against acetylated Tubulin revealed that even at stage E13.5, only half of the centrosomes in *Pax6**LOF* cortex extended cilia. To escape some technical restrictions of the IHC analysis at stage E15.5 (as pointed in the results), we applied again EM. As expected, the EM data revealed a much stronger reduction of primary cilia in E15.5 compared with at E13.5 *Sey/Sey* cortex. Thus, only ~6 % or ~35 % of the centrioles were connected to a primary cilium at apical surface of E15.5 *Sey/Sey* or WT cortex, respectively. These data reveals a dramatic loss of primary cilia at the ventricular surface in *Pax6*-deficient cortex. The question why only 35 % of WT centrioles are connected to cilia although 50 % show appendages appears to relate to the fact that not every mother centriole is located at the ventricular surface. Centrioles, which migrate basally to build up the spindle pole bodies or migrate apically after mitosis, show the characteristic appendages but are not connected to primary cilia.

In order to study more directly whether in *Pax6**LOF* an affected centriole maturation occurs, that may relates to migration problems of the daughter cell towards IZ and CP, I took advantage of the recently published method by Wang et al. (2009), reported to be applicable for studies in developing wild type cortex. The *Sey/Sey* embryos have severe malformations not only in the cortex, but also in the entire forebrain including the nose and eyes (Hill et al 1991) and are known as bad survivors upon *in vivo* manipulation. Therefore, I mastered and introduced in the Lab the shortened version of this method. Accordingly, 24 hours after *in vivo* electroporation of the Kaede-Centrin1 expression vector (encoding a photo switchable tag of Centrin1 used as specific marker of the centrosome) in E13.5 WT and *Pax6*-deficient brains, the electroporated brains were photo-switched *ex vivo* and 300 μ m thick sections were maintained for 48 hours as slice cultures. Despite different *pro* and *contra* for application of this version of the method (pointed already in the results), a very important priority of the applied shorter

version is the fact that the pregnant mother mouse is not operated a second time, which would severely diminish the number of survived embryos (Wang et al 2009). Despite such a precaution, the *Sey*^{+/+} pregnant mice did not survive the *in utero* electroporation. Therefore, the experiments were performed with *Pax6*^{fl/fl} females plugged with *Pax6*^{fl/fl}; *Emx1CreI*^{+/-} male mice thus carrying embryos in which the function of Pax6 was eliminated only in developing cortex *via* conditional inactivation, based on the Cre-LoxP strategy (Tuoc et al 2009).

So far, four embryos survived the electroporation procedure and were analysed. The results from the performed IHC analysis indicated a reduced number of centrosomes in VZ of *Pax6*^{LOF} cortex. Despite that no statistical relevance was found, the results can be accepted as a first hint that in *Pax6*-deficiency in addition to the differentiating cells, also cells carrying the mother centrosome (that otherwise should re-enter the cell cycle for RGP renewal) leave the VZ. Analysis of the distinct locations of mother and daughter centrosomes reveals a statistical relevant loss of mother centrosomes in the VZ indicating that indeed cells containing the mother centrosome (normally RGPs which re-enter the mitotic cycle (Wang et al 2009)) leave the ventricular zone prematurely and are lost as radial glia progenitor cells.

III.2. Pax6 dependent molecular mechanism controls the centrosome function

Aiming at identification of Pax6 interacting proteins that could influence the centrosome structure and function, I analysed a possible interaction, between Pax6 and three candidates for Pax6 protein partners, selected after a yeast-two-hybrid screen performed in our laboratory. The protein Kif2a, is a Kinesin motor protein involved in microtubules depolymerisation (Wordeman 2005), possible related to assembly of the centrioles. Hook2 is a linker protein linking cargo proteins or complexes to motor proteins (Szebenyi et al 2007) whose *C. elegans* homologue (zyc-12) connects the centrosome to the nucleus (Gonczy 2004). The third one, Nedd9, is a scaffolding protein of the Cas family, involved in the β -1 integrin pathway located in the centrosomes. However, after co-transfection with *Pax6* in NIH3T3 cells, none of the potential binding partners showed a co-

localisation with Pax6: while all three proteins were located in the cytoplasm, TF Pax6 was exclusively localized in the nucleus. Furthermore, co-immunoprecipitation of Pax6 and the potential binding partners failed in all three cases, indicating no interaction potency between Pax6 and the studied three centrosome-associated proteins.

To study furthermore whether Pax6 in general has the ability to interact with the centrosome through protein / protein interactions, an IHC with antibodies for γ -Tubulin and Pax6 was performed. The IHC confirmed that as a transcription factor, during the interphase Pax6 is exclusively located in the cell nucleus. During the mitosis, the nuclear membrane is degraded and Pax6 is evenly distributed all over the cytoplasm, however, an accumulation at the spindle poles has not been detected. As recently reported by Asami et al., (2011), the RGPs in *Pax6*-deficient cortex show abnormal cleavage angle, most probably due to a direct regulation of the spindle-specific expression of the *Spag5* gene. In the presented here work, I showed data indicating that a direct regulation of *Odf2* expression by TF Pax6 is a novel important molecular mechanism involved in centrosome dysfunction in *Pax6*LOF cortex.

Odf2 came into the focus of my study because it is a protein specifically expressed at the subdistal appendages, and similarly to TF Pax6 exerts a restricted expression in the developing forebrain. Moreover, *Odf2*-deficient cells also show loss of primary cilia (Ishikawa et al 2005) as seen and shown in this work for RGPs in the *Sey/Sey* mutant. Intriguingly, QIAGEN SABiosciences identified Pax6 as a relevant transcription factor for *Odf2* in a chromatin immunoprecipitation assay (http://www.sabiosciences.com/chipqpcrsearch.php?factor=Over+200+TF&species_id=0&ninfo=n&ngene=n&nfactor=y&gene=ODF2).

Upon co-expression of *Odf2*-promoter-*luciferase* and *CMV-Pax6* expression constructs in NIH3T3 cells *in vitro*, only a slight transactivation of the reporter was measured, possibly due to the fact that *Odf2* is endogenously expressed in this cell line and / or other factors are absent. Interestingly, three Pax6 consensus-binding sequences were identified in the *Odf2* promoter. Remarkably, the results from the performed EMSA clearly indicated that one of these sites strongly binds Pax6 and is involved in transcriptional regulation of *Odf2* expression *in vitro*. Thus, these *in vitro* results reveal that *Odf2* is a direct downstream target of TF Pax6.

To prove whether a genetic interplay between Pax6 and *Odf2* exists also *in vivo*, a detailed expression analysis were undertaken using *in situ* hybridisation on brain sections as well as a quantitative PCR analysis with isolated mRNA samples from cortex of embryos of both genotypes (wild type and *Sey/Sey*). In a striking accordance with the discovered defect of centrosome structure and function mostly during late neurogenesis, both approaches indicated that the expression of *Odf2* was severely down regulated in the *Pax6*-deficient cortex, much more pronounced at E15.5, as compared with E13.5. The results from the quantitative rt-PCR analysis confirmed the conclusion for approximately ~50 % reduction of *Odf2* mRNA in the whole cortex at this later stage. Given that *Odf2* is expressed not only in RGP, but also in differentiating cells (Wilsch-Brauninger et al 2012), the reduction of *Odf2* mRNA in cortical RGP in a lack of Pax6 might be even stronger than 50 %, compared to controls.

To analyse whether the protein level is reduced in Pax6-deficient brains, an IHC was performed on E13.5 and E15.5 brain sections. As expected, the reduction of Odf2 protein was strongest at E15.5, where almost no Odf2 protein was detectable anymore. While in WT cortex Odf2 was clearly expressed at almost every centrosome at both E13.5 and E15.5, in the *Sey/Sey* mutant, a remarkable higher number of γ -Tubulin⁺ centrioles were missing Odf2 expression already at E13.5.

To sum up, the results from the performed *in vitro* and *in vivo* analysis, revealed that TF Pax6 directly regulates the expression of *Odf2*. Thus, as a consequence of disrupted function of *Pax6*, the maturation of the mother centrioles is disrupted and they fail to extend primary cilia at the VZ surface as seen in the *Small eye* mutant.

Interestingly, in parallel of the inhibition of *Odf2* expression in *Sey/Sey* cortex, we found *via* IHC a massive down regulation of Ninein expression at subdistal appendages. This is in accordance with previous publications (Ibi et al 2011, Ishikawa et al 2005) showing that a loss of Odf2 causes a loss of Ninein at the subdistal appendages. Previous report also indicated a down regulation of *Ninein* on mRNA level in the *Sey/Sey* brain (Asami et al 2011). Whether the inhibited *Ninein* expression could be caused by the down regulation of *Odf2* can only be speculated. Giving the fact, that Odf2 is not a transcription factor, a direct regulation between Odf2 and *Ninein* seems implausible. On the other hand, no

data are available up to now, for a direct regulation of *Ninein* expression by TF Pax6. One possibility for further experimentation could be that Pax6 exerts an indirect control on *Ninein* expression *via* another still unknown factor.

Ninein is an important centrosome protein located at the minus ends of microtubules, connecting them with the subdistal appendages of the mother centriole to build up the microtubules aster. Loss of Ninein and therefore a defect in the connection between the subdistal appendages and the microtubules system is assumed to be involved in distortion of INM (Bornens 2002). It should be noticed, however, that Ninein is not exclusively expressed at the subdistal appendages of the mother centriole, and is involved in capping the minus ends of microtubules, not only at the centrosome but also in unbound microtubules (Bornens 2002, Moss et al 2007, Ohama & Hayashi 2009). Therefore, even a full loss of Ninein could not explain the specific and complete loss of subdistal appendages in Pax6-loss-of-function brain.

To directly examine the role of *Odf2* expression level in cortical RGPs, I performed knock down experiments *in vivo via in utero* electroporation using *Odf2* short-hairpin constructs. Two of the tested constructs showed a strong capacity to knock down *Odf2* expression up to >95 %. Remarkably, the *Odf2KD* *in vivo* caused a massive loss of electroporated RGPs (GFP⁺/Pax6⁺) in VZ, compared to the controls. Depending on the used short hairpin construct, a loss of ~80 %, respectively ~75% was visible. Interestingly, knock down of *Ninein* causes a very similar effect (Wang et al 2009), suggesting a role of the subdistal appendages for the re-entry of RGPs into the cell cycle. The same effect after knock down of *Ninein*, respectively of *Odf2*, is in accordance with previous publications stating that a loss of *Odf2* causes a loss of subdistal appendages and therefore a loss of Ninein (Ibi et al 2011, Ishikawa et al 2005).

A loss of connection to the apical surface could lead to increase of so called outer subventricular zone progenitors (OSVZPs). These progenitors show the same molecular characteristics like RGPs but exhibit an ectopic position in the outer SVZ. It would be possible that a disturbed centrosome function especially at the connection between centrosome and microtubules aster also affect the adherence junction complex, which is essential for the connection of the apical process of the RGPs. However, the loss of Pax6 expression in the outer SVZ in *Sey/Sey* cortex indicates that this is not the case.

Indeed, the results from the performed analysis of RGPs exit from mitotic cycle revealed that the number of cells, which re-entered the cell cycle after the last cell division within the last 24 hours, was dramatically reduced after *Odf2KD*. While in the control almost 60 % of the electroporated cells re-entered the mitotic cycle, only ~26 % did so after *Odf2KD*. This indicates that cells containing abnormally assembled mother centrosome (with reduced or missing subdistal appendages) fail to re-enter the cell cycle and possibly prematurely differentiate. Interestingly, the number of renewing RGPs (GFP⁺/BrdU⁺/Ki67⁺) was reduced not only in VZ; but also in SVZ, suggesting that in absence of Odf2, not only the re-entry of RGPs into the cell cycle was affected, but also generation of IPs failed.

III.3. Put the things together

In this work, I have shown that a loss of Pax6 during cortical neurogenesis leads to a down regulation of *Odf2* expression in RGPs. Without Odf2, the formation of subdistal appendages of the mother centrioles fails. As a consequence, the mother centrosomes in apical RGPs fail to assemble primary cilia at the ventricular surface. This is in accordance with previous publications stating that Odf2 is essential for the assembly of subdistal appendages at the mother centriole, the recruitment of Ninein to the subdistal appendages and for the assembly of primary cilia in F9 cells (Ibi et al 2011, Ishikawa et al 2005). The loss of primary cilia would lead to dramatic consequences for RGPs because these sensory organs of the cells mediate signalling of several pathways. As a second consequence of *Odf2* dis-regulation in *Pax6LOF*, the recruitment of Ninein to the abnormal or missing subdistal appendages fails. In accordance with reported loss of RGPs at the apical VZ in the absence of Ninein at the subdistal appendages (Wang et al 2009), *Odf2KD* caused a similar phenotype, as reported in this work. Furthermore, I presented evidence that such mis-located RGPs actually exit from the mitotic cycle, more evident during the late cortical neurogenesis, shown previously as a specific defect in corticogenesis after conditional *Pax6KO in vivo* in which generation of upper layer neurons were almost fully abrogated (Tuoc et al 2009). Together, the presented here novel data strongly suggests that regulation of *Odf2* expression in subdistal appendages of the mother centrioles in RGPs is a main

Pax6-dependent molecular mechanism involved in specification of neuronal subtypes during later stages of cortical neurogenesis.

An interesting question is why a protein like Odf2, which is not exclusively expressed in RGPs but also in many other different cell types (Carlisle et al 2012, Ibi et al 2011, Kunimoto et al 2012, Schweizer & Hoyer-Fender 2009) is regulated by such a cell type specific TF as Pax6. One possibility may be that *Odf2* expression in differentiated cells is regulated by a transcription factor, which is missing in stem cells. It seems possible that such a transcription factor is also not present in RGPs of developing cortex and therefore a RGP specific TF (Pax6) overtakes regulation of *Odf2* expression. As mentioned before, the number of subdistal appendages in different cell types is not fixed, implicating that also the amount of Odf2 should be different. Therefore, another possibility would be that *Odf2* is specifically regulated in each distinct cell type by specific transcription factors.

The molecular mechanism that regulates the correct position and proper function of INM in RGPs is most likely microtubules based. A breakdown of connection between centrosome and microtubules system appears to cause an incomplete or missing recruitment of the mother centriole to the cell membrane at the ventricular surface. The missing anchorage could then explain why the centrosome moves basally to the nucleus. On the other hand, when the connection between centrosome and nucleus is disturbed, the nucleus fails to move apically. It is a plausible mechanism to explain the defects in centrosome location that accompanied the defective INM in *Pax6LOF* cortex (Tamai et al 2007).

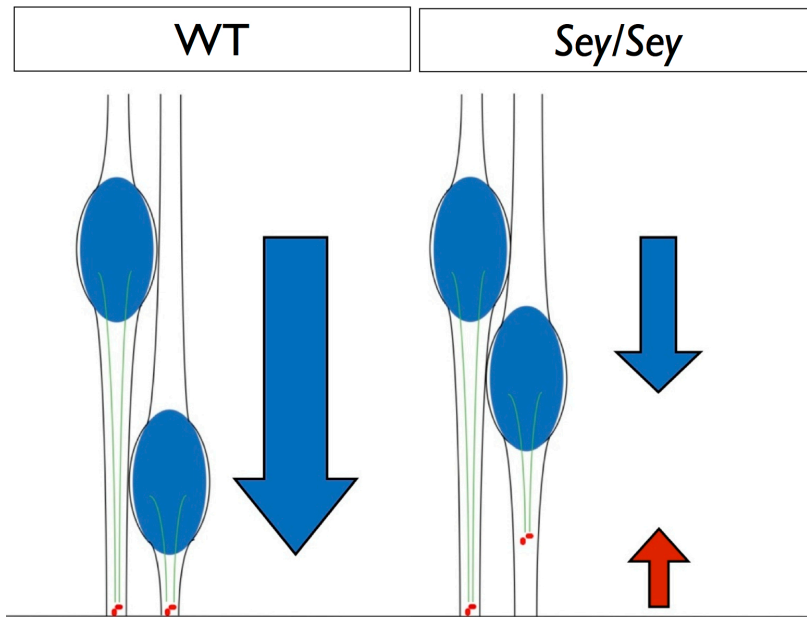


Fig. V.1. Schematic overview of mechanistic consequences due to loss of Odf2. The Centrosome (red) anchored at the cell membrane at the ventricular surface pulls down the nucleus (blue) in WT RGPs. The missing anchorage of the centrosome in *Sey/Sey* RGPs leads to basal movement of the centrosome and a slower or incomplete basal to apical transition of the nucleus. Adopted from Tamai et al 2007.

In my view, the most interesting effect of loss of Odf2 in RGPs is the failure of RGPs to re-enter into the cell cycle after division. The reasons for this are still not clear. Interestingly, the mother centrosome remains not only in the stem cells of the developing cortex but also in other kind of stem cells (Yamashita et al 2007).

The results of Wang et al., (2009) as well the presented in this thesis work data strongly support the view that a proper maturation of the mother centriole is necessary that RGPs re-enter the cell cycle, thus maintaining the progenitor pool throughout the cortical neurogenesis. The reasons for that can only be speculated. Most likely, the microtubules aster is an intrinsic factor for this mechanism. The mother centriole as the centre of the aster, might be the meeting point of intrinsic factors for re-entry into the cell cycle. The cell, which contains the mother centrosome, also contains the factors for cell cycle re-entry. Without a proper microtubules aster these factors are evenly distributed over both daughter cells and both daughter cells fail to enter the cell cycle again.

During early neurogenesis Pax6 is strongly expressed in the rostral lateral cortex with lowest expression in the caudal medial cortex. During late neurogenesis the Pax6 expression becomes more uniform, therefore increases in

the caudal medial cortex (Mi et al 2013). These authors showed a shortening of the cell cycle during late neurogenesis in *Sey/Sey* embryos indicating that *Pax6* is an important regulator of the cell cycle during late neurogenesis (Mi et al 2013). These findings together with our previous results (Tuoc et al 2009) indicate the importance of *Pax6* for the generation of upper layer neurons during late neurogenesis. Recent report revealed existence of fate restricted *Cux2*⁺ RGPs at the onset of neurogenesis, which enter into neurogenic divisions not before the beginning of late neurogenesis (Franco et al 2012). Most probably the regulation of *Odf2* by *Pax6* is of importance in this population of *Cux2*⁺ progenitors. This would be an interesting question for further investigations.

TF *Pax6* is known for more than 20 years as a powerful developmental regulator, however little is still known about the molecular mechanisms involved. As intrinsic determinant of cortical RGPs, *Pax6* regulates the mitotic cycle of these cells at transcriptional level, including *Cdk6* (Mi et al 2013) and *Spag5* genes (Asami et al 2011), the last one encoding for a microtubules associated protein with a role for determination of the cleavage angle during cell mitosis. Here, I showed a novel mechanism for regulation of RG division that involves a transcriptional control by *Pax6* on the expression of *Odf2*, specifically in the subdistal appendages of the mother centriole, that causes severe structural defects of the centrosome and its function. The regulation of the appendage protein *Odf2* is only a brick in the complex molecular mechanisms controlled by TF *Pax6* in developing brain.

IV. MATERIAL AND METHODS

IV.1. Material

IV.1.1. Biological material

IV.1.1.1. Bacterial strains

Escherichia coli strain DH5 α was used for subcloning and keeping of plasmid DNA.

IV.1.1.2. Cell lines

For *in vitro* cell culture experiments NIH3T3 cells (embryonic mouse fibroblasts) were used (Jainchill et al 1969).

IV.1.1.3. Vectors

Vector	Gene	Origin	Application
pGFP-V-RS	Odf2 SH Nr.58; 59; 60; 61 Control K07	OriGene	Odf2 knock down
pCS2+	Pax6-Flag;	Dep. mol. cell biol.	<i>in vitro</i> over expression
pCMV-HA	Nedd9; Hook2; Kif2a; Odf2	Dep. mol. cell biol.	<i>in vitro</i> over expression
pCIG2	GFP	Francois Guillemot	<i>in vivo</i> over expression
pSilencer2.0-U6	Odf2 SH Nr.1-8	Ambion	knock down experiments
pCDNA3.1	hHook2	Helmut Krämer	Subcloning
CMV-Pax6	Pax6	Dep. mol. cell biol.	<i>in vitro</i> over expression
pSP64-Pax6	Pax6	Dep. mol. cell biol.	<i>in vitro</i> over expression

IV.1.1.4. Oligonucleotides

The Oligonucleotides were purchased from Sigma-Aldrich

Sequence	Name	Application
CATAGTCGACCACCATGTGGGC	Nedd9 forNedd9 for Sall	Subcloning
GATCTCGAGTTCAAAAGGTGGCC	Nedd9 revNedd9 rev XhoI	Subcloning
CTAAGTCGACCACCATGACTTCC	Tax1bp1 forTax1bp1 for Sall	Subcloning
GAAGTCGAGTCTAGTCGAAGTTGAG	Tax1bp1 revTax1bp1 rev XhoI	Subcloning
CATAGTCGACCACCATGGCCATTG	Lzts2 for Sall	Subcloning
GTTTGCGGCCGCTCTAGATCTCAG	Lzts2 rev NotI	Subcloning
CATAGTCGACCACCATGGCAAC	Kif2a for Sall	Subcloning
GATCTCGAGTTTAGAGGGCTCGG	Kif2a rev XhoI	Subcloning
CTTCGTCGACCACCATGAGTGTGG	Hook2 for Sall	Subcloning
GTTTGCGGCCGCTTCAGTGC	Hook2 rev NotI	Subcloning
CCTCGTCGACCACCATGAAGTAC	Nedd9 for Sall2	Subcloning
GGAGAATTCATACCATGTGGGCGAG	Nedd9 for EcoRI	Subcloning
GATTCGGCCGCTCAAAAGGTGG	Nedd9 rev NotI	Subcloning
GGAGAATTCATACCATGGCCATTG	Lzts2 for EcoRI	Subcloning
CAGAATTCAAACCATGAGCGTGGAC	hHook for EcoRI	Subcloning
GACCTCGAGTCAGTGCTTGTCACTG	hHook rev XhoI	Subcloning
CTTCTAGGCCTGTACGGAAGTG	pCMV-HA for Seq Primer	Sequencing
GAAGAATTCACCATGGCAACG	Kif2a for EcoRI	Subcloning
GAAGAATTCATACCATGGCAACGGC	Kif2a for EcoRI 2.0	Subcloning
GATTCTCGAGTTAGAGGGCTCGGG	Kif2a rev XhoI 2.0	Subcloning
GAGGAATTCATACCATGACATCC	Tax1bp1 for EcoRI	Subcloning
CCGAGGATCCACCATGGCCTC	Centrin2 for BamHI	Subcloning
CGCCGAATTCATAGAGGCTGGTC	Centrin2 rev EcoRI	Subcloning
CGCGAATTCATGAGTCTGATTAAAC	Kaede for EcoRI	Subcloning
GACCTCGAGTTACTTGACGTTGTCC	Kaede for XhoI	Subcloning
CTTCTCGAGCACCATGGCCTC	Centrin2 for XhoI	Subcloning
GAACCCGGGATAGAGGCTGG	Centrin2 rev SmaI	Subcloning
CTTCCCGGATGAGTCTGATTAAAC	Kaede for SmaI	Subcloning
GTAGCGGCCGCTTACTTGACG	Kaede rev NotI	Subcloning
TCCACGGTCGCCAAGGCATTGTCCAGGGAA	CasL KO for	Genotyping
CGGACTTGAAGAAGTCGTGCTGCTTCATGT	G2CasL KO rev1	Genotyping
GCCATTTAGTATGTTTGCTTTGGGGC	CasL KO rev2	Genotyping
CCTACAGCTCCTGGGCAA	pCIG2/pCIK for Sequenzierung	Sequencing
GCTTCGGCCAGTAACGTT	pCIG2 rev Sequenzierung	Sequencing
CAAAAAATTCCAACACACTATTGC	pCI rev Sequenzierung	Sequencing
CTTTTCCATCTCCCTCAATAA	pCIK rev	Subcloning
GGACTCGGGGATGGAAGAGGAAG	Cdk5rap2 for	Subcloning
CATGAGCCCGGTCTGCTGG	Cdk5rap2 rev	Subcloning
CGTAGGCAAAAGGGAGAG	pCIK rev Sequenzierung	Sequencing
GTTCGGCTTCTGGCG	pCIK for Sequenzierung	Sequencing
CAGTTCTTTGATGTCTATAGTTCC	pCIK for/rev Sequenzierung	Sequencing
CTTCTCGAGCACCATGGCGTC	Centrin1 for XhoI	Subcloning
GAACCCGGGTAAATAAAGGTTGGTC	Centrin1 rev SmaI	Subcloning
CAGAGTGGAGACAATGATTCGTGGAGATTATAAC	Pax6 binding sequence in Odf2 1	EMSA

AC	Promotor forward Primer	
GTGTTATAATCTCCACGAATCATTGTCTCCACTCT	Pax6 binding sequence in Odf2 1	
G	Promotor reverse Primer	EMSA
TTGCACGCACAAAATGAACCGTCAAGGGTTGACG	Pax6 binding sequence in Odf2 2	
AAC	Promotor forward Primer	EMSA
GTTCGTCAACCCTTGACGGTTCATTTGTGCGTGC	Pax6 binding sequence 2 in Odf2	
AA	Promotor reverse Primer	EMSA
GTGGGAAGGTAGTTCACGCTCCAGGGAGGAGCT	Pax6 binding sequence 3 in Odf2	
GGTG	Promotor forward Primer	EMSA
CACCAGCTCCTCCCTGGAGCGTGAACCTACCTCC	Pax6 binding sequence 3 in Odf2	
CAC	Promotor reverse Primer	EMSA
CCCGAATTCCCACCATGAAGG	Odf2 Eco for	Subcloning
CACCTCGAGTCAGGCAGGGG	Odf2 Xho rev	Subcloning
GGTGAATTCCCACCATGAAGGAC	Odf2 Eco for2	Subcloning
CAACTCGAGTCAGGCAGGGG	Odf2 Xho rev2	Subcloning
CAAGTCGACCCACCATGAAGGACCG	Odf2 Sal for	Subcloning
CTTGCGGCCGCTCAGGCAGGG	Odf2 Not for	Subcloning
ATGAAGGACCGATCTTCAACTCC	Odf2 for	Subcloning
TCAGGCAGGGGGCGATC	Odf2 rev	Subcloning
AGCCCCAAAATGGTTAAGGTTGC	mHPRT-for	q-rtPCR
TTGCAGATTCAACTTGCCTCAT	mHPRT-rev	q-rtPCR
ACCA TGAAGGACCGCTCTTC	Odf2-for	q-rtPCR
CGCACATTCACAGTGTCCCC	Odf2-rev	q-rtPCR

IV.1.1.5. Enzymes

IV.1.1.5.1. Restriction enzymes

Enzyme	Company
BamHI	NEB/Fermentas
EcoRI	NEB/Fermentas
NotI	NEB/Fermentas
SalI	NEB/Fermentas
SmaI	NEB/Fermentas
XhoI	NEB/Fermentas

IV.1.1.5.2. DNA-Polymerase

Enzyme	Company	Application
Taq Polymerase	Promega	Genotyping
Phusion	Finnzymes	Subcloning

IV.1.1.5.3. DNA Ligases

Enzyme	Company
T4-Ligase	NEB

IV.1.1.5.4. DNA Phosphatase

Enzyme	Company
Antarktic Phosphatase	NEB

IV.1.1.6. Antibodies

IV.1.1.6.1. Primary Antibodies

Target Protein	Host	Origin	Dilution	Application
Acetylated Tubulin	Mouse IgG2b	Sigma	1:200	IHC
GFP	Chicken IgGY	Abcam	1:500	IHC
HA-Tag	Rat	Roche	1:500	Westernblot
Ninein	Rabbit	Abcam	1:500	IHC
Odf2	Rabbit	Self-made S.H.-F.	1:50	IHC
Pax6	Rabbit	Covance	1:300/1:1000	IHC/Westernblot/EMSA
Pax6	Mouse	DSHB	1:200	IHC
Phosphorylated Histon H3	Mouse IgG1	Cell signalling	1:100	IHC
Sox2	Rabbit	Millipore	1:200	IHC
tGFP	Mouse IgG2b	Origene	1:100	IHC
Tuj	Mouse IgG1	Millipore	1:200	IHC
β -Actin	Mouse IgG1	Sigma	1:2000	Westernblot
γ -Tubulin	Rabbit	Sigma	1:500	IHC

Antibodies for IHC / ICC were diluted in blocking solution; antibodies for Westernblot were diluted in 5 % milk powder in TBST

IV.1.1.6.2. Secondary antibodies

IV.1.1.6.2.1. Secondary antibodies for Westernblot

Target protein	Host	Origin	Dilution
Anti Rabbit IgG	Goat	Covance	1:10,000
Anti mouse IgG	Goat	Covance	1:5,000
Anti Rat IgG	Goat	Covance	1:10,000

Antibodies were diluted in 5 % milk powder in TBST

*IV.1.1.6.2.1. Secondary antibodies for immunohistochemistry /**immunocytochemistry*

As secondary antibodies for IHC and ICC Alexa Fluor[®]-coupled antibodies from Molecular Probes were used in a dilution of 1:400 in blocking solution. Antibodies were coupled to fluors 488, 555, 568 and 647, produced in mouse, rabbit, chicken, guinea pig, goat and rat.

IV.1.2. Culture mediaIV.1.2.1. Culture media for *E.coli* cultures

Name	Ingredients
Luria-Bertania (LB)-medium	1 % (w/v) Pepton 0.5 % (w/v) Yeast extract 0.5 % (w/v) NaCl pH 7,5 Diluted in milliQH ₂ O
LB-Agar plates	1.5 % (w/v) Agar in LB-medium
Ampicillin-medium	50 µg/ml Ampicillin in LB-medium
Kanamycin-medium	50 µg/ml Kanamycin in LB-medium

IV.1.2.2. Culture media for eukaryotic cell culture

Name	Ingredients
DMEM with FCS and Pen/Strep	85 % (v/v) DMEM 10 % (v/v) FCS 5 % (v/v) Penicillin/Streptomycin (5000 u)
Brain slice culture medium	50 % (v/v) Eagle's Basal Medium 25 % (v/v) Hank's balanced salt solution 5 % (v/v) FCS 1 % (v/v) 100x N2 supplement 1 % (v/v) 100x Penicillin/Streptomycin 1 % (v/v) 100x Glutamin 0.66 % (w/v) D-(+)-glucose (Sigma)
Brain preparation solution	Earl's Balanced Salt Solution

All media and supplements were ordered from Gibco BRL Life Technologies.

IV.1.3. Buffers and solutions

Name	Ingredients
Binding buffer (EMSA)	25 mM HEPES; pH 7.4 10 % (v/v) glycerol 75 mM NaCl 0.25 mM EDTA 1 mM DTT 0.1 % (v/v) Nonidet P-40 1 mM MgCl ₂ Protease inhibitor
Blocking solution (IHC / ICC)	0.1 % (v/v) Triton X-100 10 % (v/v) normal goat serum in PBS
Blocking solution (<i>in situ</i> hybridisation)	10 % normal sheep serum in KTBT
CaCl ₂ Solution	60 mM CaCl ₂ 15 % (v/v) Glycerol 10 mM PIPES pH 7.0
DNA loading buffer	25 % (w/v) Ficoll 100 mM EDTA 0.05 % (w/v) Bromophenol Blue
Epon A	60 ml Epon 50 ml DDSA
Epon B	40 ml Epon 22.5 ml MNA

Epon final solution	Epon A: Epon B 6:4 1.8 % (v/v) DMP-30
Ethidiumbromide	10 mg/ml Ethidiumbromide working solution 5 µg/ml
Hybridisation buffer	50 ml Formamide 25 ml 20 x SSC pH4.5 1g blocking powder 1 ml 0.5 M EDTA 1 ml of 100 mg / ml total RNA 0.1 ml of 100mg/ml Heparin 0.1 ml Tween-20 1 ml 10 % CHAPS add to 100 ml H ₂ O
KTBT	100 ml 1 M Tris-Cl pH 7.5 60 ml 5 M NaCl 20 ml 1 M KCl 20 ml Tween-20 add to 2 l H ₂ O
2x Laemmli-probe-buffer	62.5 mM Tris, pH 6.8 2 % (w/v) SDS 10 % (v/v) 2-β-Mercaptoethanol 0,001 % (w/v) Bromophenol Blue 10 % (v/v) Glycerol
10 x Laemmli electrophoreses buffer	0,25 M Tris 2 M (w/v) Glycin 1 % SDS
Lysis buffer for CoIP	1 x PBS 1 % (v/v) Nonidet P40 1 % 100 x ProteoBlock™ Proteinase inhibitor cocktail (Fermentas)
Lysis buffer for genotyping of embryonic mouse tissue	100 mM Tris; pH 8.5 200 mM NaCl 5 mM EDTA 0.2 % SDS 250 µg/ml Proteinase K
Lysis buffer for luciferase assay	150 mM HEPES; pH 5.2 0.25 % (v/v) Triton X-100
NTMT	100 ml 1 M Tris pH 9.5 20 ml 5 M NaCl 50 ml 1 M MgCl ₂ 1 ml Tween-20 0.24 g Levamisole add to 1 l H ₂ O
Osmium	1% (v/v) aqueous solution of OsO ₄

	0.15 M Sörensen
Paraformaldehyd (PFA)	4 % (w/v) Paraformaldehyd in 1 x PBS (pH 7.4)
Postfixation	4 % (w/v) PFA 0.2 % (v/v) Glutaraldehyde in 1x PBS (pH7.4)
Proteinase K	50 ml 1M Tris Cl pH 8.0 10 ml 0.5 M EDTA 0.5 ml Proteinase K (10 mg/ml) add to 1 l H ₂ O
10 x PBS	1.3 M NaCl 70 mM Na ₂ HPO ₄ +2H ₂ O 30 mM KH ₂ PO ₄ pH 7.4
0.3 M Sörensen solution1	41.37g KH ₂ PO ₄ x H ₂ O ad to 1 l H ₂ O
0.3 M Sörensen solution 2	42.58g Na ₂ HPO ₄ ad to 1 l H ₂ O
0.3 M Sörensen final solution	18.2 % (v/v) solution 1 81.8 % (v/v) solution 2 Mixing short before usage
TBST	20 mM Tris pH 7.5 300 mM NaCl 0.2 % (v/v) Triton [®] X-100
0.5 x TE-buffer	45 mM Tris-borate; pH 8.0 1 mM EDTA
Transferbuffer	1 M Tris 0.2 M Glycin 0,4 mM MgCl ₂ 0,04 % (w/v) SDS 8 % (v/v) Methanol

If no other indications, solutions and buffer were assembled in milliQH₂O.

IV.1.3.1. Gels for SDS-PAGE

Component	Separation gel (20 ml)	Collecting gel
30 % Aclamid M-Bis	6.7 ml	13.3 ml
1.5 M Tris	5.2 ml	5.2 ml
SDS	0.2 ml	0.1 ml
10 APS	0.2 ml	0.2 ml
TEMED	0.008 ml	0.008 ml
H2O	7.9 ml	1.3 ml

IV.1.4. Chemicals

Name	Company
1 kb DNA Ladder	GeneCraft / NEB
100 bp DNA Ladder	GeneCraft / Fermentas
Acrylamid M-Bis	Roth
Agarose	Roth
Blocking powder	Boehringer
Bromdesoxyuridin (BrdU)	Sigma-Aldrich
Diethylpyrocarbonate (DEPC)	Sigma-Aldrich
DMP-30	SERVA
Dodecenylbersteinacidanhydrid (DDSA)	SERVA
Epon	SERVA
Ethidiumbromide	Roth
Fast Green	Sigma-Aldrich
Glutaraldehyd	SERVA
Levamisole	Sigma-Aldrich
PageRuler™ Prestained ProteinLadder	Fermentas
peqGOLD RNAPure™	PEQLAB
Methylnadicanhydrid (MNA)	SERVA
N,N,N',N',-Tetramethylendiamin (TEMED)	Sigma-Aldrich
NBT / BCIP	Roche
dNTPs	NEB
Paraformaldehyd	Sigma-Aldrich
Propylenoxid	SERVA
Sodium dodecylsulfate (SDS)	SERVA
Transfectin®	BioRad
Vectashield with DAPI	Vector Laboratories

All other chemicals were purchased from Merck.

IV.2. Methods

IV.2.1. Microbiological methods

IV.2.1.1. Culture of *E. coli*

E.coli were cultured at 37 °C over night at 220 rpm. Antibiotics were added as described.

IV.2.1.2. Storage of *E. coli* cultures

200 µl Glycerol were added to 800 µl of an over night culture and stored at -80 °C.

IV.2.1.3. Production of competent bacteria

4 ml of an over night culture were added to 400 ml LB medium and incubated at 37 °C until an OD 600 of 0.35 to 0.4. The cultured medium was aliquoted into 50 ml pre-chilled Falcon tubes and incubated for 5 to 10 minutes on ice. The cultures were centrifuged at 4 °C for 7 minutes at 16,000 x g. The supernatant were discarded and the pellets were resuspended in 10ml pre-chilled CaCl₂ solution and centrifuged at 1,100 x g at 4 °C for 5 minutes. The supernatants were discarded and the pellets were resuspended in 10 ml pre-chilled CaCl₂ solution and incubated for 30 minutes on ice. The solution were centrifuged for 5 minutes at 1,100 x g at 4 °C. The supernatants were discarded again and each pellet was resuspended in 2 ml pre-chilled CaCl₂ solution. 200 µl of the solutions were aliquoted into Eppendorf reaction tubes, immediately frozen in liquid nitrogen and stored at -80 °C.

IV.2.1.4. Transformation

Transformation by heat shock into competent *E. coli* strains (DH5 α) was performed as described by D. Hanahan (Hanahan 1983).

Cells were defrosted on ice and 50 μ l of the cells were added to the DNA (~1 ng of plasmid DNA or 5 μ l of a 20 μ l Ligation solution). Cell and DNA were incubated for 20 minutes on ice. Heat shock was performed for 90 seconds at 42 °C. 200 μ l LB medium without antibiotics were added and incubated for at least 30 min at 37 °C. The solution was added on LB-Agar plate containing selective Antibiotics and incubated at 37 °C over night.

IV.2.1.4. DNA preparation

DNA preparation was performed with DNA preparation Kits from QIAGEN[®] as indicated. These protocols are based on the alkaline lysis from H.C. Birnboim and J. Doly (Birnboim & Doly 1979). DNA preparation for *in utero* electroporation was performed with QIAGEN[®] EndoFree[®] Maxi Kit and Macherey-Nagel NucleoBond EF[®] Maxi Kit as indicated in the provided instruction manual.

IV.2.1.5. Extraction of genomic DNA from embryonic mouse tissue

Tissue from embryonic mice were digested in 500 μ l lysis buffer at 55 °C for 2 hours up to over night. DNA was precipitated with 1.2 volume isopropanol and centrifuged for 10 minutes with 13,000 rpm. The precipitated DNA was washed with 500 μ l of 70 % Ethanol. After centrifugation (10 min; 13,000 rpm) DNA was air dried and dissolved in 200 μ l H₂O.

IV.2.1.5. Polymerase chain reaction (PCR)

Polymerase chain reaction was used for amplification of DNA fragments for subcloning or genotyping (Saiki et al 1988). In general, 100 ng of DNA were used as template. For genotyping of *Pax6cKO* mice 1 μ l of Kit-prepared DNA was used. The PCR reaction programs were performed by an Eppendorf Master cycler.

For genotyping following reaction mix was prepared:

5 µl	10 x Promega GoTaq [®] Buffer
0,25 µl	dNTP mix
1 µl	DNA Solution
1 µl	forward primer
1 µl	reverse primer
1 µl	Promega GoTaq [®] Polymerase
Add to 50 µl with sterilized milliQH ₂ O	

For amplification the following program was used:

1. Initial denaturation	95 °C	2 min
2. Denaturation	95 °C	30 sec
3. Annealing	55-65 °C	30 sec
4. Extension	72 °C	~2 min/kb
5. Steps 2 to 4	30 x	
6. Final extension	72 °C	10 min

For amplification of cDNA for subcloning following reaction mix was prepared:

10 µl	Phusion [®] HF Buffer
1 µl	dNTP mix
1 µl	forward primer
1 µl	reverse primer
0.5 µl	template DNA
0.5 µl	Phusion [®] DNA Polymerase
Add to 50 µl with sterilized milliQH ₂ O	

For amplification the following program was used:

1. Initial denaturation	98 °C	30 sec
2. Denaturation	98 °C	5-10 sec
3. Annealing	55-65 °C	10-30 sec
4. Extension	72 °C	15-30 sec/kb
5. Steps 2 to 4	25-35 x	
6. Final extension	72 °C	10 min

IV.2.1.6. Quantitative real time PCR (q-rtPCR)

Total RNA was extracted from cortex cells by peqGOLD RNAPure™ and digested with RQ1 DNase. cDNA was generated from 0.5 µg of total RNA using RevertAid™ H Minus First Strand cDNA Synthesis Kit (Fermentas) and oligo(dT)₁₈ primer. Real time PCR was performed on iCycler IQ PCR System (BioRad) using cloned *Odj2* and *Hprt* fragments, respectively as standard for quantification. The specificity of the SYBR Green assay was verified by melting curve analysis.

IV.2.1.7. DNA electrophoresis

1% agarose in 0.5 x TE buffer was prepared together with 0.3 µg/ml Ethidiumbromid. The DNA was mixed with 5 x DNA loading buffer. Electrophoresis was performed in 0.5 x TE buffer under 1-6 V/cm.

IV.2.1.8. DNA purification

IV.2.1.8.1. Isolation of DNA from agarosegels

DNA was isolated and purified with QIAGEN® QIAquick Gel Extraction Kit® as indicated in the provided instruction manual.

IV.2.1.9. Enzymatic modification of DNA by restriction enzymes

For analytical DNA digestion 50 µg DNA were digested with 1 µl of the provided restriction enzyme at 37 °C for 15 to 30 minutes. An activation of the enzyme was performed at 80 °C for 10 minutes

IV.2.1.10. De-phosphorylation of DNA 5'-ends

To avoid relegation of digested vectors, vector DNA was de-phosphorylated with Antarctic phosphatases. Therefore 1 µl of the provided enzyme together with the provided buffer were added to the digestion mixture. The mix was incubated for

30 minutes at 37 °C. Inactivation of the enzyme was performed at 65 °C for 10 minutes.

IV.2.1.11. Measurement of DNA / RNA concentrations

1 µl of the nucleic acid mixture was measured by OD260 with a photospectrometer (Nanodrop 1000, Peclab). The dilute reagent was used as blank reference

IV.2.1.12. Ligation

Ligations were performed with a 3:1 molar ratio insert / vector. 100 ng of the vector were mixed with the insert DNA fragment. 1 µl of the provided T4 DNA ligase together with the provided buffer were added to the DNA mixture. Ligation were performed for two hours at 16 °C.

IV.2.1.13. Electrophoretic mobility shift assay (EMSA)

Pax6 proteins were expressed using the TNT *in vitro* transcription and translation system (Promega), according to the instruction manual. Double-stranded oligonucleotides were labelled using polynucleotide kinase and γ -P32ATP. The binding reaction was performed for 1 hour on ice in binding buffer containing 0.5 µg poly-dI-dC, double stranded oligonucleotides (with radial activity at 35,000 cpm) and 10 µl of *in vitro* translated Pax6 protein. For antibody supershift analysis, 0.5 µl of Pax6 polyclonal antibody was added and samples were incubated for additional 15 minutes. Samples were loaded onto 4 % TAE polyacrylamide gel and electrophoresed at 10 V / cm to resolve complexes. Gels were dried and processed for autoradiography.

IV.2.2. Cell culture

IV.2.2.1. Culture of NIH3T3 cells

NIH3T3 were cultured in petri dishes at 37 °C and 5 % CO₂ in Dulbeccos modified Eagles Medium (DMEM) with 10 % FCS and 5 % Penicillin / Streptomycin. NIH3T3 cells for immunocytochemistry (ICC) were cultured on 12 mm cover slips in 6-well plates. For cell transfer to new culture dishes adherent cells were washed once with PBS and with 1 ml of a 0.25 % Trypsin solution incubated for 5 minutes. Trypsin were inactivated by DMEM medium containing 10 % FCS. Cells were spun down and re-suspended in an adequate volume of DMEM medium containing 10 % FCS and transferred into new culture dishes. For ICC preparation 1×10^5 cells per well were transferred into a 6-well plate. For protein extraction for co-immunoprecipitation assays 1×10^6 cells per 10 mm dished were transferred. For the luciferase assay 1.5×10^5 cells per well were transferred into a 12-well plate.

IV.2.2.2. Plasmid DNA transfection into NIH3T3 cells

Transfection of plasmid DNA was performed with Transfectin[®] according to suppliers instruction. Per 1 µg DNA 1 µl Transfectin[®] were used. For ICC 1 µg DNA per well were used. For transfection of cell cultured in 10 mm dishes for Protein extraction 8 µg DNA were used. For transfection of the luciferase constructs 1 µg per well of the TopFlash (OT) respectively FopFlash (OF) were used. For all other constructs 100 ng DNA per well were used.

IV.2.2.3. Immunocytochemistry

NIH3T3 cells cultured on coverslips were washed 3 times for 5 minutes with PBS. Fixation was performed with 4 % paraformaldehyde in PBS for 20 minutes at room temperature followed by 3 times washing with PBS for 5 minutes. Cells were incubated for 5 minutes with 0.2 % Triton X-100 in PBS at room temperature for permeabilisation of the cells. Incubation with 10 % BSA-TBS was performed for blocking of unspecific antibody binding. Primary antibodies were incubated in PBS for 30 minutes at 37 °C followed by 3 times washing with PBS. The secondary antibodies were incubated like the primary antibodies. After final 3 times washing with PBS cells were covered with Vectashild Mounting Medium containing DAPI and sealed with nail polish. Cells were analysed with confocal microscopy (TCS SP5, Leica).

IV.2.2.4. Reportergene assay

For analyses of Pax6 activation of the Odf2 promoter the Dual Glo Luciferase assay system provided from Promega was used. TopFlash vector containing a firefly luciferase under the control of an Odf2 promoter was transfected with or without a Pax6 expression plasmid. 24 hours after transfection cells were scratched from the bottom of the wells and centrifuged for 10 minutes at 800 x g. The pellet was re-suspended and digested in 30 µl Lysisbuffer for 30 minutes at room temperature. After incubation the suspension was centrifuged at 13,000 x g for 1 min at room temperature. The supernatant were transferred into 96-well plate for luciferase measurement. The luciferase activity measurement was performed according to supplier's instruction with Luminometer Centro LB 960. The results were analysed with Microsoft Excel.

IV.2.2.5. Extraction of proteins after expression in NIH3T3 cells

Cells were harvested as described previously and the quantity was calculated with a Neubauer counting chamber. The cells were washed once with PBS and digested in 1 ml lysis buffer per 10^7 cells for 30 minutes on ice. The suspension was centrifuged for 10 minutes at $10,000 \times g$ at 4°C . The supernatant were stored at -20°C and later on used for Westernblot analysis.

IV.2.3. Protein biochemical assays

IV.2.3.1. SDS-PAGE

Proteins were separated with Sodiumdodecylsulfate polyacrylamide gel electrophoresis (SDS-PAGE). Before probes were loaded to the gel they were mixed with Laemmli probe buffer and heated for 3 minutes at 95°C . The denaturated proteins were then separated in a Mini-PROTEAN Tetra Cell chamber, filled with Laemmli electrophoresis buffer at 100 V.

IV.2.3.2. Transfer of proteins to an Immobilon-P Membrane

For antibody detection of specific proteins the proteins were transferred onto an Immobilon-P Membrane (Millipore). Therefore the membrane was activated by methanol and transferred onto the SDS-PAGE gel. The gel together with the membrane was clamped between Whatmen-paper and transfer occurred in a Mini-PROTEAN Tetra Cell chamber at 1.5 A for 45 minutes.

IV.2.3.3. Protein detection by antibodies

After protein transfer to the Immobilon-P Membrane the membrane was blocked against unspecific antibody binding by incubation with 5 % milk powder solution for 1 hour at room temperature. The primary antibodies were incubated at 4 °C over night in 5 % milk powder solution. The membrane was washed 3 times with TBST for 10 minutes at room temperature. Incubation with horseradish peroxidase conjugated antibody occurred for 1 hour at room temperature. After intensive washing for one hour chemoluminescence activation by ECL Western Blotting Substrate (Pierce) followed according to instruction manual. Chemoluminescence was detected by a radiographic film.

IV.2.3.4. Quantitative protein analysis

In order to analyse different quantities of a protein the SDS-PAGE gel was loaded with the same amount of cells. Therefore cells were counted before lysis with a Neubauer counting chamber. As a loading control a Westernblot analysis of β -Actin was performed in order to be able to compare the different experiments.

IV.2.3.5. Technics for protein-protein interaction analysis

IV.2.3.5.1. Co-immunoprecipitation analysis of HA-tagged proteins

HA-tagged proteins were transfected in NIH3T3 like described previously. After 24 hours cells were harvested by trypsinisation. After inactivation of Trypsin by DMEM containing 10 % FCS cells were counted with a Neubauer counting chamber. Interaction analysis of HA-tagged proteins (Kif2a, Hook2, Nedd9) was performed with the ProFound™ Mammalian HA Tag IP/Co-IP Kit. The experiments were performed according to the instruction manual.

IV.2.4. Animals

IV.2.4.1. Animals

For *Pax6*-loss-of-function experiments *Pax6/Small eye (Sey/Sey)* mutant mice were used. For *in-utero* electroporation experiments CD1 wild type mice were used. For *in-utero* electroporation in *Pax6cKO* embryos *Pax6^{fl/fl}* mice were crossed with *Emx1Cre^{+/-};Pax6^{fl/fl}* mice (Gorski et al 2002). The day of vaginal plug (VP) were considered as embryonic day 0 (E0) and the day of birth were considered as postnatal day 0 (P0).

IV.2.4.2. Animal treatments

IV.2.4.2.1. BrdU injections

Pregnant mice were intraperitoneal injected at E14.5 with 100 µl per 10 g of body weight BrdU solution (0.014 g BrdU in 1 ml PBS). Embryonic brains were dissected after 24 hours.

IV.2.4.2.2. *In utero* electroporation

The CD1 WT mice for *in utero* electroporation received a painkiller one day before and three days after operation via drinking water. On day of operation (embryonic day E13.5) the mice were anaesthetized by intraperitoneal injection of Ketamine (2 mg / 30 g), Xylazine (0.4 mg / 30 g) and Acepromazine (0.06 mg / 30 g) solution in 0.9 % NaCl. Injection capillaries from glass micropipettes were pulled and broken to get an inner diameter of 10 - 20 µm. The mice were fixed with their back on a warm plate and deep anaesthesia was verified by the absence of pain reflexes and the abdomen was cleaned with 70 % ethanol. The uterine horns were exposed through a 2 cm caesarean cut along the abdominal midline. The uterine horns were arranged on a sterile gaze pad and kept warm with a pre warmed 0.9 % NaCl solution. 2 µl of Plasmid DNA with a concentration between 2 and 2.5 µg/µl mixed with 1 µl of a FastGreen solution (0.1 % in PBS) were injected in one hemisphere of the lateral ventricle of the selected embryo by a mouth pipette. Tweezer electrodes were positioned laterally to the head orientated with the plus pole to the injected hemisphere. Three electric pulses of 50

milliseconds with a brake of 950 milliseconds were performed with 30 Volts. Maximum 3 embryos per uterus horn were injected. Regularly, 2 embryos at the left side and 2 at the right side were chosen with at least one untreated embryo in between. The uterine horns were placed back by an o-ringed forceps. Before closure of the abdominal wall with 4 to 6 stiches (Ethicon 5-0 surgical suture) 500 µl Traumeel was applied and the abdominal skin was closed with 3 to 4 clips. The mice were transferred into a clean cage with papers on a 37 °C warming plate until wake up (30-45 minutes). The mice were sacrificed as the experiment demanded. The experiments ran under the file numbers 33.14-42502-04-057/08 and 33.9-42502-04-12/0734.

IV.2.5. Histology

IV.2.5.1. Cryo conservation and sectioning of mouse brains

Murine embryos were removed by caesarean section from time pregnant mice. The mice were killed by cervical dislocation. For genotyping a tissue sample was taken from the tail of the embryo. The brains were dissected in ice cold PBS and afterwards fixed in 4% PFA in PBS on ice for the following fixation times:

E12.5 (embryo) 2 hours

E13.5 (brain) 1,5 hours

E14.5 (brain) 1,5-2 hours

E15.5 (brain) 2 hours

E16.5 (brain) 2,5 hours

After fixation the brains were washed three times in ice cold PBS_{DEPC} for 20 minutes and then transferred in 25% sucrose until the brains sank down. Afterwards the brains were embedded in Tissue Tek and frozen on dry ice. The frozen blocks were stored on -20 C° until sectioning with a Cryostat were proceed. After sectioning the sections were collected on SuperFrost microscope slides and dried on a 30 C° heating plate. The sections were stored at -80° until use.

IV.2.5.2. Organotypic embryonic mice cortical slice culture and photo switch by UV light

E14.5 mice embryos were dissected in EBSS (Invitrogen) at 4°C. Brains were embedded in 2% low-melting agarose (Invitrogen) in EBSS and cooled to 4°C for vibratome sectioning. Brains were sectioned into 300 µm thick slices. Cross sections of cortex were transferred to Minicell cell culture inserts (0,4µm; 30mm Diameter; Millipore) in 6 wells. For photo switch of the Kaede-protein each well was exposed for 5 seconds to a 350 – 400 nm UV light diode.

The cortex slices were incubated with 1,5 ml Brain slice culture medium at 37 °C and 5% CO₂ for 3 days.

For fixation cortex sections were transferred into 4% PFA in PBS and incubated for 30 min. After 3 times 10' washing in PBS the slices were transferred into 25% sucrose in PBS for 30 min and processing for cryosectioning.

IV.2.5.3. Immunohistochemistry

Cryomatrix was removed by 15 minutes washing in PBS. The slides were blocked in 0.1 % Triton X-100 in PBS with 10 % normal goat serum for 1 hour at room temperature. Primary antibodies were diluted in blocking solution and incubated on the slides at 4 °C over night. After washing 3 times for 10 minutes with PBS. Secondary antibody (diluted in blocking solution) was incubated on the slides for 2 hours at room temperature. In case of double or triple immunostaining incubation with the next primary antibody starts at this point. After complete antibody incubation the slides were washed 3 times for 20 minutes with PBS. The slides were covered with Vectashild mounting-medium containing DAPI and sealed with nail polish. The slices were analysed with fluorescence microscope (DMI6000 B, Leica) or confocal microscope (TCS SP5, Leica)

IV.2.5.4. Generation of DIG-labelled anti-sense RNA probes

For preparation of DNA template 15 µg of a cDNA containing plasmid were linearized by a certain restriction enzyme. The sample was purified by phenol-chloroform extraction. The sample was precipitated with 7.5M NH₄Ac and 100 % Ethanol. Afterwards the DNA was washed once with 70 % ethanol and dissolved in 10 µl H₂O_{DEPC}. To estimate the amount of the template it was loaded on a 1 % minigel for electrophoresis. The template was stored at -20 C°.

To produce the DIG labelled antisense RNA probes for *in-situ* hybridisation following reaction was arranged:

- | | |
|--------------------------------|--------|
| • H ₂ O | 9,5 µl |
| • 5x Transcription buffer | 4 µl |
| • 0,1 DTT | 2 µl |
| • Nucleotid-mix (DIG labelled) | 2 µl |
| • Template (1µg/µl) | 1 µl |
| • RNasin | 0,5 µl |
| • RNA polymerase (T3, T7, SP6) | 1 µl |

The reaction was incubated for 2 hours at 37 C°. Then spun down and incubated with 2 µl DNase I (1U/µl) for 10 minutes at 37 °C. The probe was purified and precipitated by adding 2 µl 0,2 M EDTA, 2,5µl 4 M LiCl and 75 µl -20C° ethanol. The mix was incubated for 2 hours at -80C°. Then centrifugation for 15 minutes at 4 C° followed and the pellet was washed once with 100 µl 70 % ethanol. After centrifugation the pellet was dried at room temperature and lysed in 50 µl H₂O and incubated for 10 minutes at 65 C°. To estimate the amount of the probe it was loaded on a 1 % Minigel for electrophoresis.

16 µm cryo-sections were labelled with digoxigenin (DIG)-labelled probes. The slides were incubated with following solutions:

Solution	Time	Temperature
4 % PFA in PBS	15 min	RT
PBS	5 min	RT
PBS	5 min	RT
Proteinase K	4 min	37 °C
0.2 % glycine in PBS	5 min	RT
PBS	5 min	RT
PBS	5 min	RT
Postfixation	5 min	RT
PBS	5 min	RT
PBS	5 min	RT

Prehybridisation was performed in an airtight box humidified with formamid in 2 x SSC pH4.5 for two hours at 70 °C. The DIG labelled probes were diluted in the hybridisation buffer due to the determined concentration. After denaturation for 3 minutes at 80 °C the probes were applied on the sections over night at 70 °C in the humidified box.

The next day the slides were incubated with the following solutions:

Solution	Time	Temperature
2 x SSC pH 4.5	5 min	RT
2 x SSC pH 4.5; 50 % Formamide	30 min	65 °C
2 x SSC pH 4.5; 50 % Formamide	30 min	65 °C
2 x SSC pH 4.5; 50 % Formamide	30 min	65 °C
KTBT	10 min	RT
KTBT	10 min	RT

The slides were incubated in blocking solution for 2 hours at room temperature. As next step, the slides were incubated with an anti-DIG antibody coupled to alkaline phosphatase in blocking solution (1: 2,000) over night at 4 °C. On the third day following steps were proceeded:

Solution	Time	Temperature
KTBT	5 min	RT
KTBT	5 min	RT
KTBT	5 min	RT
KTBT	30 min	RT
KTBT	30 min	RT
KTBT	30 min	RT
NTMT	5 min	RT
NTMT	5 min	RT
NTMT	5 min	RT

For staining slides were incubated with a 2 % NBT / BCIP in NTMT solution in a dark wet chamber. When adequate staining was reached, staining reaction was stopped by 3 times washing with PBT. The slides were mounted with Mowiol and sealed with nail polish.

IV.2.5.5. Electron microscopy of E15.5 embryonic cortex

Cortex hemispheres were dissected and fixated in 0.15 M Sörensen-buffer containing 3 % PFA and 3 % glutaraldehyde at least for one hour. After fixation the following steps were proceed:

Solution	Time	Temperature
0.15M Sörensen buffer	10 min	4°C
Osmium	1.5 h	4°C
0.15 M Sörensen buffer	10 min	4°C
30 % Ethanol	10 min	4°C
50 % Ethanol	10 min	4°C
70 % Ethanol	o/n	4°C
90 % Ethanol	10 min	4°C
100 % Ethanol	10 min	4°C
100 % Ethanol	10 min	4°C
Propylenoxid	15 min	4°C
Propylenoxid	15 min	4°C
Epon; Propylenoxid 1:1	1 h	4°C
Epon Propylenoxid 3:1	16 h	4°C

The tissue was embedded in Epon for 24 hours at 60 °C and semi-thin cuttings was performed to trim the cutting block. Then ultra thin cuttings were performed and analysed by electron microscopy in neuronal pathology of the medical centre of the university of Göttingen.

IV.2.6. Software

DNA sequences analysis and oligonucleotide creation were performed with Amplify 3X. MatInspector software was used to search for possible Pax6 binding sites within the Odf2 promoter sequence. Pictures and figures were edit with Adobe® Photoshop®. Statistical analysis was performed with Microsoft Excel® and Apple Numbers®.

V. LITERATURE

- Asami M, Pilz GA, Ninkovic J, Godinho L, Schroeder T, et al. 2011. The role of Pax6 in regulating the orientation and mode of cell division of progenitors in the mouse cerebral cortex. *Development* 138: 5067-78
- Ashery-Padan R, Marquardt T, Zhou X, Gruss P. 2000. Pax6 activity in the lens primordium is required for lens formation and for correct placement of a single retina in the eye. *Genes Dev* 14: 2701-11
- Azimzadeh J, Bornens M. 2007. Structure and duplication of the centrosome. *J Cell Sci* 120: 2139-42
- Azimzadeh J, Marshall WF. 2010. Building the centriole. *Curr Biol* 20: R816-25
- Badano JL, Mitsuma N, Beales PL, Katsanis N. 2006. The ciliopathies: an emerging class of human genetic disorders. *Annual review of genomics and human genetics* 7: 125-48
- Baltz JM, Williams PO, Cone RA. 1990. Dense fibers protect mammalian sperm against damage. *Biology of reproduction* 43: 485-91
- Barnes BG. 1961. Ciliated secretory cells in the pars distalis of the mouse hypophysis. *Journal of ultrastructure research* 5: 453-67
- Baumer N, Marquardt T, Stoykova A, Spieler D, Treichel D, et al. 2003. Retinal pigmented epithelium determination requires the redundant activities of Pax2 and Pax6. *Development* 130: 2903-15
- Berger J, Berger S, Tuoc TC, D'Amelio M, Cecconi F, et al. 2007. Conditional activation of Pax6 in the developing cortex of transgenic mice causes progenitor apoptosis. *Development* 134: 1311-22
- Bernstein E, Caudy AA, Hammond SM, Hannon GJ. 2001. Role for a bidentate ribonuclease in the initiation step of RNA interference. *Nature* 409: 363-6
- Bettencourt-Dias M, Glover DM. 2007. Centrosome biogenesis and function: centrosomics brings new understanding. *Nat Rev Mol Cell Biol* 8: 451-63
- Birnboim HC, Doly J. 1979. A rapid alkaline extraction procedure for screening recombinant plasmid DNA. *Nucleic acids research* 7: 1513-23
- Borello U, Pierani A. 2010. Patterning the cerebral cortex: traveling with morphogens. *Curr Opin Genet Dev* 20: 408-15
- Bornens M. 2002. Centrosome composition and microtubule anchoring mechanisms. *Curr Opin Cell Biol* 14: 25-34
- Bornens M. 2012. The centrosome in cells and organisms. *Science* 335: 422-6
- Bornens M, Azimzadeh J. 2007. Origin and evolution of the centrosome. *Advances in experimental medicine and biology* 607: 119-29
- Bultje RS, Castaneda-Castellanos DR, Jan LY, Jan YN, Kriegstein AR, Shi SH. 2009. Mammalian Par3 regulates progenitor cell asymmetric division via notch signaling in the developing neocortex. *Neuron* 63: 189-202
- Burfeind P, Hoyer-Fender S. 1991. Sequence and developmental expression of a mRNA encoding a putative protein of rat sperm outer dense fibers. *Dev Biol* 148: 195-204
- Campbell K. 2005. Cortical neuron specification: it has its time and place. *Neuron* 46: 373-6
- Campbell K, Gotz M. 2002. Radial glia: multi-purpose cells for vertebrate brain development. *Trends Neurosci* 25: 235-8
- Carlisle FA, Steel KP, Lewis MA. 2012. Specific expression of Kcna10, Pxn and Odf2 in the organ of Corti. *Gene Expr Patterns* 12: 172-9

- Caviness VS, Jr., Takahashi T. 1995. Proliferative events in the cerebral ventricular zone. *Brain & development* 17: 159-63
- Chalepakakis G, Stoykova A, Wijnholds J, Tremblay P, Gruss P. 1993. Pax: gene regulators in the developing nervous system. *Journal of neurobiology* 24: 1367-84
- Chalepakakis G, Tremblay P, Gruss P. 1992. Pax genes, mutants and molecular function. *Journal of cell science. Supplement* 16: 61-7
- Chenn A, Zhang YA, Chang BT, McConnell SK. 1998. Intrinsic polarity of mammalian neuroepithelial cells. *Mol Cell Neurosci* 11: 183-93
- Collombat P, Mansouri A, Hecksher-Sorensen J, Serup P, Krull J, et al. 2003. Opposing actions of Arx and Pax4 in endocrine pancreas development. *Genes Dev* 17: 2591-603
- Collombat P, Xu X, Ravassard P, Sosa-Pineda B, Dussaud S, et al. 2009. The ectopic expression of Pax4 in the mouse pancreas converts progenitor cells into alpha and subsequently beta cells. *Cell* 138: 449-62
- Costa MR, Wen G, Lepier A, Schroeder T, Gotz M. 2008. Par-complex proteins promote proliferative progenitor divisions in the developing mouse cerebral cortex. *Development* 135: 11-22
- Delgehyr N, Sillibourne J, Bornens M. 2005. Microtubule nucleation and anchoring at the centrosome are independent processes linked by ninein function. *J Cell Sci* 118: 1565-75
- Donkor FF, Monnich M, Czirr E, Hollemann T, Hoyer-Fender S. 2004. Outer dense fibre protein 2 (ODF2) is a self-interacting centrosomal protein with affinity for microtubules. *J Cell Sci* 117: 4643-51
- Eggenchwiler JT, Anderson KV. 2007. Cilia and developmental signaling. *Annual review of cell and developmental biology* 23: 345-73
- Estivill-Torrus G, Pearson H, van Heyningen V, Price DJ, Rashbass P. 2002. Pax6 is required to regulate the cell cycle and the rate of progression from symmetrical to asymmetrical division in mammalian cortical progenitors. *Development* 129: 455-66
- Farkas LM, Huttner WB. 2008. The cell biology of neural stem and progenitor cells and its significance for their proliferation versus differentiation during mammalian brain development. *Curr Opin Cell Biol* 20: 707-15
- Fawcett DW. 1975. The mammalian spermatozoon. *Dev Biol* 44: 394-436
- Fietz SA, Huttner WB. 2011. Cortical progenitor expansion, self-renewal and neurogenesis-a polarized perspective. *Current opinion in neurobiology* 21: 23-35
- Fish JL, Dehay C, Kennedy H, Huttner WB. 2008. Making bigger brains-the evolution of neural-progenitor-cell division. *J Cell Sci* 121: 2783-93
- Fode C, Ma Q, Casarosa S, Ang SL, Anderson DJ, Guillemot F. 2000. A role for neural determination genes in specifying the dorsoventral identity of telencephalic neurons. *Genes Dev* 14: 67-80
- Franco SJ, Gil-Sanz C, Martinez-Garay I, Espinosa A, Harkins-Perry SR, et al. 2012. Fate-restricted neural progenitors in the mammalian cerebral cortex. *Science* 337: 746-9
- Fujita S. 1962. Kinetics of cellular proliferation. *Exp Cell Res* 28: 52-60
- Georgala PA, Carr CB, Price DJ. 2011a. The role of Pax6 in forebrain development. *Developmental neurobiology* 71: 690-709
- Georgala PA, Manuel M, Price DJ. 2011b. The generation of superficial cortical layers is regulated by levels of the transcription factor Pax6. *Cereb Cortex* 21: 81-94

- Gerdes JM, Liu Y, Zaghloul NA, Leitch CC, Lawson SS, et al. 2007. Disruption of the basal body compromises proteasomal function and perturbs intracellular Wnt response. *Nat Genet* 39: 1350-60
- Goetz SC, Anderson KV. 2010. The primary cilium: a signalling centre during vertebrate development. *Nature reviews. Genetics* 11: 331-44
- Gonczy P. 2004. Centrosomes: hooked on the nucleus. *Curr Biol* 14: R268-70
- Gorski JA, Talley T, Qiu M, Puelles L, Rubenstein JL, Jones KR. 2002. Cortical excitatory neurons and glia, but not GABAergic neurons, are produced in the Emx1-expressing lineage. *J Neurosci* 22: 6309-14
- Gotz M, Barde YA. 2005. Radial glial cells defined and major intermediates between embryonic stem cells and CNS neurons. *Neuron* 46: 369-72
- Gotz M, Hartfuss E, Malatesta P. 2002. Radial glial cells as neuronal precursors: a new perspective on the correlation of morphology and lineage restriction in the developing cerebral cortex of mice. *Brain research bulletin* 57: 777-88
- Gotz M, Huttner WB. 2005. The cell biology of neurogenesis. *Nat Rev Mol Cell Biol* 6: 777-88
- Gotz M, Sommer L. 2005. Cortical development: the art of generating cell diversity. *Development* 132: 3327-32
- Gotz M, Stoykova A, Gruss P. 1998. Pax6 controls radial glia differentiation in the cerebral cortex. *Neuron* 21: 1031-44
- Gunhaga L, Marklund M, Sjodal M, Hsieh JC, Jessell TM, Edlund T. 2003. Specification of dorsal telencephalic character by sequential Wnt and FGF signaling. *Nat Neurosci* 6: 701-7
- Hammond SM, Bernstein E, Beach D, Hannon GJ. 2000. An RNA-directed nuclease mediates post-transcriptional gene silencing in *Drosophila* cells. *Nature* 404: 293-6
- Hanahan D. 1983. Studies on transformation of *Escherichia coli* with plasmids. *Journal of molecular biology* 166: 557-80
- Haubensak W, Attardo A, Denk W, Huttner WB. 2004. Neurons arise in the basal neuroepithelium of the early mammalian telencephalon: a major site of neurogenesis. *Proc Natl Acad Sci USA* 101: 3196-201
- Heins N, Malatesta P, Cecconi F, Nakafuku M, Tucker KL, et al. 2002. Glial cells generate neurons: the role of the transcription factor Pax6. *Nat Neurosci* 5: 308-15
- Hill RE, Favor J, Hogan BL, Ton CC, Saunders GF, et al. 1991. Mouse small eye results from mutations in a paired-like homeobox-containing gene. *Nature* 354: 522-5
- Hinchcliffe EH, Sluder G. 2001. "It takes two to tango": understanding how centrosome duplication is regulated throughout the cell cycle. *Genes Dev* 15: 1167-81
- Hoyer-Fender S. 2010. Centriole maturation and transformation to basal body. *Semin Cell Dev Biol* 21: 142-7
- Hoyer-Fender S, Neesen J, Szpirer J, Szpirer C. 2003. Genomic organisation and chromosomal assignment of ODF2 (outer dense fiber 2), encoding the main component of sperm tail outer dense fibers and a centrosomal scaffold protein. *Cytogenet Genome Res* 103: 122-7
- Hoyer-Fender S, Petersen C, Brohmann H, Rhee K, Wolgemuth DJ. 1998. Mouse Odf2 cDNAs consist of evolutionary conserved as well as highly variable sequences and encode outer dense fiber proteins of the sperm tail. *Mol Reprod Dev* 51: 167-75

- Huber D, Geisler S, Monecke S, Hoyer-Fender S. 2008. Molecular dissection of ODF2/Cenexin revealed a short stretch of amino acids necessary for targeting to the centrosome and the primary cilium. *European journal of cell biology* 87: 137-46
- Huber D, Hoyer-Fender S. 2007. Alternative splicing of exon 3b gives rise to ODF2 and Cenexin. *Cytogenet Genome Res* 119: 68-73
- Ibi M, Zou P, Inoko A, Shiromizu T, Matsuyama M, et al. 2011. Trichoplein controls microtubule anchoring at the centrosome by binding to Odf2 and ninein. *J Cell Sci* 124: 857-64
- Imai JH, Wang X, Shi SH. 2010. Kaede-centrin1 labeling of mother and daughter centrosomes in mammalian neocortical neural progenitors. *Current protocols in stem cell biology* Chapter 5: Unit 5A 5
- Ishikawa H, Kubo A, Tsukita S. 2005. Odf2-deficient mother centrioles lack distal/subdistal appendages and the ability to generate primary cilia. *Nat Cell Biol* 7: 517-24
- Jainchill JL, Aaronson SA, Todaro GJ. 1969. Murine sarcoma and leukemia viruses: assay using clonal lines of contact-inhibited mouse cells. *Journal of virology* 4: 549-53
- Januschke J, Llamazares S, Reina J, Gonzalez C. 2011. Drosophila neuroblasts retain the daughter centrosome. *Nature communications* 2: 243
- Januschke J, Reina J, Llamazares S, Bertran T, Rossi F, et al. 2013. Centrobin controls mother-daughter centriole asymmetry in Drosophila neuroblasts. *Nat Cell Biol*
- Kawasaki H, Taira K. 2003. Short hairpin type of dsRNAs that are controlled by tRNA(Val) promoter significantly induce RNAi-mediated gene silencing in the cytoplasm of human cells. *Nucleic acids research* 31: 700-7
- Kobayashi T, Dynlacht BD. 2011. Regulating the transition from centriole to basal body. *J Cell Biol* 193: 435-44
- Kochanski RS, Borisy GG. 1990. Mode of centriole duplication and distribution. *J Cell Biol* 110: 1599-605
- Kunimoto K, Yamazaki Y, Nishida T, Shinohara K, Ishikawa H, et al. 2012. Coordinated ciliary beating requires Odf2-mediated polarization of basal bodies via basal feet. *Cell* 148: 189-200
- LaMonica BE, Lui JH, Wang X, Kriegstein AR. 2012. OSVZ progenitors in the human cortex: an updated perspective on neurodevelopmental disease. *Current opinion in neurobiology* 22: 747-53
- Lui JH, Hansen DV, Kriegstein AR. 2011. Development and evolution of the human neocortex. *Cell* 146: 18-36
- Malatesta P, Hartfuss E, Gotz M. 2000. Isolation of radial glial cells by fluorescent-activated cell sorting reveals a neuronal lineage. *Development* 127: 5253-63
- Mallamaci A, Stoykova A. 2006. Gene networks controlling early cerebral cortex arealization. *Eur J Neurosci* 23: 847-56
- Marin O, Rubenstein JL. 2003. Cell migration in the forebrain. *Annual review of neuroscience* 26: 441-83
- May SR, Ashique AM, Karlen M, Wang B, Shen Y, et al. 2005. Loss of the retrograde motor for IFT disrupts localization of Smo to cilia and prevents the expression of both activator and repressor functions of Gli. *Dev Biol* 287: 378-89
- Meinhardt H. 2001. Organizer and axes formation as a self-organizing process. *The International journal of developmental biology* 45: 177-88

- Meraldi P, Nigg EA. 2002. The centrosome cycle. *FEBS Lett* 521: 9-13
- Mi D, Carr CB, Georgala PA, Huang YT, Manuel MN, et al. 2013. Pax6 Exerts Regional Control of Cortical Progenitor Proliferation via Direct Repression of Cdk6 and Hypophosphorylation of pRb. *Neuron* 78: 269-84
- Miyata T, Kawaguchi D, Kawaguchi A, Gotoh Y. 2010. Mechanisms that regulate the number of neurons during mouse neocortical development. *Current opinion in neurobiology* 20: 22-8
- Mogensen MM, Malik A, Piel M, Bouckson-Castaing V, Bornens M. 2000. Microtubule minus-end anchorage at centrosomal and non-centrosomal sites: the role of ninein. *J Cell Sci* 113 (Pt 17): 3013-23
- Molyneaux BJ, Arlotta P, Menezes JR, Macklis JD. 2007. Neuronal subtype specification in the cerebral cortex. *Nat Rev Neurosci* 8: 427-37
- Moritz M, Agard DA. 2001. Gamma-tubulin complexes and microtubule nucleation. *Current opinion in structural biology* 11: 174-81
- Moss DK, Bellett G, Carter JM, Liovic M, Keynton J, et al. 2007. Ninein is released from the centrosome and moves bi-directionally along microtubules. *J Cell Sci* 120: 3064-74
- Murcia NS, Richards WG, Yoder BK, Mucenski ML, Dunlap JR, Woychik RP. 2000. The Oak Ridge Polycystic Kidney (orpk) disease gene is required for left-right axis determination. *Development* 127: 2347-55
- Muzio L, DiBenedetto B, Stoykova A, Boncinelli E, Gruss P, Mallamaci A. 2002. Emx2 and Pax6 control regionalization of the pre-neuronogenic cortical primordium. *Cereb Cortex* 12: 129-39
- Nakagawa Y, Yamane Y, Okanoue T, Tsukita S, Tsukita S. 2001. Outer dense fiber 2 is a widespread centrosome scaffold component preferentially associated with mother centrioles: its identification from isolated centrosomes. *Mol Biol Cell* 12: 1687-97
- Nieto M, Monuki ES, Tang H, Imitola J, Haubst N, et al. 2004. Expression of Cux-1 and Cux-2 in the subventricular zone and upper layers II-IV of the cerebral cortex. *The Journal of comparative neurology* 479: 168-80
- Nigg EA, Raff JW. 2009. Centrioles, centrosomes, and cilia in health and disease. *Cell* 139: 663-78
- Noctor SC, Flint AC, Weissman TA, Dammerman RS, Kriegstein AR. 2001. Neurons derived from radial glial cells establish radial units in neocortex. *Nature* 409: 714-20
- Nonaka S, Shiratori H, Saijoh Y, Hamada H. 2002. Determination of left-right patterning of the mouse embryo by artificial nodal flow. *Nature* 418: 96-9
- O'Leary DD. 1989. Do cortical areas emerge from a protocortex? *Trends Neurosci* 12: 400-6
- O'Leary DD, Chou SJ, Sahara S. 2007. Area patterning of the mammalian cortex. *Neuron* 56: 252-69
- O'Neill GM, Fashena SJ, Golemis EA. 2000. Integrin signalling: a new Cas(t) of characters enters the stage. *Trends Cell Biol* 10: 111-9
- Ohama Y, Hayashi K. 2009. Relocalization of a microtubule-anchoring protein, ninein, from the centrosome to dendrites during differentiation of mouse neurons. *Histochem Cell Biol* 132: 515-24
- Oko R, Clermont Y. 1988. Isolation, structure and protein composition of the perforatorium of rat spermatozoa. *Biology of reproduction* 39: 673-87
- Olson GE, Sammons DW. 1980. Structural chemistry of outer dense fibers of rat sperm. *Biology of reproduction* 22: 319-32

- Ou YY, Mack GJ, Zhang M, Rattner JB. 2002. CEP110 and ninein are located in a specific domain of the centrosome associated with centrosome maturation. *J Cell Sci* 115: 1825-35
- Paintrand M, Moudjou M, Delacroix H, Bornens M. 1992. Centrosome organization and centriole architecture: their sensitivity to divalent cations. *Journal of structural biology* 108: 107-28
- Pazour GJ, Dickert BL, Vucica Y, Seeley ES, Rosenbaum JL, et al. 2000. Chlamydomonas IFT88 and its mouse homologue, polycystic kidney disease gene tg737, are required for assembly of cilia and flagella. *J Cell Biol* 151: 709-18
- Pinon MC, Tuoc TC, Ashery-Padan R, Molnar Z, Stoykova A. 2008. Altered molecular regionalization and normal thalamocortical connections in cortex-specific Pax6 knock-out mice. *J Neurosci* 28: 8724-34
- Puelles L. 2001. Brain segmentation and forebrain development in amniotes. *Brain research bulletin* 55: 695-710
- Quinn JC, Molinek M, Martynoga BS, Zaki PA, Faedo A, et al. 2007. Pax6 controls cerebral cortical cell number by regulating exit from the cell cycle and specifies cortical cell identity by a cell autonomous mechanism. *Dev Biol* 302: 50-65
- Rakic P. 1988. Specification of cerebral cortical areas. *Science* 241: 170-6
- Rakic P. 2009. Evolution of the neocortex: a perspective from developmental biology. *Nat Rev Neurosci* 10: 724-35
- Rallu M, Machold R, Gaiano N, Corbin JG, McMahon AP, Fishell G. 2002. Dorsoventral patterning is established in the telencephalon of mutants lacking both Gli3 and Hedgehog signaling. *Development* 129: 4963-74
- Reiner O, Sapir T, Gerlitz G. 2012. Interkinetic nuclear movement in the ventricular zone of the cortex. *Journal of molecular neuroscience : MN* 46: 516-26
- Rivkin E, Tres LL, Kierszenbaum AL. 2008. Genomic origin, processing and developmental expression of testicular outer dense fiber 2 (ODF2) transcripts and a novel nucleolar localization of ODF2 protein. *Mol Reprod Dev* 75: 1591-606
- Rohatgi R, Milenkovic L, Scott MP. 2007. Patched1 regulates hedgehog signaling at the primary cilium. *Science* 317: 372-6
- Rosenbaum JL, Witman GB. 2002. Intraflagellar transport. *Nat Rev Mol Cell Biol* 3: 813-25
- Ross AJ, May-Simera H, Eichers ER, Kai M, Hill J, et al. 2005. Disruption of Bardet-Biedl syndrome ciliary proteins perturbs planar cell polarity in vertebrates. *Nat Genet* 37: 1135-40
- Ruiz i Altaba A, Jessell TM, Roelink H. 1995. Restrictions to floor plate induction by hedgehog and winged-helix genes in the neural tube of frog embryos. *Mol Cell Neurosci* 6: 106-21
- Saiki RK, Gelfand DH, Stoffel S, Scharf SJ, Higuchi R, et al. 1988. Primer-directed enzymatic amplification of DNA with a thermostable DNA polymerase. *Science* 239: 487-91
- Salmon NA, Reijo Pera RA, Xu EY. 2006. A gene trap knockout of the abundant sperm tail protein, outer dense fiber 2, results in preimplantation lethality. *Genesis* 44: 515-22
- Sanes DH, Reh TA, Harris WA. 2006. *Development of the nervous system*. Amsterdam ; Boston: Elsevier. xiii, 373 p. pp.

- Sansom SN, Griffiths DS, Faedo A, Kleinjan DJ, Ruan Y, et al. 2009. The level of the transcription factor Pax6 is essential for controlling the balance between neural stem cell self-renewal and neurogenesis. *PLoS Genet* 5: e1000511
- Sansom SN, Livesey FJ. 2009. Gradients in the brain: the control of the development of form and function in the cerebral cortex. *Cold Spring Harbor perspectives in biology* 1: a002519
- Sauer FC. 1935. Mitosis in the neural tube. *Journal of Comparative Neurology* 62: 377-405
- Schneider L, Clement CA, Teilmann SC, Pazour GJ, Hoffmann EK, et al. 2005. PDGFRalpha signaling is regulated through the primary cilium in fibroblasts. *Curr Biol* 15: 1861-6
- Schuurmans C, Guillemot F. 2002. Molecular mechanisms underlying cell fate specification in the developing telencephalon. *Current opinion in neurobiology* 12: 26-34
- Schweizer S, Hoyer-Fender S. 2009. Mouse Odf2 localizes to centrosomes and basal bodies in adult tissues and to the photoreceptor primary cilium. *Cell Tissue Res*
- Shao X, Murthy S, Demetrick DJ, van der Hoorn FA. 1998. Human outer dense fiber gene, ODF2, localizes to chromosome 9q34. *Cytogenet Cell Genet* 83: 221-3
- Simons M, Gloy J, Ganner A, Bullerkotte A, Bashkurov M, et al. 2005. Inversin, the gene product mutated in nephronophthisis type II, functions as a molecular switch between Wnt signaling pathways. *Nat Genet* 37: 537-43
- Simpson TI, Price DJ. 2002. Pax6; a pleiotropic player in development. *Bioessays* 24: 1041-51
- Sorokin S. 1962. Centrioles and the formation of rudimentary cilia by fibroblasts and smooth muscle cells. *J Cell Biol* 15: 363-77
- Soung NK, Kang YH, Kim K, Kamijo K, Yoon H, et al. 2006. Requirement of hCenexin for proper mitotic functions of polo-like kinase 1 at the centrosomes. *Mol Cell Biol* 26: 8316-35
- Spear PC, Erickson CA. 2012. Interkinetic nuclear migration: a mysterious process in search of a function. *Dev Growth Differ* 54: 306-16
- St-Onge L, Sosa-Pineda B, Chowdhury K, Mansouri A, Gruss P. 1997. Pax6 is required for differentiation of glucagon-producing alpha-cells in mouse pancreas. *Nature* 387: 406-9
- Stoykova A, Fritsch R, Walther C, Gruss P. 1996. Forebrain patterning defects in Small eye mutant mice. *Development* 122: 3453-65
- Stoykova A, Treichel D, Hallonet M, Gruss P. 2000. Pax6 modulates the dorsoventral patterning of the mammalian telencephalon. *J Neurosci* 20: 8042-50
- Supp DM, Witte DP, Potter SS, Brueckner M. 1997. Mutation of an axonemal dynein affects left-right asymmetry in inversus viscerum mice. *Nature* 389: 963-6
- Szebenyi G, Hall B, Yu R, Hashim AI, Kramer H. 2007. Hook2 localizes to the centrosome, binds directly to centriolin/CEP110 and contributes to centrosomal function. *Traffic* 8: 32-46
- Tamai H, Shinohara H, Miyata T, Saito K, Nishizawa Y, et al. 2007. Pax6 transcription factor is required for the interkinetic nuclear movement of neuroepithelial cells. *Genes Cells* 12: 983-96

- Tarabykin V, Stoykova A, Usman N, Gruss P. 2001. Cortical upper layer neurons derive from the subventricular zone as indicated by Svet1 gene expression. *Development* 128: 1983-93
- Taverna E, Huttner WB. 2010. Neural progenitor nuclei IN motion. *Neuron* 67: 906-14
- Toresson H, Potter SS, Campbell K. 2000. Genetic control of dorsal-ventral identity in the telencephalon: opposing roles for Pax6 and Gsh2. *Development* 127: 4361-71
- Tsai JW, Lian WN, Kemal S, Kriegstein AR, Vallee RB. 2010. Kinesin 3 and cytoplasmic dynein mediate interkinetic nuclear migration in neural stem cells. *Nat Neurosci* 13: 1463-71
- Tuoc TC, Radyushkin K, Tonchev AB, Pinon MC, Ashery-Padan R, et al. 2009. Selective cortical layering abnormalities and behavioral deficits in cortex-specific Pax6 knock-out mice. *J Neurosci* 29: 8335-49
- Vera JC, Brito M, Zuvic T, Burzio LO. 1984. Polypeptide composition of rat sperm outer dense fibers. A simple procedure to isolate the fibrillar complex. *J Biol Chem* 259: 5970-7
- Vogel T, Ahrens S, Buttner N, Kriegstein K. 2009. Transforming Growth Factor {beta} Promotes Neuronal Cell Fate of Mouse Cortical and Hippocampal Progenitors In Vitro and In Vivo: Identification of Nedd9 as an Essential Signaling Component. *Cereb Cortex*
- Wallingford JB, Mitchell B. 2011. Strange as it may seem: the many links between Wnt signaling, planar cell polarity, and cilia. *Genes Dev* 25: 201-13
- Walther C, Gruss P. 1991. Pax-6, a murine paired box gene, is expressed in the developing CNS. *Development* 113: 1435-49
- Wang X, Tsai JW, Imai JH, Lian WN, Vallee RB, Shi SH. 2009. Asymmetric centrosome inheritance maintains neural progenitors in the neocortex. *Nature* 461: 947-55
- Wang X, Tsai JW, LaMonica B, Kriegstein AR. 2011. A new subtype of progenitor cell in the mouse embryonic neocortex. *Nat Neurosci* 14: 555-61
- Watanabe D, Saijoh Y, Nonaka S, Sasaki G, Ikawa Y, et al. 2003. The left-right determinant Inversin is a component of node monocilia and other 9+0 cilia. *Development* 130: 1725-34
- Weinstein DC, Hemmati-Brivanlou A. 1999. Neural induction. *Annual review of cell and developmental biology* 15: 411-33
- Wildanger D, Patton BR, Schill H, Marseglia L, Hadden JP, et al. 2012. Solid immersion facilitates fluorescence microscopy with nanometer resolution and sub-angstrom emitter localization. *Adv Mater* 24: OP309-13
- Wilsch-Brauninger M, Peters J, Paridaen JT, Huttner WB. 2012. Basolateral rather than apical primary cilia on neuroepithelial cells committed to delamination. *Development* 139: 95-105
- Wilson SW, Rubenstein JL. 2000. Induction and dorsoventral patterning of the telencephalon. *Neuron* 28: 641-51
- Wordeman L. 2005. Microtubule-depolymerizing kinesins. *Curr Opin Cell Biol* 17: 82-8
- Yamashita YM. 2009. The centrosome and asymmetric cell division. *Prion* 3: 84-8

- Yamashita YM, Mahowald AP, Perlin JR, Fuller MT. 2007. Asymmetric inheritance of mother versus daughter centrosome in stem cell division. *Science* 315: 518-21
- Zamore PD, Tuschl T, Sharp PA, Bartel DP. 2000. RNAi: double-stranded RNA directs the ATP-dependent cleavage of mRNA at 21 to 23 nucleotide intervals. *Cell* 101: 25-33

VI. SUPPLEMENTAL MATERIAL

VI.1. Abbreviations

Short name	Full name
°C	Degree in Celsius
μ	Micro
μg	Microgram
μl	Microliter
μM	Micro molar
A	Ampere
AB	Antibody
AP	Anterior-posterior
AVE	Anterior visceral endoderm
BMP	Bone morphogenic protein
BrdU	5-bromo-2-desoxy-uridine
cDNA	Complementary desoxy-ribonucleic acid
CGE	Caudal ganglionic eminence
ChIP	Chromatin immunoprecipitation
cKO	Conditional knock out
CNS	Central nervous system
Cre	Cyclization recombination
CTX	Cortex
DV	Dorsal-ventral
DIG	digoxigenin
DAPI	4'-6'-diamidino-2-phenylindole
DEPC	Diethylpyrocarbonate
DP	Dorsal pallium
DNA	Desoxy-ribonucleic acid
DNase	Desoxyribonuclease
DMEM	Dulbeccos modified Eagle's minimal essential medium
dNTPs	Desoxyribonucleotides
DTT	Dithiothreitol
E	Embryonic day
EBBS	Earl's balanced salt solution
EDTA	Ethylenediaminetetracetic acid
e.g.	Exempli gratia / for example
et al.	Et alteres / and others
FCS	Fetal calf serum
FGF	Fibroblast growth serum
Fig.	Figure
g	Grams
x g	x Gravity
GABA	γ-aminobutyric acid
GE	Ganglion eminence
GFP	Green fluorescence protein
HBBS	Hank's balanced salt solution

HEPES	Hydroxyethyl-piperazineethansulfonic acid
h	Hour
ICC	Immunocytochemistry
i.e.	It est/that is
IHC	Immunohistochemistry
INM	Interkinetic nuclear migration
IN	Interneuron
IP	Intermediate/basal progenitor
ISH	<i>In situ</i> hybridisation
IZ	Intermediate zone
LGE	Lateral ganglion eminences
M	Molar
m	Milli
MGE	Medial ganglion eminences
min	Minute
ML	Medial-lateral
ml	Milliliter
mm	Millimeter
mM	Millimolar
mRNA	Messenger RNA
MTOC	Microtubules organizing centre
NBT/BCIP	Nitro blue tetrazolium/bromo-chloro-indolyl phosphate
NE	Neuroepithelial cell
NGS	Normal goat serum
NIH	National Institute of Health
ng	Nanogram
OD	Optical density
Odf	Outer dense fibre
OSVZ	Outer subventricular zone
OSVZP	Outer subventricular zone progenitor
nm	Nanometer
PAGE	Polyacrylamid gel electrophoresis
PFA	Paraformaldehyde
PBS	Phosphate buffered saline
PCR	Polymerase chain reaction
pH	Potential hydrogenii
qPCR	Quantitative PCR
RA	Retinoid acid
RGP	Radial glia progenitor
RNA	Ribonucleic acid
RNase	Ribonuclease
Rpm	Rounds per minute
RT	Room temperature
RT-PCR	Real time polymerase chain reaction
s	Second
SDS	Sodium dodecylsulfate
<i>Sey</i>	Small eye
Shh	Sonic hedgehog
sh	Short hairpin

SVZ	Subventricular zone
TBE	Tris-borate-EDTA
TE	Tris-EDTA
TF	Transcription factor
Tris	Tris(hydroxymethyl)aminomethane
U	Unit
V	Volt
v/v	Volume/Volume
v/w	Volume/weight
VZ	Ventricular zone

VI.2. Statistical analysis of electron microscopy micrographs

WT	Centrioles with appendages	Centrioles without appendages
Brain1	15	10
Brain2	24	28
Brain3	30	33
Total each	69	71
Total	140	

WT	Centrioles with appendages %	Centrioles without appendages %
Brain1	60	40
Brain2	46.15	53.85
Brain3	51.26	52.74
Average	51.26	48.74
Standard deviation	6.21	6.21

<i>Sey/Sey</i>	Centrioles with appendages	Centrioles without appendages
Brain1	5	35
Brain2	17	40
Brain3	9	30
Total each	31	105
Total	136	

<i>Sey/Sey</i>	Centrioles with appendages %	Centrioles without appendages %
Brain1	12.5	87.5
Brain2	29.82	70.18
Brain3	23.08	76.92
Average	21.8	78.2
Standard deviation	7.13	7.13

	WT Centrioles with appendages %	<i>Sey/Sey</i> Centrioles with appendages %
Brain1	60	12.5
Brain2	46.15	29.82
Brain3	51.26	23.08
Average	51.26	21.8
Standard deviation	6.21	7.13

VI.3. Number of appendages

The number of appendages was counted from centrioles containing appendages. Centrioles without appendages were not considered. The average number of appendages was calculated for every brain.

	WT	<i>Sey/Sey</i>
Brain1	1.6	1.2
Brain2	1.54	1.06
Brain3	1.4	1.44
Average Total	1.51	1.23
Standard deviation	0.08	0.16

VI.4. Quantification of primary cilia by IHC of E13.5 WT and Sey/Sey cortex

WT	Cilia	Width	Stack thickness	Stacks	Cilia/ μm^2
Brain 1	29	88	0.25	41	0.032
Brain 2	19	88	0.25	28	0.031
Brain 3	23	88	0.25	37	0.028
Brain 4	28	88	0.25	40	0.032
Average					0.031

<i>Sey/Sey</i>	Cilia	Width	Stack thickness	Stacks	Cilia/ μm^2
Brain 1	15	88	0.25	32	0.021
Brain 2	18	88	0.25	48	0.017
Brain 3	10	88	0.25	33	0.013
Average					0.017

	Average Cilia/ μm^2	Cilia %	Standard deviation
WT	0.031	100	
<i>Sey/Sey</i>	0.017	56.47	10.02

VI.5. Cilia quantification by EM at E15.5 cortex

	WT Centrioles	WT Centrioles connected to cilia	<i>Sey/Sey</i> Centrioles	<i>Sey/Sey</i> Centrioles connected to cilia
Brain 1	25	11	40	3
Brain 2	52	44	57	6
Brain 3	63	20	39	0
Total	140	75	136	9

	WT %	<i>Sey/Sey</i> %
Brain 1	44	7.5
Brain 2	38.46	10.53
Brain 3	22.22	0
Average	34.89	6.01
Standard deviation	9.24	4.42

VI.5. Statistical analysis of Kaede-Centrin1 approach

VI.5.1. Analysis of control brains

VZ	Yellow	Green	Yellow %	Green %
Brain 1	436	533	44.99	55.01
Brain 2	287	603	32.24	67.75
Brain 3	138	127	52.08	47.92
		Average	43.11	56.89
		Standard deviation	8.2	8.2

CP	Yellow	Green	Yellow %	Green %
Brain 1	195	593	24.75	75.25
Brain 2	131	583	18.35	81.65
Brain 3	64	158	28.83	71.17
		Average	23.97	76.03
		Standard deviation	4.31	4.31

Yellow Centrosomes	VZ	CP	VZ %	CP %
Brain 1	436	195	69.1	30.9
Brain 2	287	131	68.66	31.34
Brain 3	138	64	68.32	31.68
		Average	68.69	31.31
		Standard deviation	0.32	0.32

VI.5.2. Analysis of *Pax6cKO* brains

VZ	Yellow	Green	Yellow %	Green %
Brain 1	209	350	37.39	62.61
Brain 2	365	609	37.47	62.53
Brain 3	235	609	27.84	72.16
Brain 4	117	153	43.33	56.67
		Average	36.51	63.49
		Standard deviation	5.55	5.55

CP	Yellow	Green	Yellow %	Green %
Brain 1	439	1425	23.55	76.45
Brain 2	411	578	41.56	58.44
Brain 3	295	447	39.76	60.24
Brain 4	317	286	52.57	47.43
		Average	39.36	60.64
		Standard deviation	10.36	10.36

Yellow Centrosomes	VZ	CP	VZ %	CP %
Brain 1	209	439	32.25	67.75
Brain 2	365	411	47.04	52.96
Brain 3	235	295	44.34	55.66
Brain 4	117	317	26.96	73.04
		Average	37.65	62.35
		Standard deviation	8.31	8.31

VI.5.3. Locations of Yellow centrosomes

	Control %	<i>Pax6cKO</i> %
VZ	68.69	37.65
CP	31.31	62.35

VI.5.4. Location of Centrosomes

VI.5.4.1. Location of centrosomes in control brains

Control	VZ	CP	VZ %	CP %
Brain 1	969	788	55.15	44.85
Brain 2	890	714	55.49	44.51
Brain 3	265	222	54.41	45.59
		Average	55.02	44.98
		Standard deviation	0.45	0.45

VI.5.4.2. Location of Centrosomes in *Pax6cKO* brains

<i>Pax6cKO</i>	VZ	CP	VZ %	CP %
Brain 1	559	1864	23.07	76.93
Brain 2	974	989	49.62	50.38
Brain 3	844	742	53.21	46.78
Brain 4	270	603	30.92	69.07
		Average	39.21	60.79
		Standard deviation	12.59	12.59

VI.5.4.3. Comparison of centrosome localisation in control and *Pax6cKO* brains

	Control %	<i>Pax6cKO</i> %
VZ	55.02	39.21
CP	44.98	60.79

VI.6. Luciferase assay

VI.6.1. Data from Luciferase assay

Odf2-promoter-luciferase									
Firefly luciferase	632240	691220	2772210	7374490	16269810	562620	12300272	9892926	40919735
	315220	481840	2216340	11055930	16152230	5443830	16312532	13181538	45330685
	369050	474730	2362120	12489080	18598730	5372840	14442927	8856372	41744025
Renilla Luciferase	41154860	122454200	29666280	118475560	137859010	17569810	52545426	46069864	134346470
	25094810	66038970	25210490	128184150	171828620	138419400	62040682	55793443	137964267
	26484290	114518480	26432910	142448130	142951820	119628710	59171181	40638698	131322863
FLuc/RLuc	0,015362463	0,005644723	0,093446499	0,062244821	0,118017749	0,032021974	0,234088349	0,214737469	0,304583626
	0,012561163	0,007296298	0,087913404	0,086250367	0,094001977	0,039328519	0,262932828	0,236256042	0,328568302
	0,013934676	0,004145444	0,089362844	0,08767458	0,130104884	0,04491263	0,244087185	0,217929521	0,317873248
Average	0,013952767	0,005695488	0,090240916	0,078723256	0,114041537	0,038754374	0,247036121	0,222974344	0,317008392
Percent	1,101033394	0,991086685	1,035522504	0,790678942	1,034866349	0,826280248	0,947587535	0,963059091	0,960806192
	0,900263212	1,281066252	0,974207805	1,095614834	0,824278415	1,014814963	1,064349731	1,059566036	1,036465628
	0,998703394	0,727847063	0,99026969	1,113706224	1,140855236	1,15890479	0,988062735	0,977374873	1,00272818

Odf-promoter-luciferase/Pax6									
Firefly Luciferase	248400	356810	10299090	15578990	12523910	9879660	9171600	8061629	47216195
	372530	519400	5502040	17614280	27551700	7801670	11122148	8217189	55116939
	234930	676380	5397260	10859460	26799200	6232380	8688096	5597425	47658346
Renilla Luciferase	30666970	38619780	78988060	126443010	116468120	130554510	45223392	36364920	130681826
	23675450	64322390	61191550	155638150	200796750	140104690	45646832	35629092	139951235
	20388340	74724030	61368830	113284730	193633430	122803660	36020145	26477760	127919643
FLuc/RLuc	0,00809992	0,009239048	0,130387935	0,123209579	0,107530799	0,075674598	0,202806548	0,221686972	0,361306514
	0,015734865	0,008074949	0,089915029	0,113174565	0,137211882	0,055684574	0,243656515	0,230631446	0,393829601
	0,011522763	0,009051707	0,087947904	0,095859874	0,138401721	0,050750768	0,241201028	0,211401002	0,37256472
Average	0,011785849	0,008788568	0,102750289	0,110748006	0,127714801	0,060703313	0,229221363	0,221239807	0,375900278
Percent	0,580524261	1,622169581	1,444887098	1,565097596	0,942909067	1,952672408	0,820959085	0,994226367	1,13973801
	1,127723579	1,417779863	0,996388706	1,437625565	1,203174616	1,436859066	0,986319386	1,03434073	1,242331782
	0,826912842	2,183531035	0,984166361	1,093359948	1,063770373	1,129988768	0,988175713	0,97004298	1,172054341

VI.6.2. From the data of the Luciferase experiment

following result was calculated:

	Odf2-Promoter-Luciferase	Odf2-Promoter-Luciferase/Pax6
Average	1	1.20
Standard deviation		0.34

VI.7. Knock down of *Odf2* in vivo

VI.7.1. Sequences of short-hairpin constructs

Construct	Sequences	
SH1	GATCCGTGAAAGGGGACACCGTGAATTCAAGAGATTACGGGTGTCCCCTTTCATTTTTTGAAA	sence
	AGCTTTTCCAAAAAATGAAAGGGGACACCGTGAATCTCTTGAATTCACGGGTGTCCCCTTTCACG	antisence
SH2	GATCCGCCGAGAAACAGATGACTTGTTCAAGAGACAAGTCATCTGTTTCTCGGTTTTTGAAA	sence
	AGCTTTTCCAAAAAACCAGAGAAACAGATGACTTGCTCTTGAACAAGTCATCTGTTTCTCGGCG	antisence
SH3	GATCCGAACTCCTCCAGGAGATCTCAAGAGAGTATCTCCTGGAGGAGTTCTTTTTTGAAA	sence
	AGCTTTTCCAAAAAAGAACTCCTCCAGGAGATCTCTTGAAGTATCTCCTGGAGGAGTTCTG	antisence
SH4	GATCCGATTGGAGGCTGATGAAGTTTCAAGAGAACTTCATCAGCCTCCAATCTTTTTTGAAA	sence
	AGCTTTTCCAAAAAAGATTGGAGGCTGATGAAGTTCTCTTGAAGTTCATCAGCCTCCAATCTG	antisence
SH5	GATCCGTAAACAGCTGAGTCAGAAAGTTCAAGAGACTTCTGACTCAGCTGTTTATTTTTTGAAA	sence
	AGCTTTTCCAAAAATAAACAGCTGAGTCAGAAAGTCTCTTGAAGTCTGACTCAGCTGTTTACG	antisence
SH6	GATCCACCAAGGAACAGGCACTCTTTCAAGAGAAGAGTGCCTGTTCTTGGTTTTTTTGAAA	sence
	AGCTTTTCCAAAAAACCAAGGAACAGGCACTCTTCTCTTGAAGAGTGCCTGTTCTTGGTG	antisence
SH7	GATCCGGCCTCTTATGCAATGTGTTCAAGAGACACATTGTCATAAGAGGCCCTTTTTTGAAA	sence
	AGCTTTTCCAAAAAAGGCCCTTATGCAATGTGTCTCTTGAACACATTGTCATAAGAGGCCG	antisence
SH8	GATCCATGACCGGGTGACAGATCTTTCAAGAGAAGATCTGTCACCCGGTCATTTTTTTTGAAA	sence
	AGCTTTTCCAAAAAATGACCGGGTGACAGATCTTCTCTTGAAGATCTGTCACCCGGTCATG	antisence
K07	GCACTACCAGAGCTAACTCAGATAGTACT	sence
	CGTGATGGTCTCGATTGAGTCTATCATGA	antisence

Red marked are the sequences of the constructs, which was used for the *Odf2* knock down experiments.

VI.7.2. Results of quantification of electroporated cells after knock down of *Odf2*

Control	Pax6 ⁺ /GFP ⁺	GFP ⁺
Brain 1	341	3,291
Brain 2	655	6,688
Brain 3	222	2,084
Total	1,218	12,063

SH3	Pax6 ⁺ /GFP ⁺	GFP ⁺
Brain 1	114	10,491
Brain 2	143	6,410
Brain 3	510	20,885
Total	767	37,786

SH5	Pax6⁺/GFP⁺	GFP⁺
Brain 1	637	20,230
Brain 2	511	20,323
Brain 3	243	12,896
Total	1,391	53,449

VI.7.3. Statistical analysis of quantification

	Control %	SH3 %	SH5 %
Pax6 ⁺ /GFP ⁺	9.31	1.88	2.45
GFP ⁺	90.69	98.12	97.55
Standard deviation	0.29	0.58	0.49

VI.7.4. Statistical analysis of electroporated RGPs

(Pax6⁺/GFP⁺) normalized to control

	Control %	SH3 %	SH5 %
Pax6 ⁺ /GFP ⁺	100	20.19	26.33
Standard deviation		6.18	5.28

VI.8. Cell cycle index

VI.8.1. Results of cell cycle analysis

Control	GFP ⁺ /BrdU ⁺ /Ki67 ⁺	GFP ⁺ /BrdU ⁺ /Ki67 ⁻
Brain 1	538	325
Brain 2	1955	1569
Brain 3	1100	850

SH3	GFP ⁺ /BrdU ⁺ /Ki67 ⁺	GFP ⁺ /BrdU ⁺ /Ki67 ⁻
Brain 1	867	2266
Brain 2	364	1195
Brain 3	939	2426

VI.8.2. Statistical analysis of quantification of cell cycle exit after knock down of Odf2

Control	GFP ⁺ /BrdU ⁺ /Ki67 ⁺ %	GFP ⁺ /BrdU ⁺ /Ki67 ⁻ %
Brain 1	62.34	43.59
Brain 2	55.48	44.52
Brain 3	56.41	37.66
Average	58.08	41.92
Standard deviation	3.04	3.04

SH3	GFP ⁺ /BrdU ⁺ /Ki67 ⁺ %	GFP ⁺ /BrdU ⁺ /Ki67 ⁻ %
Brain 1	23.35	76.65
Brain 2	27.67	72.33
Brain 3	27.90	72.10
Average	26.31	73.69
Standard deviation	2.10	2.10

VI.9. Figure index

- Fig. I.1. Schema showing the primary brain vesicles of forebrain (prosencephalon), midbrain (mesencephalon) and hindbrain (rhombencephalon)(**A**). The primary vesicles get further subdivided in later stages of development, as indicated in (**B**) (Sanes et al 2006)..... 4
- Fig. I.2. Schema showing the different signalling centres and migrating signalling molecules in developing forebrain: FGF8 secreted by the anterior neural ridge (ANR), sonic hedgehog (Shh) by prechordal plate and Wnts and BMPs by the roof plate (RP). After expansion of the telencephalic vesicles Fgfs are expressed anteriorly at the commissural plate (CoP) and septum. The roof plate and the cortical hem secretes morphogeneic factors from Wnts, Tgfs and BMPs families, while the ventral mesendoderm secretes Shh. The anti-hem secretes Fgf7, Tgfa and Sfrp2 (Borello & Pierani 2010) 6
- Fig. I.3. Patterning of cerebral cortex. (A) Based on specific expression of regulatory molecules, the embryonic cortex is subdivided into dorsl (DP), lateral (LP), ventral (VP) and medial (MP) pallium. A complex interplay between TFs Pax6 and Gsh1/2 as well as Ngn1/2 and Mash/Dlx1/2 establishes a sharp boundary between pallium and subpallium (specifically, with the ventral lateral ganglion eminences (vLGE) (Schuurmans & Guillemot 2002). (B) Schema of the different functional areas of the mouse telencephalon (Sansom & Livesey 2009). (C) Schema of the current view of cortical arealization. The correct molecular identity is already encoded in radial units in the germinative zone and maintained by information from outside. VZ: ventricular zone; IZ: intermediate zone; SP: subplate; CP: cortical plate; MZ: marginal zone; MN: migrating neuron; RG: radial glia cell; NB: nucleus basalis; MA: monoamine subcortical centres; TR: thalamic radiation; CC: cortigo-cortical connections. The timing of neurogenesis (E40-E100) refers to the embryonic age in macaque monkey (Rakic 2009).. 8
- Fig. I.4. Schema of bith places of different neuronal subtypes. GABAergic interneurons are born in the VZ of the lateral and medial ganglion eminences (LGE/MGE) while glutamatergic projection neurons are born in the VZ of the neocortex (**A**) Glutamatergic neurons migrate relatively short distances within the cortex while GABAergic interneurons migrate long distances from LGE and MGE into the cortex (**B**) (Wilson & Rubenstein 2000)..... 8
- Fig. I.5. Schema of the different cell division modes of RGPs: (**A**) Symmetric proliferative divisions to expand the progenitor pool, leading thereby to lateral expansion of the cortex; (**B**) asymmetric neurogenic divisions produce RGPs and neurons during early neurogenesis *via* a direct mode of neurogenesis; (**C**) asymmetric differentiative divisions during mid- and late neurogenesis to produce a RGPs and an IPs, the last of which move into SVZ and after limited amplifications, symmetrically divides to generate neurons *via* indirect mode of neurogenesis (Fish et al 2008). (**D**) The time scale shows when the neurons of the different layers are produced. Lower layers (VI, V) are produced first, followed by a subsequent generation of upper layers (IV-II) according to an “inside first outside last” intrinsic program (Molyneaux et al 2007). 10
- Fig. I.6. Schema showing the different progenitor cell types in vertebrates. During evolution additional germinative layers with additional progenitor subtypes

- developed to fulfil the higher requirements of a mammalian neocortex (Fietz & Huttner 2011). 11
- Fig. I.7. Although RGP's span through the whole thickness of the neocortex, the cell bodies including the nucleus are exclusively located in VZ (A). The interkinetic nuclear migration guarantees mitosis at the ventricular surface therefore it is strongly connected to the cell cycle (B) (Reiner et al 2012) .. 12
- Fig. I.8. Pax6-deficient cortex shows almost a complete loss of neurons of layer 3-2 and 4 (**B and D**) compared to control (**A and C**) (Tuoc et al 2009). Interkinetic nuclear migration (INM) and centrosome localisation are disturbed in Pax6 loss-of-function. The nucleus migrates fast from the basal part of the VZ to the apical surface in WT animals. The centrosome (arrowhead) stays at the ventricular surface during nucleus migration (**E+E'**). In Pax6 LOF cortex, the nuclear migration is incomplete or absent; instead the centrosome (arrowhead) is moving towards the nucleus (**F and F'**) or nucleus migration is retarded and the centrosome (arrowhead) 'jumps' up and down (**G and G'**) (Tamai et al 2007). 14
- Fig. I.9. Schematic illustration of the centrosome structure. The mother centriole (red) shows distal and subdistal appendages. At the subdistal appendages are microtubules of the microtubules aster anchored. The daughter centriole (green) misses these structures (**A**). The mother centriole in the function of basal body of the primary cilium binds to the membrane *via* its distal appendages (**B**). Electronmicroscopy pictures of the centrosome, showing the distal (1 and arrowhead) and subdistal (**2 and arrow**) appendages of the mother centriole (**C**). Fluorescence of the centrosome as MTOC. Centrin (green) marking the centrioles, Ninein (red) marking the mother centriole, microtubules (white) staining shows that only the mother centriole functions as MTOC (**D**). Electronmicroscopy picture of the mother centriole shows that the microtubules are anchored at the subdistal appendages (**E**). Analysis of the centriole mobility shows that the mother centriole has a stable position due to its connection to the microtubules aster while the daughter centriole is able to move around (**F**) (Bornens 2012) 16
- Fig. I.10. Schematic illustration of the centrosome cycle. After mitosis centriole disorientation occurs, meaning the new-formed daughter centriole is detached from the mother centriole. At G1 S-phase transition centrosome duplication starts which is accomplished at the end of the S-phase. During G2 phase, the new centrosome matures - that means it recruits PCM. Before the cell enters mitosis, centrosome separation starts to build up the spindle pole bodies during cell division (Meraldi & Nigg 2002) 18
- Fig. I.11. Odf2 deficient cells miss the characteristic appendages at the mother centriole (arrows) (A). As a consequence of that *Odf2* knock out cells show a loss of Ninein at the subdistal appendages (B). A second important defect in *Odf2*^{-/-} cells is the loss of primary cilia (C) (Ishikawa et al 2005). 20
- Fig. I.12. Countless proteins accumulate in the centrosome, and especially in the PCM. Here are shown some of the most important proteins like γ -Tubulin and Centrin, which localize outside respectively inside of the centrioles and are the most common marker protein for the centrioles. Pericentrin localized predominantly around the centrioles and in the PCM is a marker for the whole centrosome. Ninein is predominantly localized at the subdistal appendages although it is also expressed at the proximal ends of the centrioles adopted from Bornens, 2002 (Bornens 2002). 21

- Fig. II.1. IHC with phosphorylated histone H3 (pH3) antibody on brain sections from E13.5 and E15.5 *Sey/Sey* and wild type embryos as indicated. **(A and B)** In WT animals note that two germinative zones (VZ, arrowheads; SVZ arrows) are visible. RGPs divide direct at ventricular surface while IPs divide mostly in SVZ located basally from VZ surface. **(C and D)** In *Sey/Sey* animals less cells divide at the ventricular surface. Instead cells divide in the basal part of the VZ indicating a defect of INM. At E15.5 this phenotype is more drastic than at E13.5..... 26
- Fig. II.2. IHC for γ -Tubulin shows a disturbed localisation of centrosomes in *Pax6LOF* cortex. **(A)** In WT, centrosomes form a line at the ventricular surface. **(B)** In *Sey/Sey* cortex centrosomes are scattered in the basal part of RGPs 27
- Fig. II.3. Schematic overview of the hypothesized effect of Pax6 loss of function on centrosome structure and behaviour. A loss of distal/subdistal appendages due to a lack of Pax6 would explain miss-orientation and ectopic position of the centrosome due to a missing anchorage to the cell membrane. As a consequence assembly of the primary cilium at the ventricular surface would be disturbed. 27
- Fig. II.4. STED microscopy picture of Ninein (red) at the centrosome of a NIH3T3 cell combined with a confocal picture of γ -Tubulin (green). Although the resolution of STED microscopy is much higher then confocal microscopy, STED microscopy is not able to visualize details of the appendages at the centrioles. 28
- Fig. II.5. Electron microscopy pictures of centrioles at the ventricular surface of WT E15.5 embryos. Counting reveals that 50 % of the centrioles possesses subdistal appendages (arrowheads). Most centrioles possessing subdistal appendages are the basal body of a primary cilium **(B-F)**. 29
- Fig. II.6. Electron microscopy pictures of centrioles at cortical ventricular surface of *Sey/Sey* E15.5 embryos. Around 78 % of the centrioles miss appendages (arrows) while only around 22 % of the centriole show subdistal appendages even when they are connected to a primary cilium **(C+E)**. Most centrioles are not located directly at the ventricular surface even when they are mother centrioles identified by the vesicle at their distal end **(A+D)**. 30
- Fig. II.9. IHC for γ -Tubulin (red), acetylated Tubulin (green) and DAPI. On cross brain sections at E13.5, the *Sey/Sey* cortex shows reduced primary cilia (arrowheads) at the ventricular surface **(A)** as compared to WT **(B)**. Higher magnification pictures ((in the frames) indicates a misorientation of some cilia (arrows) in *Sey/Sey* **(D)** but not in WT cortex **(C)**. Statistical analysis reveals a reduction oinprimary cilia number in *Sey/Sey* cortex by more than 40 % (43.53 %; ± 10.02 ; $p = 0.015$) compared to the WT..... 32
- Fig. II.10. IHC for γ -Tubulin (red) and acetylated tubulin (green). Due to the strong expression of acetylated tubulin in the apical process of RGPs an identification of primary cilia is not possible..... 33
- Fig. II.11. Quantitative analysis of centrioles connected to primary cilia using electron microscopy. Considerably less centrioles were connected to primary cilia (arrowheads) in *Sey/Sey* then in WT cortex. Centrioles in *Sey/Sey* cortex showed very often a vesicle at their distal end (arrows). However they failed to connect to the cell membrane and to assemble a primary cilium. Statistical analysis **(C)** indicates a strong reduction of the number of primary cilia at the ventricular surface compared with the wild type (WT: 34.89 % ± 9.24 ; *Sey/Sey*: 6.01 ± 4.42 ; $p = 0.031$). 34

- Fig. II.12. Schematic overview of the Kaede-Centrin1 approach to evaluate the centrosome maturation. The embryos were electroporated at E13.5. At E14.5 the mouse was sacrificed and the electroporated brains were cutted into 300 μm slices followed by photo conversion by exposure to UV light (350 – 400 nm) for 5 seconds. After two cell cycles (48 hours) it is possible to distinguish between mother centrosome (yellow/green and red) and daughter centrosome (green)..... 37
- Fig. II.13. Confocal microscopy of WT cortex after *in utero* electroporation of Kaede-Centrin fusion protein at E13.5, photo switch *ex vivo* at E14.5 and 48 hours of incubation (37 °C; 5 % CO₂; humidified). Analysis showed yellow and green marked centrosomes indicating that photo switch was successful. Green marked centrosomes located basally from VZ indicate a proper cell division of RGP and proper migration of differentiating cells. Distribution of the centrosomes indicates a higher percentage of mother centrosomes (yellow) in the VZ. Statistical analysis was not performed. 38
- Fig. II.14. Statistical analysis of Kaede-Centrin1 experiment. The analysis indicated a general reduction of centrosome number in the VZ of *Pax6* deficient cortex although there is no statistical relevance (WT: 55.02 % \pm 0.45; *Sey/Sey*: 44.98 % \pm 12.59; $p = 0.3$). Clearer was the result from analysis of the location of the mother centrosomes. While in WT almost 70 % of the mother centrosomes are located in the VZ, only less than 40 % are in *Pax6* deficient cortex indicating a loss of cells containing the mother centrosome (WT: VZ: 68.69 % \pm 0.32, CP: 31.31 % \pm 0.32; *Sey/Sey*: VZ: 37.65 % \pm 8.31, CP: 62.35 % \pm 8.31; ** = $p < 0.01$; $p = 0.0074$). 40
- Fig. II.15. Confocal microscope pictures of control (A) and *Pax6* deficient cortex (B) after electroporation of Kaede-Centrin1-plasmid, photo switch after 24 h and 48 h incubation *in vitro*. The *Pax6*-deficient cortex shows remarkably lower number of mother centrosomes (green and red / yellow; arrowheads) in the VZ as compared with the control cortex (A, VZ and B, VZ). In the *Pax6*-deficient cortex more mother centrosomes are distributed in basal regions (the intermediate zone, IZ and cortical plate, CP). 42
- Fig. II.16. Co-transfections and Co-immunoprecipitations (CoIPs) of *Pax6* with of potential *Pax6* protein binding partners. Nedd9 protein was distributed in the cytoplasm (arrowheads) showing no co-localisation with *Pax6*, which is exclusively expressed in the nucleus. Kif2a and Hook2 showed at least a partially co-localisation (arrows) (A and B). CoIPs were performed with the centrosome associated proteins Kif2a (D), Hook2 (E) and Nedd9 (F). None of the proteins showed a positive interaction with *Pax6 in vitro*. 44
- Fig. II.17. Immunohistochemistry (IHC) with antibodies for *Pax6* (green) and γ -Tubulin (red). *Pax6* and centrioles of interphase cells show no co-localisation. During mitosis the nuclear membrane is degraded and *Pax6* is evenly distributed in the cytoplasm (Arrow). Therefore an interaction would be only possible during cell division. 45
- Fig. II.18. View on the ventral part of an E12.5 WT embryo after whole mount *in situ* hybridisation for *Odf2* in a WT E12.5 embryo. Expression pattern of *Odf2* reveals a strong expression of *Odf2* in the developing CNS, including a strong expression in E12.5 forebrain of WT embryos. Collaboration with Prof. Hoyer-Fender. 46
- Fig. II.19. Luciferase reporter with the control of the *Odf2* promoter. Co-expression of *Pax6* revealed an increased reporter gene activity of ~20 % compared to single expression of reporter construct. Reporter construct

- (Control) = 1; Pax6 + Reporter construct = 1,2; $\pm 0,34$; ** = $p < 0.01$; $p = 0,0084$ 47
- Fig. II.20. Left panel: Sequence of the *Odf2* promoter containing possible Pax6 binding sites (coloured); right panel: EMSA of the three Pax6-binding sequences (SQ1, SQ2, SQ3) in *Odf2* promoter.. The third binding sequence (red; SQ3) showed a very strong binding to Pax6 (arrow), which band was supershifted (arrowhead) in the additional presence of Pax6 antibodies..... 49
- Fig. II.21. *In situ* hybridisation analysis of *Odf2* expression at E13.5 and E15.5 of WT and *Sey/Sey* brains as indicated. ISH at E13.5 reveals a slight reduction of *Odf2* expression in *Sey/Sey* embryos (A, B). At E15.5 ISH shows a much stronger down regulation of *Odf2* in *Sey/Sey* embryos (C, D)..... 50
- Fig. II.22. Quantitative rtPCR (E15.5). Quantitative rtPCR showed a reduction of more then 50 % in the *Sey/Sey* cortex (D) as compared with control ($53.95 \% \pm 6.24$; ** = $p < 0.01$; $p = 0.009$). 51
- Fig. II.23. IHC with antibodies for γ -Tubulin (red) and *Odf2* (green) revealed a reduction of *Odf2* at the centrioles of E13.5 *Sey/Sey* embryos compared with WT. At E15.5 no *Odf2* was detectable at the centrioles indicating a complete loss respectively massive down regulation of *Odf2*..... 52
- Fig. II.24. IHC with antibodies for γ -Tubulin (red) and Ninein (green) at E15.5 showed a strong reduction of Ninein at the centrioles indicating a loss of subdistal appendages in *Sey/Sey* cortex..... 53
- Fig. II.25. Functional test of *Odf2* short-hairpin constructs. The constructs SH3 and SH5 caused a strong knock down of *Odf2*. Construct K07 is a non-targeting construct used as control. Construct 58, 59, 60, 61 were from Origene, constructs SH1-SH8 were generated with pSilencer 2.0-U6 vector. Ligation of SH4 construct with pSilencer2.0-Ug vector failed..... 55
- Fig. II.26. Analysis of the neocortex after *Odf2* knock down *in vivo*. Electroporation of embryo brains with *Odf2* SH constructs SH3 and SH5 and the control plasmid K07 together with GFP was done at E13.5 and the analysis was made at E16.5. Each SH construct was electroporated together with GFP-plasmid to mark the electroporated cells. **(A)** After electroporation of a control plasmid 9.3 % (± 0.29) of electroporated cell were $\text{GFP}^+/\text{Pax6}^+$. After electroporation of SH3 respectively SH5 1.88 % (± 0.58) respectively 2.45 % (± 0.49) were $\text{GFP}^+/\text{Pax6}^+$ indicating a loss of RGP. Normalized to control, *Odf2* knock down causes a reduction of RGP amount of ~80 % ($20.19 \% \pm 6.18 \text{ GFP}^+/\text{Pax6}^+$) respectively ~75 % ($26.33 \pm 5.28 \text{ GFP}^+/\text{Pax6}^+$)(*** = $p < 0.001$; SH3: $p = 0.00053$; SH5: $p = 0.00027$). Diagram representing the whole amount of electroporated cells indicated a reduction of $\text{GFP}^+/\text{Pax6}^+$ cells (represented in yellow) after knock down of *Odf2* compared to control **(B)**. Diagram representing $\text{GFP}^+/\text{Pax6}^+$ normalized to control indicates a massive reduction of electroporated RGP after the knock down of *Odf2* **(C)**..... 56
- Fig. II.27. Analysis of cell cycle exit index after knock down of *Odf2*. **(A, B and C)** After electroporation of control plasmid K07 at E13.5, BrdU injection 24 hours later and analysis of E15.5 brains, 58.08 % (± 3.04) of the electroporated cells were in the cell cycle ($\text{GFP}^+/\text{BrdU}^+/\text{Ki67}^+$) (arrows). **(D)** However, after electroporation of SH3, only 26.31 % (± 2.1) of the RGP were still in the cell cycle, and a higher number (73.69; ± 2.1) exited from the mitotic cycle ($\text{GFP}^+/\text{BrdU}^+/\text{Ki67}^+$) (arrowheads) (***) = $p < 0.001$; $p = 0.00051$). The diagrams showing the cell cycle index after electroporation of

control plasmid and <i>Odf2</i> knock down construct SH3 indicating a strong diminishing of cells within the cell cycle (black bars).....	58
Fig. V.1. Schematic overview of mechanistic consequences due to loss of Odf2. The Centrosome (red) anchored at the cell membrane at the ventricular surface pulls down the nucleus (blue) in WT RGP. The missing anchorage of the centrosome in <i>Sey/Sey</i> RGP leads to basal movement of the centrosome and a slower or incomplete basal to apical transition of the nucleus. Adopted from Tamai et al 2007.	68

VII. ACKNOWLEDGEMENTS

First of all I want to thank my supervisor Prof. Dr. Anastassia Stoykova to give me the opportunity to perform my PhD thesis in her laboratory on this interesting topic. She was incredible helpful in countless discussions and in preparing my thesis. She gave me the opportunity to develop my own project and to gain my knowledge in this interesting field of biology. Without her this thesis would not have been possible. Thank you very much!

Furthermore, I want to thank Prof. Dr. Sigrid Hoyer-Fender for her support concerning the topic of centrosomes. Without her support many of the presented experiments would not have been possible. Additionally, I want to thank her for many fruitful discussions and for giving me the opportunity to collect credit points for teaching during her practical courses.

I want to thank Prof. Dr. Andreas Wodarz for his support during the thesis committee meetings and for critical comments and helpful suggestions.

Additionally, I want to thank the department of molecular cell biology, especially Kirsten Backs, Sigurd Hille, Sharif Mahsur and Ahmed Mansouri for fruitful discussions and if it was necessary distraction.

Special thanks go to Dr. Tamara Rabe, Dr. Alexander Klimke, Thomas Schulz, Dr. Tran Cong Tuoc and the “godfather of IHC” Dr. Anton Tonchev for support and discussions and so on.

I want to appreciate technical assistance as well as many discussions with Martina Daniel and the support for in utero electroporation by Silke Schlott. Without them this thesis would not have been possible.

Furthermore, I want to thank Heike Fett and Christian Dietl from the BTL for maintenance and provision of the mice.

Of course, I want to thank my parents for the unbelievable support not only during the time of the PhD preparation.

I want to thank my friends Andi, Silke, Lisa Blunck as well as Philip Moest for their support, nice evenings, football discussions and so on.

And finally I want to thank my girlfriend Dörte Linhop for her support

VIII. CURRICULUM VITAE

Curriculum vitae

Personal data

Name: Marco Andreas Tylkowski
Date of birth: August 5th 1981
Place of birth: Wedel
Nationality: German

Academic education

10/1999 – 12/2008	Biology studies, Georg-August University Göttingen, Germany
03/2008 – 12/2008	Diploma thesis, Research group of Prof. Hoyer- Fender, Dep. of developmental Biology, Georg- August University Göttingen, Germany
Since 05/2009	Research assistant, Research group of developmental Neurobiology, Max Planck Institute for biophysical Chemistry, Göttingen, Germany
Since 09/2009	PhD student of the Göttingen Graduate School for Neurosciences, Biophysics, and Molecular Biosciences (GGNB), Georg-August University School of Science (GAUSS) Program: Molecular physiology of the brain (CMPB)

Work experience

01/2009 – 02/2009	Research assistant, Research group of Prof. Hoyer- Fender, Dep. of developmental Biology, Georg- August University Göttingen, Germany
2011 - 2013	Tutor of the annual lecture course (1 week) of the International Max Planck Research School for Neuroscience (MSc/PhD)

Contact:

Research group for molecular developmental Neurobiology
Max Planck Institute for biophysical Chemistry
Am Fassberg 11
37077 Göttingen, Germany
Phone: + 49 551 201 1469
E-mail: marco.tylkowski@mpibpc.mpg.de